RELATIONSHIP BETWEEN LIGHTNING IMPULSE CURRENT INJECTED AND THE DEGREE OF ELECTRICAL DEGRADATION OF THE MOV

Mathews Musa Mashaba

A dissertation submitted to the Faculty of Engineering and the Built Environment, University of the Witwatersrand, Johannesburg, in fulfilment of the requirements for the degree of Master of Science in Engineering

Johannesburg, 2017

Declaration

I declare that this dissertation is my own, unaided work, other than where specifically acknowledged. It is being submitted for the degree of Master of Science in Engineering in the University of the Witwatersrand, Johannesburg. It has not been submitted before for any degree or examination in any other university.

Signed this _____day of _____20____

_____

Mathews Musa Mashaba

Abstract

Surge Protective Devices (SPDs) are used to protect electrical and electronic equipment against damages and operational malfunctions caused by surges. The commonly employed SPDs are composed of Metal Oxide Varistors (MOVs). MOVs are typically known for being inexpensive and for withstanding reasonable high values of current transients; they degrade over time depending on the severity and frequency of the surges they are subjected to. When MOVs are not properly monitored, the equipment they are meant to protect may remain unprotected and susceptible to surges. Reference voltage and leakage current of the MOV are commonly measured to deduce the operational status of the MOV. However, measuring the reference voltage only provides a pass or fail status of the MOV and not the degree of degradation, and measuring the leakage current and other dielectric parameters of the MOV (such as return voltage, decay voltage, etc.) is not always practical depending on the manner in which the MOVs are connected, especially the low voltage MOVs. This results in limited preventative maintenance techniques since the degree of degradation of the MOV is not known and other parameters of the MOV cannot always be measured. Therefore, the preventative maintenance mechanisms are sought. Extensive studies have been done to investigate the electrical and microstructural degradation of MOVs. However, the relationship between the current impulse injected and the degree of electrical degradation of the MOV have not been clearly defined. Therefore, defining this relationship can help to achieve preventative maintenance on lightning protection composed of MOVs by characterising and quantifying the degree of degradation of the MOV caused by a lightning impulse current without physically measuring dielectric parameters of the MOV. Thus, the study done in this dissertation answers the research question entitled: ***What is the relationship between an 8/20 µs lightning impulse current applied and the degree of degradation of the MOV?*** This question is answered through proposing a mathematical model that characterises the percentage of degradation of the MOV caused by a lightning impulse current. The mathematical model is specifically for MOVs with sizes ranging from 5 mm to 40 mm. The proposed model is tested against experimental test results and is found to match them by at least 75%. The discrepancy in matching is due to the assumption used in the matching process that all the MOVs exhibit the same response when subjected to the same impulse current. Nonetheless, the proposed model provides a minimum possible degradation level caused by a particular impulse current. The proposed model is thus deemed suitable to describe the relationship between the lightning impulse current injected and the degradation of the MOV.

This dissertation is dedicated to Hlengiwe Mnisi

Thank you for your love, support and encouragement. Most of it all, thank you for believing in me

Acknowledgements

I would like to sincerely thank my supervisor Professor Ken J. Nixon for his guidance and support which led to the completion of this study. Also, I would like to thank Mr. Hugh Hunt for his inputs in building up the research question and concluding this dissertation.

Special acknowledgments are extended to the following individuals/entities:

- Maynard Kumm (from Transnet Freight Rail, Technology Management) for his support in helping me to understand lightning protection and lightning related problems in Rail Network.
- Transnet Centre of Systems Engineering (TCSE) for their financial support in funding this study.
- Transnet Freight Rail for granting me the opportunity to further my studies
- John Kannemeyer (from Transnet Freight Rail, Technology Management) my manager, for his understanding and support throughout my studies.
- Gerhard Breedt (from Transnet Freight Rail, Technology Management) for helping with some of the tools used in conducting the experimental tests.
- Hlengiwe Mnisi; my lovely fiancée for your continuous love, support and motivation.

Lastly, I would to like to extend my utmost gratitude to my family for their endless support and love.

Thank you Lord Almighty, without You I wouldn't be where I am.

Contents

List of Figures

List of Tables

1. Introduction

Lightning and switching surges propagate through incoming and outgoing power and signal cables to reach electrical and electronic equipment, and subsequently may cause damage and operational malfunction. Surge Protective Devices (SPDs) are used to protect the electrical and electronic equipment against the catastrophic and harmful effects of surges. Most SPDs, especially the ones used in low-voltages are composed of Metal Oxide Varistors (MOVs) [1-3]. MOVs are bipolar ceramic semiconductor devices with a non-linear voltage-current characteristics; their resistance decreases with an increase in voltage magnitude [1, 2]. A MOV acts as an open circuit during normal operating voltage and conducts current during voltage transients or when its voltage is elevated above the rated Maximum Continuous Operating Voltage (MCOV).

After exposure to a surge, a MOV is expected to retain its original properties (electrically and microstructurally) without a noticeable damage [1]. However, the operational reliability and capability of a MOV is substantially influenced by the temperature and other factors of the surrounding environment and its capability to withstand a surge. MOVs can age, degrade, or reach their end of life over time due to the following reasons: surges that exceed the surge current ratings of the varistor; the rate of occurrence of surge events; duration of the surge; or the combination of these events. Repetitive surge events of significant amplitude over a period of time can overheat the MOV and eventually degrade it.

Numerous studies have been undertaken to determine the degradation of a MOV. Most of these studies utilise methods and diagnostic techniques which focus on observing the degradation of the MOV's microstructure and how the change in microstructure actually affects the electrical performance of the MOV with respect to its specification [1, 3]. However, not much attention has been focused on quantifying the electrical degradation of the MOV caused by a single lightning impulse.

1.1 Problem statement

Various mechanisms and methods of measuring the degradation of the MOV through determining the change in the parameters of a MOV such as leakage current, reference voltage, decay voltage (Ohmic conductivity), polarisation/depolarisation current (polarisation conductivity) exist. However, most of these methods (except leakage current and reference

voltage measurements) are commonly applied off-line, where the MOV is isolated and no longer in service, to determine the degree of degradation the surges caused on the MOV when it was in service. Removing the MOV from service to conduct tests in order to deduce its degree of degradation does not form part of preventative maintenance. The reference voltage of the MOV is commonly measured to determine the operational status while the MOV is in service. However, measuring the reference voltage gives only pass or fail status of the MOV and not the degree of degradation of the MOV caused by a specific lightning impulse current. Therefore, measuring the reference voltage while the MOV is in service only gives an indication of whether the MOV requires replacement or not, which serves as a corrective maintenance and it does not provide any means of preventative maintenance. Furthermore, it is not always feasible to measure the reference voltage of every MOV while it is in service due to accessibility and the manner in which the MOVs are connected. Recently, more studies have been conducted to devise mechanisms of achieving preventative maintenance on the surge protective devices [4], however, these mechanisms rely on monitoring the electrical parameters (such as leakage current, reference voltage, etc.) of the MOV whilst the MOV is in service. This type of preventative maintenance has limitations since it cannot be undertaken for every MOV depending on the manner the MOVs are connected, especially the low voltage MOVs.

Other existing methods of measuring the degree of degradation only determine the degradation of the MOV when it was in service, but not the degree of degradation caused by a specific lightning impulse current. Pulse rating curves of the MOV exist and provide an estimated life span of the MOV when it is subjected to surges of constant magnitudes, but, in reality, the magnitudes and patterns of surges are not similar. Furthermore, the degree of degradation caused by a single lightning impulse current is not defined. Therefore, a relationship between the lightning impulse current and the degree of degradation of the MOV is to be defined. This leads to the research question this study aims to answer:

What is the relationship between an 8/20 µs lightning impulse current applied on a MOV and the corresponding degree of degradation of the MOV?

Answering this question will provide knowledge on quantifying the degree of degradation a particular 8/20 µs lightning impulse current can cause on the MOV without necessarily measuring physical parameters of the MOV. Furthermore, it will help to estimate the end of life of the MOV in order to timeously replace the MOV while it offers acceptable protection

level and as a result, the preventative maintenance shall be achieved. Additionally, the answer of this dissertation will provide knowledge which can be extended to gauge the risk level of the environment the MOV is used in and also, to determine the feasibility of using the MOV in a particular environment.

1.2 Approach taken

This section discusses the approach taken to answer the research question addressed by this dissertation in order to characterise the relationship between the lightning impulse current injected and the degree of degradation of the MOV.

1.2.1 Proposed mathematical model of MOV degradation

The research question will be answered by proposing a mathematical model that defines the relationship between the lightning impulse current and the degree of degradation of the MOV. The model is developed using the pulse rating curves of MOVs with sizes ranging from 5 mm to 40 mm, which provide the number of impulses of particular lightning impulse current each MOV can withstand. The number of impulses denotes the estimated life span and the degradation of the MOV. The aforementioned MOVs are selected because they commonly encounter challenges addressed in the problem statement since they are mostly used in low voltage equipment.

Different types of varistor models (discussed in **Chapter 2**) are considered for modelling the degradation of the MOV, however, the proposed model is derived and contextualised from the interpolation formula of the simplified varistor model and it is verified using the number of impulses per lightning impulse current given by the pulse rating curves of each MOV. The proposed model is applicable to different types of MOVs with sizes ranging from 5 mm to 40 mm, with each type of MOV having unique parameters. The proposed model only characterises the degradation of the MOV when it is subjected to 8/20 µs type of lightning impulse current. This model is detailed in **Chapter 3**.

1.2.2 Evaluation of the proposed model

Experimental tests are conducted to observe the degradation of the MOV through measuring the parameters of a MOV such as reference voltage and leakage current. The proposed model is then evaluated against the experimental tests results by matching the minimum percentage of change of leakage current (which indicates the degree of degradation) estimated by the

model with the percentage of change of leakage current computed from the experimental test results.

The results obtained from comparing the model with the experimental test results are then analysed to determine the accuracy of the model and to outline the possible areas of improvements on the model.

1.3 Dissertation Structure

This dissertation proposes a mathematical model that describes the relationship between the lightning impulse current injected and the degree of degradation of the MOV. In this dissertation, 'impulses' and 'impulses' are used interchangeably and they have a same meaning. The structure of this dissertation is as follows:

Chapter 2 provides a summary of IEC 61643-11 and -12 standards, and a brief background information on the composition and characteristics of the MOVs. The different forms in which the MOV fails are also discussed. This chapter further outlines the degradation of the MOV and the different diagnostic parameters and techniques used to monitor the degradation. Furthermore, it discusses the existing varistor models and outlines the knowledge gap in the existing varistor models.

Chapter 3 presents the mathematical model proposed to describe the relationship between the lightning impulse current applied and the degradation of the MOV. The model is primarily derived from the interpolation formula of the simplified varistor model and verified using the number of impulses given in the pulse rating curves.

Chapter 4 discusses the test procedures and set ups used to conduct the experimental tests in order to validate the accuracy of the proposed degradation model. This chapter further discusses the results measured and computed during the experimental tests. The results computed using the proposed degradation model are also discussed. Thereafter, the results from both experimental tests and proposed model are compared and matched to evaluate the accuracy of the model for characterising the degree of degradation of the MOV in relation to the lightning impulse current applied.

Chapter 5 provides the necessary conclusions drawn from the findings of this study when comparing the proposed model with the experimental test results. Recommendations are given

for further work to improve the proposed model and to ensure it caters for all conditions of lightning impulse currents.

Appendix A presents a paper that was accepted and presented for publication by the 2016 IEEE International Conference on High Voltage Engineering and Applications (ICHVE), in Chengdu, China, 19th – 22nd September 2016. The paper is titled: *Deducing Metal Oxide Varistor Life Span from Pulse Rating Curves for Surges of Different Magnitudes*.

Appendix B presents the pulse rating curves and the proposed model's simulation results with parameters of all the MOVs with sizes ranging from 5 mm to 40 mm. The model's simulation results are compared to the number of impulses given in the pulse rating curves to outline the percentage of error.

Appendix C shows the Matlab code used to determine the parameters of the proposed model in order to characterise the degradation of the MOVs with sizes ranging from 5 mm to 40 mm.

Appendix D presents a paper the author submitted to South African Universities Power Engineering Conference (SAUPEC) 2017 which will be held in Stellenbosch University, on the 30th January – 1st February 2017. The paper has been accepted for oral presentation. The paper is titled: *A Proposed Mathematical Model of Metal Oxide Varistor Degradation*.

Appendix E provides the list of components, equipment and tools used to conduct the experimental tests for this study. A brief description on-, and the purpose of-, each tool/equipment/component is given.

Appendix F provides the results of all the experimental tests conducted on type FNR 14K201 MOV. In total, 160 samples of the MOVs were tested, and 16 samples were used per a particular magnitude of 8/20 µs lightning impulse current.

2. Background

This chapter provides a summary of IEC 61643-11 and -12 standards, and a brief background information on the composition and characteristics of the MOVs. The different forms in which the MOV fails in are discussed. This chapter further outlines the degradation of the MOV and the different diagnostic parameters and techniques used to monitor the degradation. Furthermore, it discusses the existing varistor models and outlines the knowledge gap in the existing varistor models.

2.1 IEC 61643-11 and -12 standards

This section briefly discusses the IEC 61643-11 and -12 standards and provides a summary relevant to the tests done in this study.

2.1.1 IEC 61643-11 standard

The IEC 61643-11 standard is applicable for low-voltage surge protection devices (SPDs) which are used for protection against direct and indirect lightning and other transient overvoltages. These devices are commonly connected to 50/60 Hz power circuits with the equipment rated up to 1000 V_{rms} [5].

SPDs are classified according to a number of parameters, which include: SPD design; number of ports; Type of test, i.e. Class I, II and III tests; location the SPDs are used/installed in; accessibility; SPD mounting method; SPD disconnector location and protection functions; degree of protection (IP-code) provided by SPD enclosures; temperature and humidity range; power system the SPD is used in; SPD poles; and the SPD failure behaviour.

Type tests are conducted to evaluate the performance of the SPD against all the requirements of the relevant clauses and relevant pass criteria. SPDs tested to Class I test method are commonly subjected to partial conducted lightning current impulses, and SPDs tested to Class II or III test methods are subjected to impulses of shorter duration. The general and electrical requirements for conducting the SPD type tests or certifying the SPD are discussed in this section [5]:

2.1.1.1 SPD electrical requirements

Operating duty: The SPD shall be capable of withstanding specified discharge currents during the application of the maximum continuous operating voltage U_C without unacceptable changes in its characteristics.

Disconnectors and status indicators: The SPD shall have disconnectors, which can be either internal, external or both. Their operation shall be indicated by a corresponding status indicator. The manufacturer shall provide information about the status indicator and the actions to be taken after the change of status indication.

Insulation resistance: The insulation resistance of the SPD shall be sufficient with respect to leakage currents and protection against direct contact.

Dielectric withstand: The dielectric withstand of the SPD shall be sufficient with respect to insulation breakdown and protection against direct contact.

SPD shall be protected against overheating that may be caused by degradation or over-stresses.

Service conditions: The service conditions SPDs are exposed to, as stipulated in IEC 61643-11, are listed below:

- Frequency: 47 – 63 Hz;
- Voltage: The voltage applied continuously across the terminals of the SPD must not exceed its maximum continuous operating voltage U_C;
- Air pressure and altitude: 80 kPa (+2 000 m) – 106 kPa (-500 m);
- Normal temperature range: -5 °C to +40 °C;
- Extended temperature range: -40 °C to +70 °C;
- Normal humidity range: 5 % to 95 %; and
- Extended humidity range: 5 % to 100 %.

The normal temperature and humidity ranges address SPDs used in indoor application in weather-protected locations having neither temperature nor humidity control. The extended temperature and humidity ranges address SPDs used in outdoor application in non-weather-protected locations.

2.1.1.2 SPD type tests general requirements

The waveshape of the current impulse used for class I and II residual voltage and operating duty tests shall be 8/20 µs. The tolerances of the current waveshape passing through the device under test shall be as follows: crest value ±10 %; front time ±10 %; and the time to half value ±10 % [5]. Any overshoots or oscillations shall have an amplitude that is not more than 5 % of the crest value, and any polarity reversal after the current has fallen to zero shall not be more than 30 % of the crest value.

The standard voltage impulse waveshape used for class I and II spark over tests is 1.2/50 µs. The tolerances of the open-circuit voltage waveshape across the points where the SPD under test will be connected are as follows: crest value ±5 %; front time ±30 %; and the time to half value ±20 % [5]. Oscillations exceeding 3 % of the crest value are not allowed on the rising portion of the voltage impulse between 0 % and 80 % of the crest value. The short-circuit current of the voltage impulse generator shall be less than 20 % of the nominal discharge current (I_n) of the SPD.

The standard impulse of a combination waveform generator used for class III tests is characterized by the output voltage under open-circuit conditions and the output current under short-circuit conditions. The open-circuit voltage shall conform to the 1.2/50 µs waveshape and tolerances. The short-circuit current shall conform to the 8/20 µs waveshape and tolerances.

2.1.1.3 SPD type tests

There are several type tests conducted on a SPD to evaluate its performance against specific pass criteria and requirements stipulated in IEC 61643-11. This section briefly discusses few type tests, under SPD electrical tests, which are commonly performed on SPDs [5].

(i) Residual current I_{PE} test

The SPD shall be connected as for normal use according to the manufacturer's instructions and the voltage shall be adjusted to a reference test voltage U_{REF}. Thereafter, a residual current I_{PE} flowing through the PE terminal shall be measured and it shall not exceed the value declared by the manufacturer.

(ii) Residual voltage or measured limiting voltage

The SPDs testing for class I are applied with a sequence of 8/20 µs current impulses with an amplitude ranging up to the value of impulse discharge current I_{imp}, and the SPDs testing for class II are applied with a sequence of 8/20 µs current impulses with an amplitude ranging up to the value of nominal discharge current I_n. A residual voltage is a highest crest value measured during the flow of the surge current. The SPDs testing for class III are applied with the voltage of the combination wave generator with the open-circuit voltage ranging from 0.1 to 1.0 times the SPD open-circuit voltage (U_{OC}) as declared by the manufacturer. For every current impulse delivered by the generator into the SPD, the voltage at the output port of the SPD is measured; a measured limiting voltage is regarded as a maximum voltage recorded during this test. The measured limiting voltage shall not exceed the voltage protection level U_P declared by the manufacturer. Also, there shall be no puncture, flashover or any visible damage on the SPD, as stipulated by the IEC 61643-11 standard.

(iii) Operating duty test

The operating duty test is a type test conducted on the SPD in which service conditions are simulated by applying a stipulated number of specified impulses to the SPD while it is energized at the maximum continuous operating voltage U_C using an a.c. source according to IEC 61643-11 standard.

The test set up used for performing the operating duty tests is configured as shown in Figure 1. In the case of SPDs with follow current that is 500 A or less, the impedance of the power frequency voltage source shall be such that during the flow of follow current the crest value of the power frequency voltage measured at the SPD terminals does not fall below the crest value of its U_C by more than 10 %. On the other hand, in the case of SPDs with follow current that is above 500 A, the power frequency voltage at U_C shall have a prospective short-circuit current which is either 500 A or equal to the follow current interrupt rating I_{fi} declared by the manufacturer in accordance to IEC 61643-11.

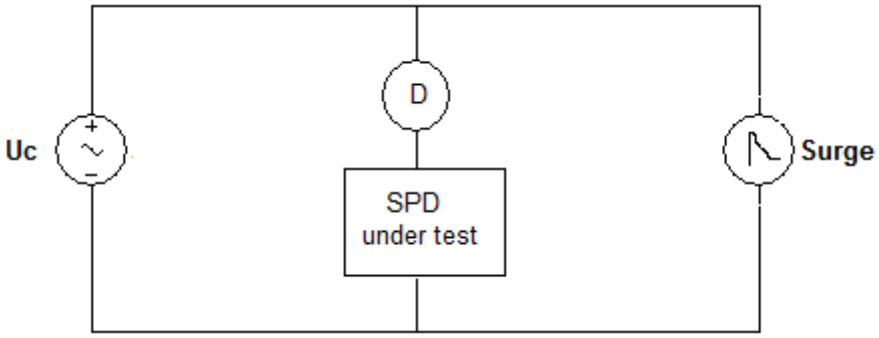

Figure 1: Test set up for operating duty test; adapted from [5]. Where U_C – Power frequency voltage source; D – SPD disconnector, as specified by the manufacturer; and Surge – impulse current as per the requirements of operating duty test in IEC 61643-11 for class I, II and III SPDs.

For Class I and II operating duty tests, three groups of five 8/20 µs current impulses with positive polarity shall be applied. Each impulse shall be synchronized to the power frequency with the interval between the impulses being 50 s – 60 s and the interval between the groups being 30 min – 35 min.

Additional duty tests are performed when testing SPDs to class I, with five current impulses having an amplitude ranging in steps up to the value of impulse discharge current I_{imp} applied through the SPD. The current impulses of positive polarity shall be initiated in correspondence to the positive crest value of the power frequency voltage source and applied into the energized SPD test sample as follows: one current impulse at 0.1 I_{imp}; one current impulse at 0.25 I_{imp}; one current impulse at 0.5 I_{imp}; one current impulse at 0.75 I_{imp}; and one current impulse at 1.0 I_{imp}. After each application of current impulse, the thermal stability is checked and the SPD test sample is cooled down to ambient temperature.

For Class III operating duty tests, the SPD is tested with three groups of impulses corresponding to the open-circuit voltage U_{OC}: the first group has five positive impulses initiated at the crest value of positive half cycle; the second group has five negative impulses initiated at the crest value of negative half cycle; and the last group has five positive impulses initiated at the crest value of positive consecutive half cycle.

After each group of impulses is applied, the SPD shall remain energized at U_C without interruption for at least 1 min to check for re-ignition. After the application of last group of impulses and the 1 min period, the SPD either remains applied or shall be re-applied within less than 30 s with U_C for another 15 min to check for thermal stability.

According to IEC 61643-11, the SPD is considered to have passed the operating duty test if:

A. The thermal stability is achieved;
B. The voltage and current records and visual inspections do not show any indications of puncture or flashover;
C. There is no visible damage that occurred during the test. After the tests, the small indents and cracks are disregarded provided that the degree of protection (IP-code) given for the SPD is still maintained;
D. The values of the measured limit voltage after the test are below or equal to SPD's voltage protection level U_P;
E. No excessive leakage current occurred after the test. The power frequency current that flows through each terminal shall not have changed by more than 20 %, or its resistive component shall not exceed a value of 1 mA;
F. No flashover, breakdown of insulation either internally (puncture) or externally (tracking) or any other manifestation of disruptive discharge shall occur on the disconnector during the test;
G. The external disconnectors as specified by the manufacturer, shall not operate during the test and shall be in the working order after the test;
H. The internal disconnectors as specified by the manufacturer, shall not operate during the test and shall be in the working order after the test; and
I. There shall be no explosion or other hazard to either personnel or the facility.

(iv) Temperature withstand test

The SPD is kept in a heated cabinet with an ambient temperature of 80 °C ± 5 K for 24 hours. There shall be no visible damage occurring during the test and the internal disconnectors of the SPD shall not operate during the test and shall be in the working order after the test.

(v) Degradation

SPD degradation is a change of original performance parameters as a result of exposure of the SPD to surge, service or unfavourable environment. Two type tests are applied to provide confidence in the SPD with respect to degradation; operating duty test and ageing test. These two tests may be combined.

The operating duty test is carried out as described in **(iii)**. The ageing test is carried out at a specified temperature with a voltage of specified magnitude and duration applied to the SPD.

2.1.2 IEC 61643-12

SPDs shall be selected according to their environmental conditions and the acceptance failure rate of the equipment and the SPDs. IEC 61643-12 standard provides information about the characteristics useful for the selection and coordination of low-voltage SPDs while considering the environment the SPDs are used in. The principles discussed in the IEC 61643-12 standard apply to SPDs connected to 50 Hz – 60 Hz a.c. and d.c. power circuits and to equipment rated up to 1 000 V_{rms} or 1 500 $V_{d.c.}$

When evaluating the installation for the use of an SPD, two main factors need to be considered [6]:

- The characteristics of the low-voltage power distribution system on which the SPD will be used; this includes the expected types and levels of overvoltage and current; and
- The characteristics of the equipment requiring protection.

In common cases lightning stress is the main factor for the selection of SPD class of test and associated current or voltage values. The evaluation of the waveshape and amplitude of current (or voltage) of the lightning surges is necessary for the proper selection of the SPD. It is important to determine if the voltage protection level of the SPD will be adequate to protect the equipment when subjected to surges.

The flowchart described in Figure 2 summarises the application of the SPD in low-voltage power distribution systems and Figure 3 summarises the selection of the SPD.

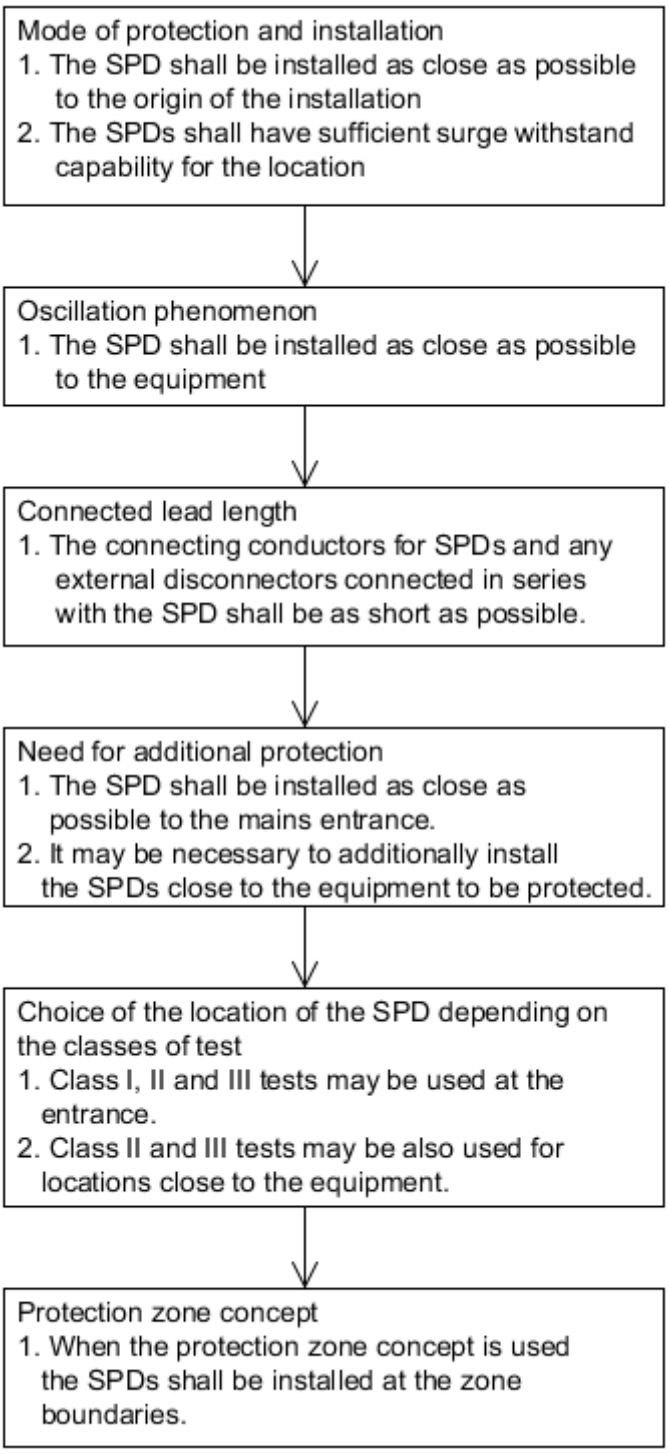

Figure 2: Flowchart for SPD application. Adapted from [6].

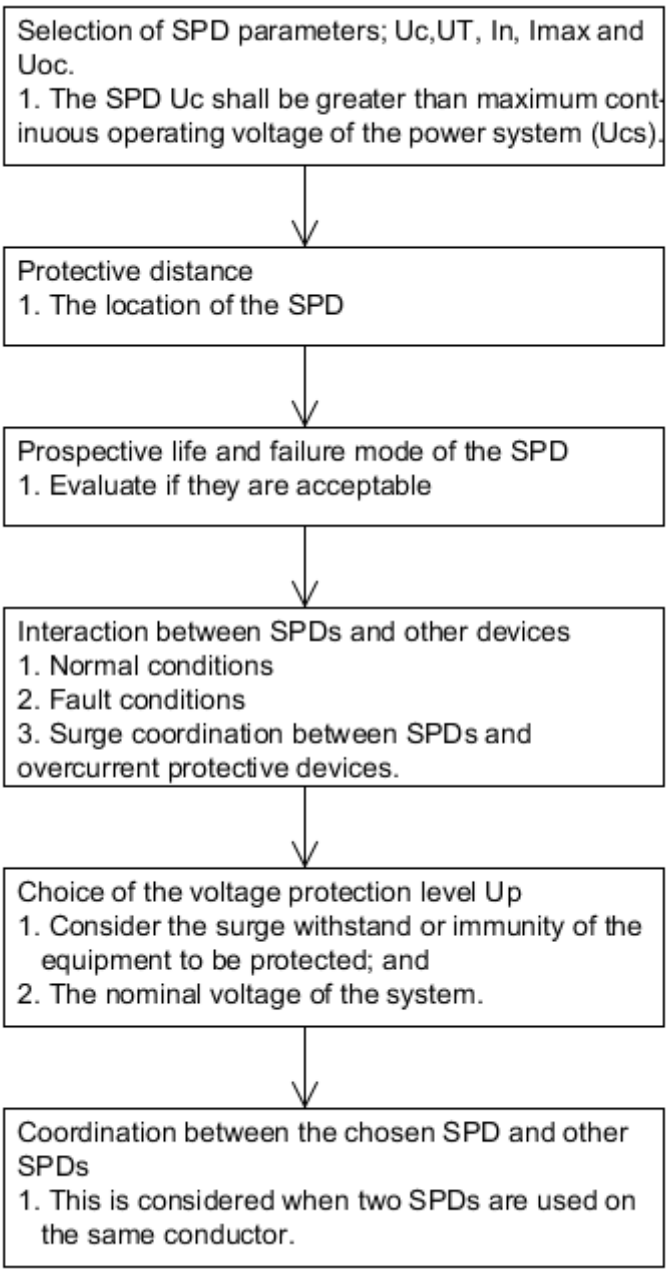

Figure 3: Flowchart of SPD selection. Adapted from [6].

2.2 Composition and Characteristics of Metal Oxide Varistors

MOVs are commonly employed as surge protective devices because they are inexpensive and they dissipate reasonably high values of transients compared to the other types of SPDs. The typical ratings of the MOVs ranges from 2.5V to 3000V and reaches current ratings of 70 000A

[7]. The energy handling capability of the MOVs can extend beyond 10 000 J especially for large units.

MOVs are composed of a mixture of Zinc Oxide (ZnO) and other metal oxides such as bismuth, cobalt, or manganese [8]. The mixture is kept intact by two metal plate electrodes. A p-n diode junction is formed between each boarder of the ZnO grain. The p-n junctions in the microstructure of the MOVs are connected both in parallel and series configurations. The parallel configuration improves the energy handling capability of the MOV, and the series configuration is improves voltage rating of the MOV. Although some p-n junctions are either forward biased or reversed biased, the MOV is bidirectional similarly to a back-to-back Zener diode. Figure 1 shows the microstructure of the MOV.

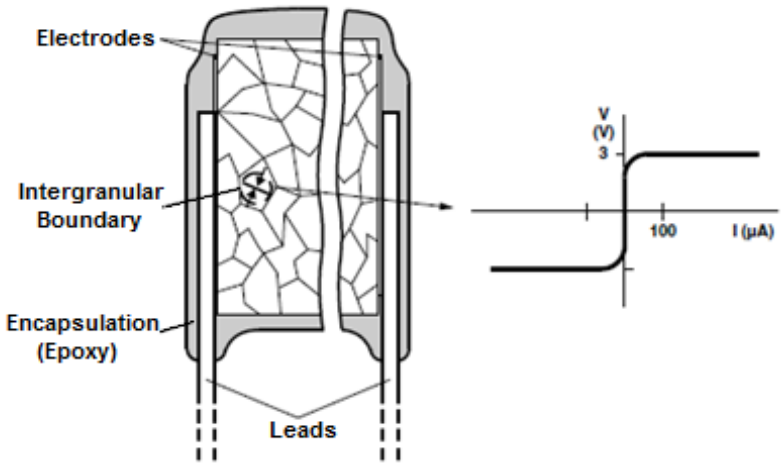

Figure 4: MOV Microstructure [9].

A reverse leakage current appears across the p-n junctions when a small voltage is applied across the electrodes of the varistor; hence the current produced across the leads of the varistor will also be small. However, when a large voltage, above MCOV is applied across the electrodes (or on either electrode), the diode boarder junction breaks down due to a combination of electron tunnelling and avalanche breakdown [8]. Thus, the varistor shows a high level of non-linear VI characteristics. Equation 1 [2] approximate the V-I characteristics of the MOV at normal varistor operation region, and Figure 2 depicts a typical V-I curve of a varistor.

$$I = kV^{\alpha} \tag{1}$$

Where:

I = current

V = voltage

k = material constant

α = degree of non-linearity

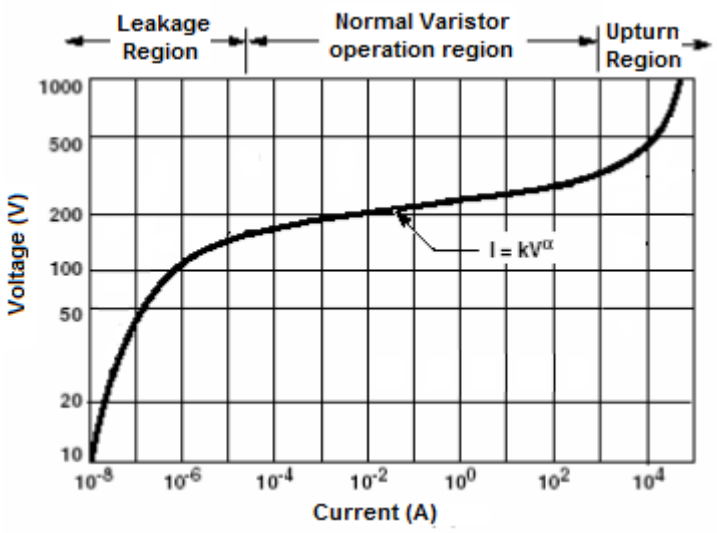

Figure 5: Typical varistor V-I curve [8].

At high voltages (voltage transients or voltage above MCOV), the resistance of the varistor is small, close to short circuit (in the range of 1 - 10 Ω) [8], this explains the capability of the varistor to clamp voltage transients to safe levels. At low voltages, the resistance is high, almost an open circuit – it behaves as an insulating material.

The maximum peak current allowable through the varistor depends on the pulse shape, duty cycle and number of pulses [9]. The ability of the varistor to withstand impulse currents is generally based on the maximum non repetitive surge current allowed through the varistor. The maximum non repetitive surge current rating of the MOV is given for one pulse of 8/20 µs shape following IEC 60060-2, with such an amplitude that the voltage of the varistor measured at 1 mA does not change by more than 10% [2, 9].

2.3 MOV Failure

MOVs are subjected to different types of failure which include long-term degradation, electrical puncture, thermal cracking, thermal runaway, etc. mainly caused by the limited capacity of the MOV to absorb energy. A surge in excess of the rated surge current or voltage may cause short circuit which

can lead to a rupture with expulsion of the material. The significant failure mechanisms of the MOV are briefly described below [2, 10, 11]:

- **Puncture** – occurs in the centre of varistor which results from non-uniform distribution of heat and current density that is caused by the higher temperature and larger current grown alternately at the centre. This phenomenon may be caused by long-duration over-voltages.
- **Cracking** – occurs due to higher thermal tensile stresses on the varistor which are caused by very large impulse currents during lightning surges.
- **Thermal runaway** – occurs due to continuous operating voltage following lightning surge current, because of the inability of the varistor to sufficiently cool temperature down, and consequently the temperature of the varistor is increased by leakage current caused by degradation of the varistor. As a result, this causes a notable disorder on the microstructure of the varistor.
- **Repeated conduction of currents** – are associated with momentary system over-voltages (swells), which lead to an increase in leakage current. The conduction is limited to a highly thermally activated low current region where the performance of the varistor is determined by the parameters of the potential barriers. This results in the movement of ions and the deformation of potential barriers.
- **Mechanical degradation** – leads to the corresponding increase in the forward voltage drop which results in electrical degradation. This degradation leads to local thermal runaway and total failure.
- **Misalignment** – results in a very small insulation path, where moisture or ion concentration may lead to high leakage. Large and unstable leakage currents may occur as a result of the oxide passivation being bridged by effects such as purple plague.

Most failure mechanisms of the MOVs result from excessive heating due to non-uniform distribution of heat. The non-uniform distribution of heat in a MOV occurs as a result of electrical properties that originate in either the fabrication process or the statistical fluctuations of properties that generally occur in polycrystalline materials [1, 2].

The disorder of ZnO varistor microstructure such as grain sizes and grain boundaries can be simulated by calculating the current densities and energy absorption capabilities using Voronoi network simulation (or other tools) [11]. By thoroughly comparing the effect of Joule heating and current localization with respect to impulse surge energy applied to ZnO varistor, puncture failure can be analysed quantitatively.

There are three basic failure modes for MOVs used within surge protective device, namely: MOVs fail as short circuit; MOVs fail as an open circuit; and MOVs fail as a linear resistance [12]. The small diameter MOVs that initially fail as a short circuit are more likely to fail as an open circuit over time due to the absorption of large continuous current.

The short circuit failure mode of MOVs is usually confined to puncture in which large fault current create plasma inside the ceramic, with temperature that is high enough to cause the ZnO ceramic to melt. The open circuit failure mode is possible if a MOV operates at steady state conditions above its rated voltage. The exponential increase in current causes overheating and as a result the wire lead and disk at the solder junction separate.

2.4 MOV typical current and voltage waveform

Figure 6 (not in scale) shows a typical 8/20 µs impulse current waveform as per IEC 61643-1 and IEC 61643-12, where I_P is the impulse current peak value, the front time is 8 µs and the time to half-value is 20 µs.

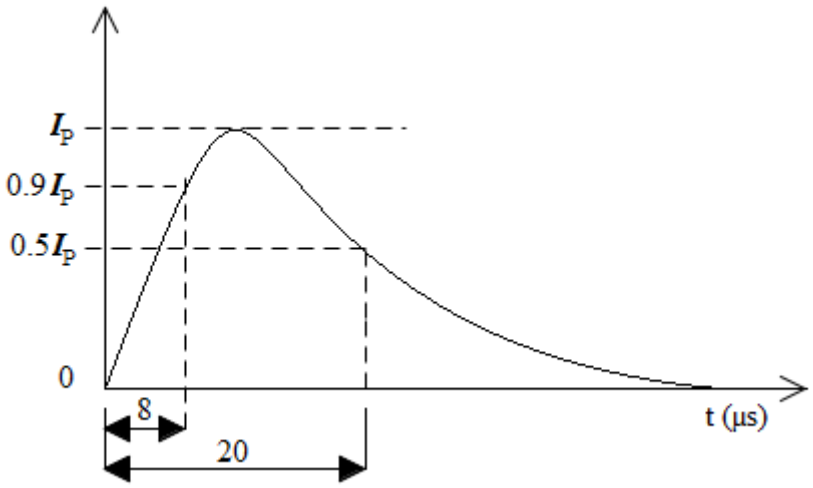

Figure 6: Typical 8/20 impulse current waveform

MOV is a voltage limiting type of SPD. Typically, when a downstream equipment protected with a MOV is subjected to current impulse as described in Figure 6, the MOV diverts all the current impulse to protective earth and limits the voltage across the downstream equipment to a voltage protection level U_P. A typical voltage waveform of how the MOV protects the downstream equipment is shown in Figure 7 as per IEC 61643-12.

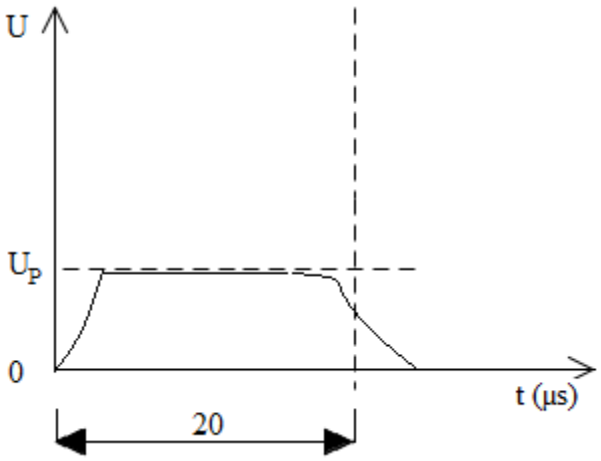

Figure 7: Typical MOV voltage waveform when subjected to current impulse

2.5 Comparison between MOVs and other SPD technologies

There are several types of SPD technologies used on low-voltage systems, but the common and widely used SPD components include Metal Oxide Varistors (MOVs), Silicon Avalanche Suppressor Diodes (SASDs) and Gas Discharge Tubes (GDTs). These SPD components can be used individually or combined to achieve an SPD technology with specific parameters.

(i) Gas Discharge Tube

Gas Discharge Tube (GDT) is a sealed glass-enclosed device containing a special gas mixture trapped between two electrodes, which conducts current when ionized by a high voltage transient [10]. GDTs conduct more current compared to the other SPD components (such as MOVs, SASD, etc.) of the same size. However, GDTs take relatively longer to trigger and as a result, they allow higher voltage transient to pass through to the protected downstream equipment before the GDT conducts significant current impulse. Therefore, in some cases, additional protective components which trigger rapider may be necessary to prevent damage to the downstream equipment or protective load, caused by let-through voltage transient which occur before the GDT conducts.

When a GDT is triggered, it creates an effective short-circuit and continues to conduct, including follow-on current, until all electrical current sufficiently diminishes and the gas discharge quenches. After the GDT is triggered, it continues to conduct at a voltage less than the high voltage that initially ionized the gas.

GDTs can handle a greater number of smaller transients or few very large transients. A typical failure of GDT occurs when triggering voltage rises to higher level to the extent that the GDT becomes ineffective; lightning surges can occasionally cause a dead short. GDT commonly fail as a permanent open-circuit.

(ii) Silicon Avalanche Suppressor Diode

Silicon Avalanche Suppressor Diode (SASD) type of SPDs include devices such as transzorbs and zeners, and are typically characterized by low clamping voltage, low surge rating, high speed, long life, and high cost [10, 13]. These components provide the fastest (theoretically in picoseconds) limiting action, but relatively low energy handling capability compared to other protective components.

SASD voltages can be clamped to less than twice the normal operation voltage. When the SASDs are subjected to current impulses within the device ratings, their life span is exceptionally long. However, when the SASD ratings are exceeded, the device may fail as a permanent short-circuit; in such cases, the protection may remain, but the normal circuit operation is terminated.

Table 1 summarises the comparison between the MOVs and other two commonly used SPD technologies [10, 13].

Table 1: Comparison between MOVs and other SPD technologies

SPD technology	Energy handling	Let-through voltage	Follow-on current	Price	Common permanent failure mode
MOVs	High	Low	Low	Low	Short/Open-circuit
SASD	Low	Low	Low	High	Short-circuit
GDT	High	High	High	Medium	Open-circuit

2.6 Degradation of the MOV

It is known that MOVs experience degradation due to single and multiple current impulses. The MOVs degrade when they are exposed to a few large surges, or many smaller surges [2]. However, many MOVs show no signs of degradation when they are operated below rated voltage. Hence, the degradation of MOVs is dependent on their composition and fabrication. Furthermore, the degradation depends on their application or use.

From the degradation tests conducted in [1] it was found that MOVs start to degrade at 8/20 μs surge current that is 1.5 times the rated MOV surge current. Degraded MOVs were found to have smaller grain size and changed diffraction peak position compared to new samples.

In high current conditions, especially above the rated surge current of a MOV, the zinc oxide junctions begin to degrade, and as a result it lowers the MCOV of the MOV. As the degradation continues, the MCOV is lowered to a level that the MOV conducts continuously, shorting or fragmenting within several seconds [2].

The life span of a MOV is generally determined by the magnitude of the internal current and its increase in temperature and voltage with time. The end of life is generally reached when the measured nominal voltage of the varistor (V_n) has changed by more than 10%. Arrhenius expression in Equation 2 defines the failure of the varistor (or life span) as the time to reach thermal runaway [2]. However, the Arrhenius expression does not consider the energy of the surge applied nor the history of surge exposure of the MOV. The environment (such as lightning surges, switching transients, temporary overvoltages, etc.) in which the MOV is exposed to is the primary factor that contribute to the degradation of a MOV. Thermal runaway, as mentioned in ***Section 2.3***, is primarily caused by large surge currents and/or long duration voltages which change the physical and/or chemical properties of the MOV. As a result, the leakage current and temperature of the MOV increase and cause the MOV to reach thermal runaway.

$$t = t_0 e^{\frac{(E_a - f(V))}{RT}} \tag{2}$$

Where:

t = time to thermal runaway

t_0 = constant time

E_a = activation energy

$f(V)$ = applied energy

R = material constant

T = temperature in kelvin

2.7 Degradation Diagnostic Parameters and Techniques

Since the MOV does not conduct at normal operating voltages (i.e. voltages below MCOV), it is then regarded as an insulator. Most diagnostic techniques refer to the MOV as an insulating material when assessing its degree of degradation. There are several recommended methods

for diagnosing and monitoring electrical equipment insulation systems (such as rotating machines, power transformers, cables, MOV, etc.) and the common and widely used methods are the Time Domain Spectroscopy (TDS) method and Frequency Domain Spectroscopy (FDS) method [14].

Time Domain Spectroscopy (TDS): TDS is based on the measurements of polarisation (also referred to as absorption) and depolarisation (also referred to as resorption) currents. These currents are used to determine the dielectric response function (which describes the behaviour) and the DC conductivity of the insulation.

Frequency Domain Spectroscopy (FDS): FDS is based on the measurements of complex permittivity components of the insulation. These components such as capacitance of insulation at different frequencies are used to determine the loss factor as the insulation degrades.

The aging of MOV involves changes in the physical and/or chemical structure of the insulation material, which subsequently change the dielectric response [15]. The degree of aging of the MOV depends on the nature of MOV, and the nature and duration of the stresses applied. There are various types of stresses which cause aging or degradation in the MOV such as electrical, mechanical, thermal, or environmental.

The quantification of electrical degradation of the MOV aims to allow reasonable estimates of service life expectancy of the MOV and to assess its reliability in operating conditions after being subjected to stresses. The commonly used non-destructive electrical degradation diagnostic parameters and techniques of a MOV include reference voltage; leakage current; return voltage characteristics; decay voltage measurement; and Polarisation/Depolarisation current measurement.

2.7.1 Reference/Nominal Voltage

The varistor nominal/reference voltage V_n represents the minimum required applied voltage for the varistor to clamp transients, which influences the MCOV of a MOV. It is a voltage across the MOV when a DC current of 1mA is applied [4]. The measurement of the reference voltage requires to be done within few seconds to avoid heating up the MOV and subsequently degrading its performance; the reference voltage is determined to establish if the MOV is in a pass or fail condition. The pass or fail condition is determined through the percentage of

deviation (tolerance) of the reference voltage before and after the MOV has been subjected to surges. The allowable changes according to IEC 60060-2 standard are not to exceed ±10% from the original values of the MOV reference voltage, depending on the type of the MOV [2, 9, 16].

The disadvantage of the reference voltage test is that it only determines the pass or fail condition of a MOV, but not the degree of degradation. It often does not provide meaningful interpretation about the extent of the MOV's degradation. Several tests are required to be done in order to scrutinise the electrical performance of the MOV before inferring the degree of degradation.

2.7.2 Leakage current

Ideally when the MOV is in non-conductive state, i.e. at voltages less than the MCOV, current is not expected to flow. However, due to real elements composing the MOV, a small amount of current does flow during this non-conductive state; which is regarded as leakage current. Leakage current is one of the main factors that indicates the level of degradation of the varistor. The total leakage current is composed of resistive and capacitive currents of an MOV [2]. The resistive component of leakage current contributes the most to the degradation of the varistor since it is thermally stimulated and it is responsible for the joule heating in the varistor. The MOV's capacitance value and applied AC voltage primarily contribute to capacitive current.

Electrical aging or degradation of MOV results only in the increase of the resistive component and not the capacitive component, this increase in the resistive component consequently increases power losses [17]. Therefore, the resistive leakage current is one of the key parameters when measuring the degradation of a varistor. The leakage current gives the following important information about the degradation level of a MOV [2, 18]:

- It determines the amount of watt loss an MOV is expected to generate when a nominal steady state operating voltage is applied.
- It determines the magnitude of steady state operating voltage that the MOV can handle without generating excessive amount of heat.

Time Domain Measurements

The stresses the MOV is subjected to may alter the dielectric insulation properties of the MOV. The dielectric insulation condition of the MOV is assessed through wide range of measurements both in time and in frequency domains [19]. The commonly used methods of quantifying the dielectric response in time domain are polarisation/depolarisation currents and recovery voltage measurements (return and decay voltages).

2.7.3 Return Voltage Characteristics

Apart from the classical measurements of insulation resistance and dielectric loss factor, the return voltage method has been recognised in power and high voltage fields as one of the effective diagnostic methods of determining insulation properties [20, 21]. The return voltage method is used to assess the insulation quality of high voltage equipment used in power transmission systems (such as power transformers, cables, MOVs, instrumentation transformers, etc.) through determining the return voltage characteristics, such as the maximum return voltage, the slope, and the time it takes to reach a peak [22 – 24].

The classical methods often do not give enough information for evaluating the insulation condition [21]. However, the use of return voltage method provides more sufficient data for analysis than classical methods. The results of return voltage method clearly present the condition of insulation. Furthermore, additional characteristics such as insulation resistance, polarisation index (absorption index) and loss factor, can be extrapolated from the measurements of diagnostic methods.

Return Voltage Measurements (RVM) are normally used in the diagnosis of insulating materials (such as cables, MOVs, etc.) and devices (such as transformer). Since a MOV behaves as an insulator during normal conditions (at voltages below MCOV), the effect of return voltage can be used to monitor the degradation of the varistor. The return voltage is based on charging and discharging of grain boundaries and space charge effect. Furthermore, it focuses on the polarisation and subsequent depolarisation of dipoles within insulating materials.

The basic principles of return voltage measurements comprise of three steps which are summarised below [1, 3, 25-27]. Figure 8 depicts the steps and typical wave shape of RVM.

(i) Charge the MOV for a pre-selected time (t_c) with a DC voltage which is much lower than the varistor's rated voltage.

(ii) Discharge the MOV for a short period of time (normally half of the charging time, $t_d = ½t_c$).

(iii) Measure the open circuit voltage build up across the MOV, which is known as the Return Voltage. Central Time Constant (ctc) indicates the time it takes to reach peak of the return voltage after discharging.

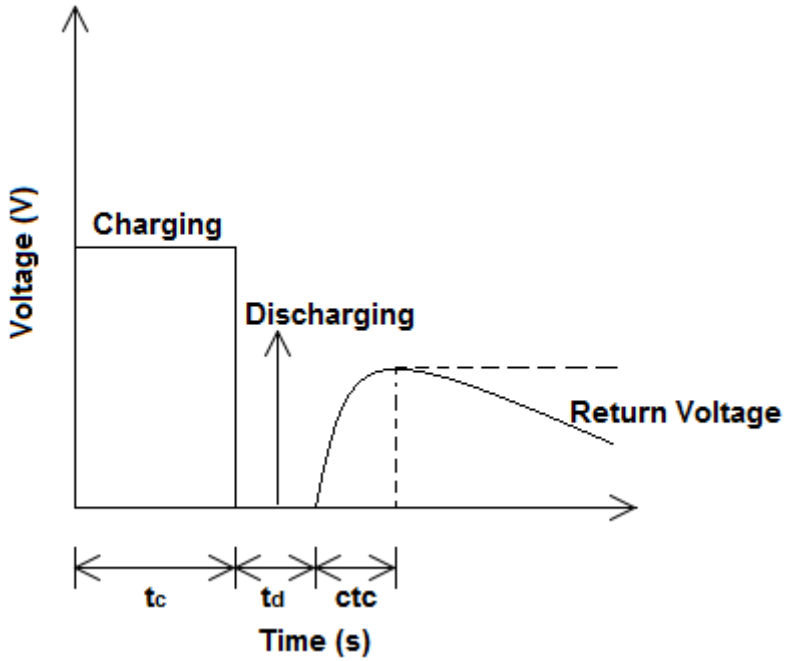

Figure 8: Typical Return Voltage Wave shape. Adapted from [3].

Rapid temperature increase is one of the indication of degradation of insulation; the increase in temperature in the MOV caused by the inability of the MOV to cool down the temperature when subjected to surges results in thermal runaway, which subsequently fails the MOV. The return voltage characteristics are able to determine the ageing or degradation of the insulator (MOV) influenced by the change in temperature. The effect of temperature causes the displacement of the polarisation maximum return voltage [20]. At high temperatures the return voltage spectrum shifts to short charging times, and at low temperatures the maximum return voltage decreases. The return voltage (RV) characteristics yield an exponential response depending on the temperature. Equation 3 describes the temperature dependence of the RV spectrum [20].

$$t_{c\ at\ T_2} = t_{c\ at\ T_1} \times \exp(-a \times \Delta T) \quad (3)$$

Where:

$t_{c\ at\ T_1}$ = charging time corresponding to maximum return voltage at temperature T_1

$t_{c\ at\ T_2}$ = new shifted value of charging time corresponding to maximum return voltage at temperature T_2

ΔT = temperature difference ($\Delta T = T_2 - T_1$)

a = constant relative to the polarisation process of an insulation material

Slope spectrum: At high temperatures a good insulation equipment can be regarded as inadequate because of the influence of temperature which can affect the accuracy or polarisation process of material/equipment. However, the temperature influence on the return voltage measurements can be disregarded if the slope of the return voltages is plotted or compared against relaxation peak time (i.e. the time it takes to reach maximum return voltage). This allows the observation of the actual condition of the insulation material or equipment regardless of the surrounding temperature the measurements.

Realisation of Return Voltage characteristics through insulation Equivalent circuit: The RV characteristics can be deduced from the change of the insulation or MOV's parameters described in the equivalent circuit diagram. Figure 9 shows the equivalent circuit diagram of insulation which is used to describe the distribution function and the correlation of polarization index with return voltage characteristics [21]. The equivalent circuit diagram(s) of the MOV, which will be discussed in ***Section 2.8***, is different from the insulation equivalent circuit diagrams. However, under the non-conductive state of the MOV, the MOV is regarded as an insulator, and therefore, during that state the equivalent circuit diagram of the insulator is assumed to also hold for the MOV.

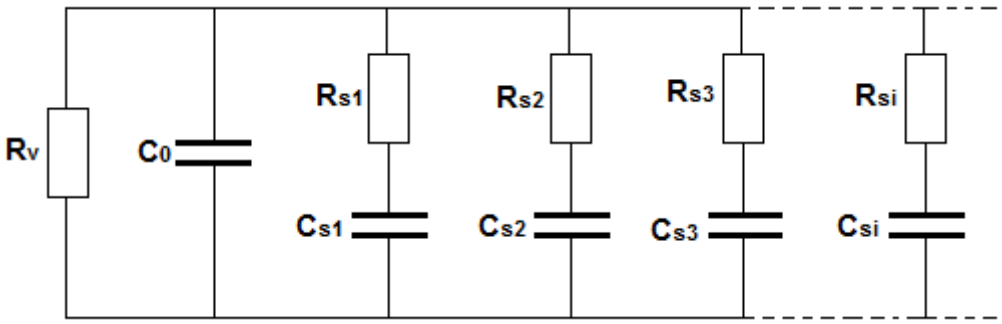

Figure 9: Equivalent circuit of insulation. Adapted from [21].

The return voltage characteristics of the insulator are better described using the equivalent circuit in Figure 4 with the following equations describing the relaxation processes [21, 28, 29].

$$\tau = R_s \cdot C_s \tag{4}$$

$$T_v = R_v \cdot C_0 \tag{5}$$

$$T_r = R_v \cdot C_s \tag{6}$$

$$T_g = R_s \cdot C_0 \tag{7}$$

$$T_s = \tau + T_v + T_r \tag{8}$$

$$T_Q = \sqrt{T_s^2 - (4 \cdot \tau \cdot T_v)} \tag{9}$$

$$T_L = \frac{2 \cdot \tau \cdot T_v}{T_s - T_Q} \tag{10}$$

$$T_K = \frac{2 \cdot \tau \cdot T_v}{T_s + T_Q} \tag{11}$$

Where:

T_L = time constant that characterizes the slope of return voltage

T_K = time constant that characterizes the time to maximum of return voltage

The return voltage characteristics are defined by the following equations [21]:

$$t_d \to t \qquad U_r(t) = U_s \cdot \frac{T_r}{T_Q}\left(e^{-\frac{t}{T_L}} - e^{-\frac{t}{T_K}}\right) \tag{12}$$

$$t_{peak} = \ln\left(\frac{T_s + T_Q}{T_s - T_Q}\right) \cdot \frac{\tau \cdot T_v}{T_Q} \tag{13}$$

$$S_r = \frac{U_C}{T_g}\left(e^{-\frac{t_d}{\tau}} - e^{-\frac{t_c + t_d}{\tau}}\right) \tag{14}$$

$$U_{max}(t_c) = U_C \cdot \left(e^{-\frac{t_d}{\tau}} - e^{-\frac{t_c + t_d}{\tau}}\right) \cdot \frac{T_r}{\sqrt{\tau \cdot T_v}} \cdot e^{-\frac{T_s}{\sqrt{2\tau \cdot T_v}} \cdot t_{peak}} \tag{15}$$

Where:

t_c = charging time

t_d = discharging time

t_{peak} = time it takes to reach maximum return voltage

U_C = charging voltage

U_s = voltage on C_s capacitance which remains after the charge time (t_c) and discharge time (t_d)

S_r = initial slope of return voltage

$U_{max}(t_c)$ = maximum return voltage

Conductivity changes: The change of insulation conductivity can be observed from two return voltage characteristics, namely: return voltage spectrum and relaxation time spectrum (time to reach peak). An increase of insulation resistance (conductivity) is expected to be observed through a decrease of return voltage spectrum and relaxation time spectrum from the reference spectra of return voltage and relaxation time respectively. The larger the spectrum decrease from the reference spectrum, the stronger the increase of insulation conductivity.

Effect of polarization resistance on conductivity resistance: The insulation resistance R_v is directly, but non-linearly proportional to the return voltage if polarization resistance is constant. However, this phenomena disappears at high values of insulation resistance, over 10^{12} Ω [21].

Change of polarization resistance: The dielectric processes of insulation are the conjunction of dielectric phenomena. Polarization spectra measurements describe the conductivity and polarization as the response of insulation, and these processes are to be separated by the analysis of obtained characteristics [21].

The change of polarization resistance can be analysed through two assumptions: Firstly, the product of the polarization resistance R_s and capacitance C_s is constant; secondly, the polarization capacitance C_s is constant, but the change of polarization resistance influences the product of R_s and C_s [21]. The increase of conductivity and the decrease of polarisation resistance are closely related with the ageing processes of insulation [21]. The changes of these dielectric phenomena can be observed through the analysis of return voltage characteristics.

Slope: Only polarization resistance R_s influences slope characteristic of return voltage. The slope is inversely, but non-linearly proportional to the polarisation resistance; i.e. the slope decreases with an increase of polarization resistance, and this is a logarithmic dependence [21]. The polarisation resistance increases through an increase in charging time.

The slope characteristic is also proportional to the geometrical capacitance of insulation. If the insulation capacitance is high, a higher slope spectrum should be expected.

Time to peak: The time to peak is proportional to both insulation and polarization resistances; i.e. the higher the resistance of the polarization process of the insulation, the longer time it takes for the return voltage to reach peak value.

However, the decrease of both resistances leads to the smoothing of relaxation times irrespective of charging times. This is likely to be observed on insulation with unsatisfactory dielectric properties [21].

The time to peak spectrum of unaged insulation should appear as points on the flat part of the spectrum that are parallel to the horizontal plane, i.e. charge time. Whereas with ageing insulation the points will move to the decline part of the figure.

Return voltage saturation: The saturation value of return voltage is only dependent on the charge voltage. There are two primary factors which cause saturation of return voltage, namely: the longer charge time and the higher resistances (R_s and R_v).

Polarization index: The polarization index is mostly influenced by the changes of insulation resistance than polarization resistances. The higher the insulation resistance, the higher the polarization index. Polarization index increases if the polarization resistance becomes smaller.

It is trivial to prove that, if polarization resistance decreases, the dielectric properties of insulation decline – this is through time to peak, slope of return voltage and the loss of dielectric increase.

2.7.4 Decay Voltage

Decay voltage diagnostic technique is also used to monitor the condition of an insulating material. The primary objective of the decay voltage measurement is to investigate the Ohmic conductivity of insulating materials. The decay voltage method is conducted by exciting the MOV with a DC charging voltage (U_{dc}) less than the MCOV for a pre-selected charging time (t_c), and thereafter, removing the DC voltage supply and measuring the decay voltage (U_d) for longer period t_{dec} (approximately 5 times the charging period, i.e. $t_{dec} = 5t_c$). When the voltage of a MOV decays, it discharges through the internal resistance of the MOV [3, 30], hence the significance of determining the Ohmic conductivity. Figure 10 shows a typical graphical representation of decay voltage curve.

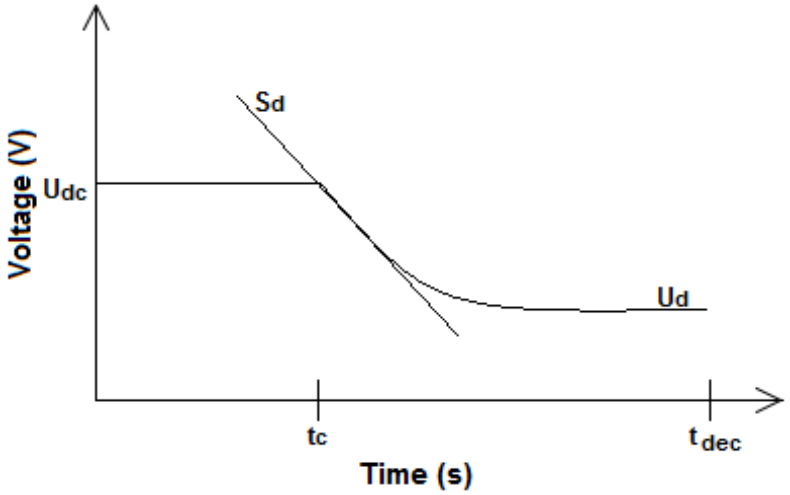

Figure 10: Decay Voltage Curve. Adapted from [3].

The decay voltage is usually measured after several hundred seconds, and at this time the polarisation process is excited by U_{dc} [3]. The steepness S_d of the initial tangent of the decay voltage is directly proportional to MOV's specific conductivity γ [3, 30, 31]. Equation 16 [3] shows the relationship between the steepness of the initial tangent of the field stress curve S'_d and specific (Ohmic) conductivity γ of a MOV.

$$S'_d = \left[\frac{dU}{dt}\right]_{t=0} = \gamma \frac{E_0}{\varepsilon_0} \tag{16}$$

Where:

E_0 = electric field strength during the charging period

γ = specific conductivity of insulation

ε_0 = permittivity of free space

Equation 17 [3] shows the expression for determining the Ohmic conductivity of the MOV with the steepness of the initial tangent extracted from the decay voltage curve. Either the specific conductivity or the steepness can be used as a quantity to describe the condition of the MOV.

$$\gamma = \frac{\varepsilon_0 S_d}{U_C} \tag{17}$$

2.7.5 Polarisation/Depolarisation current

This method is used to quantify the dielectric response of the insulating materials by monitoring the polarisation development in time when DC voltage is applied [3]. The polarisation process can be observed by measuring current through MOV; this polarisation current is proportional to the intensity of the electric field.

When the DC voltage source is removed, a reversed polarity current known as the depolarisation current is obtained [3]. Figure 11 shows a typical polarisation/depolarisation current curves. Polarisation current is measured while charging the MOV with DC voltage, and the depolarisation current is measured while discharging, when the DC voltage source is removed.

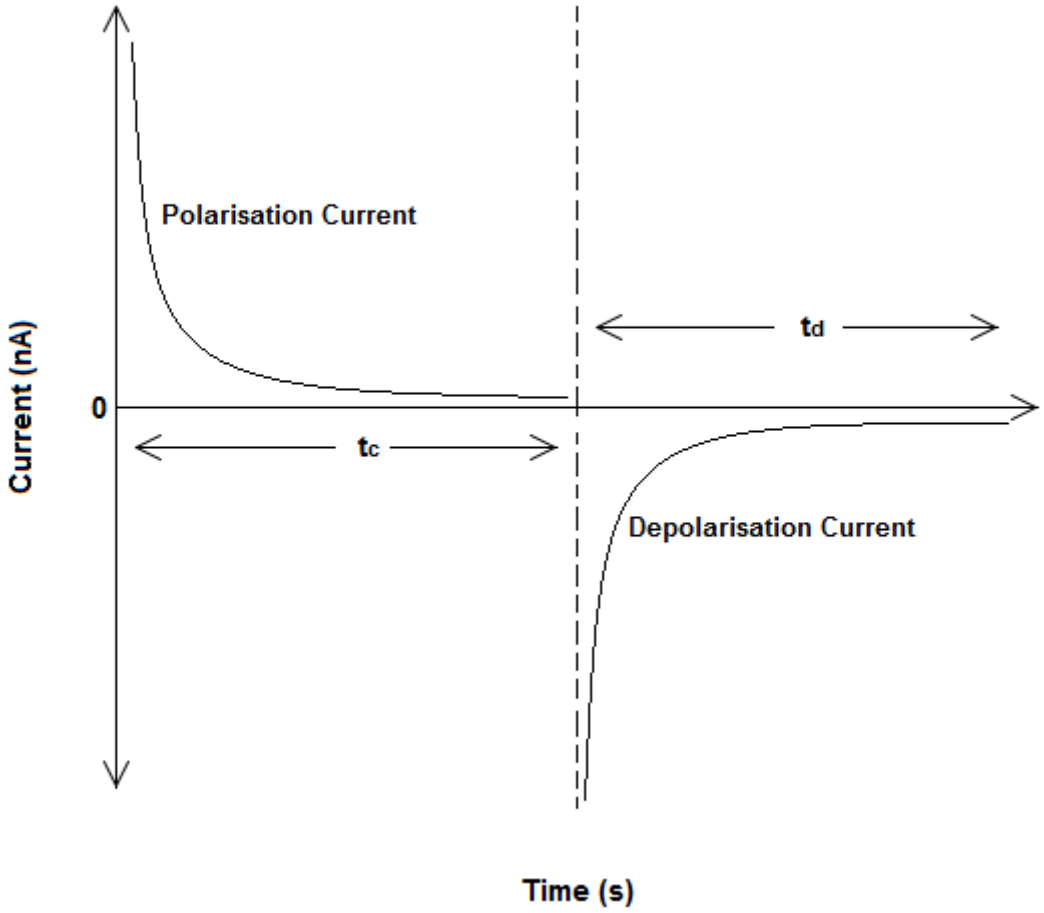

Figure 11: Polarisation/Depolarisation current curves. Adapted from [3].

If an electric field *E(t)* is applied on a dielectric material both the "free" and "bond" charges will lead to sources inside the material in a form of charge and current densities, which will eventually lead to a magnetic field B as defined by Maxwell's equations [19]. Therefore, the total current density *J(t)* through a dielectric material in an electric field *E(t)* is given by Equation 18 [19]:

$$J(t) = \sigma_0 E(t) + \varepsilon_0 \frac{\partial}{\partial t}\left\{\varepsilon_r E(t) + \int_0^t f(\tau)E(t-\tau)d\tau\right\} \quad (18)$$

Where:

σ_0 = DC conductivity

ε_r = relative permittivity of the insulation

f(t) = decaying response function which characterises the behaviour of dielectric material

E(t) = electric field caused by externally applied voltage on the insulation

J(t) = total current density through dielectric material

If a step voltage is applied on an insulation test object at time $t = 0$, with an assumption that the object is completely discharged, then the polarisation current (I_{pol}) is expressed by Equation 19 [19].

$$I_{pol}(t) = U_c C_0 \left[\frac{\sigma_0}{\varepsilon_0} + f(t)\right] \tag{19}$$

Where:

U_c = external applied voltage

C_0 = geometric or vacuum capacitance of the dielectric material

The first term from Equation 19 is related to the intrinsic conductivity of the insulation and is independent of any polarisation process; whereas the last term represents all the activated polarization processes during the voltage application [14].

Polarisation current is made up of two parts, namely: the conductivity of the material, and the activation of polarisation processes within the material which is characterised by response function. Therefore, when the external voltage (i.e. step voltage) is removed after charging time (t_c), and the test object is immediately discharged by short circuiting it to ground, and then the depolarisation current (I_{depol}) flows. Equation 20 shows the expression of depolarisation current [14, 19]. Depolarisation current represent the relaxation of polarisation processes. The sudden reduction of the voltage U_c or U_0 is regarded as a negative voltage step at time $t = t_c$ [14].

$$I_{depol}(t) = -U_c C_0 [f(t) - f(t + t_c)] \tag{20}$$

A general expression for dielectric response function is given by Equation 21 [32].

$$f(t) = \frac{A}{\left(\frac{t}{t_0}\right)^n + \left(\frac{t}{t_0}\right)^{m+1}} \tag{21}$$

Where:

f(t) = decaying response function

t = charging time

t_0 = discharging time

A, m & n = parameters obtained from curve fitting to describe polarisation effect

Discharging currents are used to determine the response function of insulation. In order to determine the dielectric response function *f(t),* the insulation must be charged for at least 10 times longer than the duration of the discharging current(s) prior to the beginning of discharging process [33]. The response function *f(t)* of the insulating material is a monotonically decaying function [19]. Therefore, for large values of charging period (t_c), the second term from Equation 20 can be neglected (i.e $f(t + t_c) \approx 0$), which result in the depolarisation current being proportional to the dielectric response function. Thus, the dielectric response function is described by Equation 22 [19, 32, 33].

$$f(t) \approx -\frac{I_{depol}(t)}{U_0 C_0} \tag{22}$$

The difference between the charging and discharging currents is used to determine the DC conductivity (σ) of the insulation as given in Equation 23 [19, 32].

$$\sigma = \frac{\varepsilon_0}{U_0 C_0} \cdot \left(I_{pol}(t) - I_{depol}(t)\right) \tag{23}$$

The crossover of the charging and discharging currents may indicate charge injection processes or memory effects of previous charging and discharging processes [32]. This may be caused by not discharging the insulation completely, thus the residual charges from polarisation processes result in inaccurate measurements.

2.7.6 Frequency Domain Measurements

In a frequency domain the dielectric response of the MOV is commonly assessed through the loss factor (*tan δ*) and complex capacitance measurements. When an AC voltage of pulsation ω is applied to an insulation material, the polarisation processes become instantaneous, the Fourier transform *F(ω)* of the dielectric response function *f(t),* and the complex susceptibility $X_e(\omega)$ are described by Equations 24 – 26 [14].

$$F(\omega) = X_e = \int_0^\infty f(t) e^{-i\omega t} dt = X_e'(\omega) - X_e''(\omega) \tag{24}$$

$$X_e'(\omega) = \int_0^\infty f(t) \cos(\omega t) dt \tag{25}$$

$$X_e''(\omega) = \int_0^\infty f(t)\sin(\omega t)dt \quad (26)$$

Where:

$X_e'(\omega)$ = represents the real part of complex electric susceptibility

$X_e''(\omega)$ = represents the imaginary part of complex electric susceptibility

Therefore, from Equations 25 and 26 the loss factor ($tan\ \delta$) of the dielectric material can be determined as described in Equation 27 [14]. The dielectric response function under frequency domain can be determined as described in Equation 28 [14] if the electric susceptibility is known. Electric susceptibility X_e is a dimensionless constant that indicate the degree of polarisation of a dielectric material in response to an applied electric field [34-36]. The electric susceptibility in relation to dielectric polarisation density and electric field is given by Equation 29 [34, 35].

$$tan\ \delta = \frac{X_e''(\omega)+\frac{\sigma}{\varepsilon_0\omega}}{1+X_e'(\omega)} \quad (27)$$

$$f(t) = \frac{2}{\pi}\int_0^\infty X_e'(\omega)\cos(\omega t)dt \quad (28)$$

$$P = \varepsilon_0 X_e E \quad (29)$$

Where:

P = dielectric polarisation density

ε_0 = electric permittivity of free space

X_e = electric susceptibility

E = electric field

The relationship between the electric susceptibility and the relative permittivity ε_r of a material is given by Equation 30 [34].

$$X_e = \varepsilon_r - 1 \quad (30)$$

The loss factor ($tan\ \delta$) includes the effect of both dielectric loss and conductivity as described in Equation 27. However, the loss factor can also be determined using both the real and imaginary parts of relative permittivity of the dielectric as descried in Equation 31 [37]. The real part of permittivity (ε_r') is a measure of how energy from external electric field is stored

in a material, and the imaginary part of permittivity (ε_r'') is a measure of how dissipative or lossy a material is to an external electric field [37]. The imaginary part of permittivity (ε_r'') is always greater than zero and is usually much smaller than the real part of permittivity (ε_r').

$$tan\ \delta = \frac{\varepsilon_r''}{\varepsilon_r'} = D = \frac{1}{Q} \tag{31}$$

Where:

D = dissipation factor

Q = quality factor

The commonly used degradation diagnostic techniques and methods both in time and frequency domain were discussed in this section. The next section discusses the existing models that describe the performance and characteristics of the varistor. The next section further outlines the knowledge gap in the existing varistor models.

2.8 Existing Varistor Models

There are several types of numerical models used to describe the performance of a metal oxide varistor when it is subjected to fast transient impulses [38-41]. Primarily, these models describe the wave shapes of the voltage across-, and the current through-, the MOV when it is subjected to transients. The numerical models of the MOV are derived from the electrical models thereof [38]. The electrical models of the MOV consist of a non-linear resistance(s) with inductance and capacitance. The use of these elementary components on the model influences the frequency range of operation of the model when compared to a performance of a MOV [38]. Non-linear resistances and inductances are normally used to improve the model to match the performance of real MOV.

Since MOVs are sometimes used in complex protection circuits where they are integrated with other protection devices, therefore, coordination between these protection devices is of paramount. Proper coordination ensures that these protection devices handle the surge energies efficiently and effectively while remaining intact and protecting the relevant equipment [42]. Improper coordination may result in misalignment between the protection devices which may result in large or low Maximum Continuous Operating Voltage (MCOV) which may lead to malfunction and/or inefficient operation of the equipment/system protected. Therefore, the

models are used to simulate the integration between the protection devices in order to achieve proper coordination between them.

The voltage-current characteristics of the ZnO varistor have three distinctive regions, namely: pre-breakdown region, breakdown region, and upturn region [43]. The breakdown (or Ohmic region) occurs at low voltages where the insulating barriers between the ZnO grains result in a very high and almost Ohmic resistivity [43]. The breakdown region occurs at threshold or breakdown voltages where the current increases abruptly relative to voltage, and their relation is described by Equation 1 ($I = kV^{\alpha}$). The degree of non-linearity α in the breakdown region is described by Equation 32.

$$\alpha = \frac{\Delta \log(I)}{\Delta \log(V)} \tag{32}$$

The upturn region occurs at high current densities where voltage increases rapidly. The increase of voltage gradually becomes linear with current where it exhibits Ohmic behaviour and is associated with the resistivity of the ZnO grains.

2.8.1 Simplified varistor model

This model is simply based on the combination of resistance, inductance and capacitance, where the resistance and inductance represent the characteristics of the conducting leads of the varistor, and the capacitance represents the properties of the device package and ZnO material [38, 44]. These elementary components are connected to a variable resistor which therefore represents the characteristics of the non-linearity of the varistor. The circuit diagram of this model is shown in Figure 12. Equation 33 [45] shows the interpolation formula of this model for V-I characteristics of the varistor.

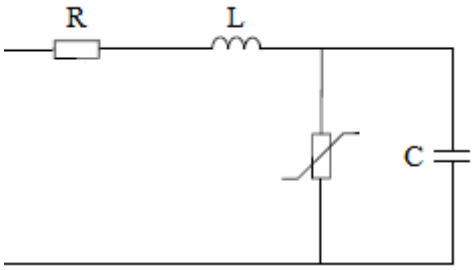

Figure 12: Simplified varistor model. Adapted from [45].

$$\log(u) = b_1 + b_2 \cdot \log(i) + b_3 \cdot e^{-\log(i)} + b_4 \cdot e^{\log(i)} \tag{33}$$

Where:

u = voltage across the varistor

i = current flowing through the varistor

b_1, b_2, b_3, & b_4 = parameters obtained from the manufacturer and are unique for each varistor type.

2.8.2 Durbak's varistor model

The Durbak's varistor model is a widely used model in the literature for transient analysis of varistor and is highly recommended by IEEE working group [41]. This model is sometimes referred to as the IEEE Frequency-dependant varistor model, however, it is commonly referred to as Durbak's model named after Daniel Durbak who originally presented it [38, 46]. The equivalent circuit diagram of this model is shown in Figure 13. In this model, the non-linear characteristics are presented by two varistor branches (A_0 and A_1) separated by a parallel combination of resistor (R_1) and inductor (L_1) which are responsible for fast front signals. The V-I characteristics of the two non-linear components can be determined through the use of ratio $\gamma = {}^{I_0}/_{I_1}$ which must be approximately 0.02 [47]. This ratio γ determines the value of the inductance L_1 which influences the frequency response of the modelled varistor. The V-I curves of A_0 and A_1 can be fitted using Equation 34 [38].

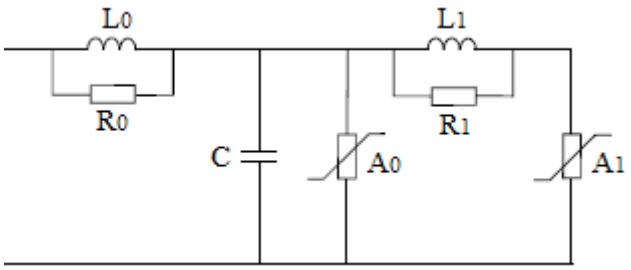

Figure 13: Durbak's Varistor Model. Adapted from [41].

$$U = kb^I I^c \tag{34}$$

Where:

U = voltage across the varistor

I = current through the varistor

k, b, & c = coefficients obtained from fitting of the curves given by the IEEE working groups

2.8.3 Knowledge Gaps for Degradation model

The existing varistor models (simplified varistor model, Durbak's model and standard V-I model – equation 1) simulate the V-I characteristics of a varistor when it is subjected to lightning and switching surges. However, they do not describe the degradation and the expected life span of the varistor when it subjected to those surges. The Arrhenius model (in ***Section 2.3***) is a model which gives an indication of the time when the varistor reaches thermal runaway, which is regarded as failure. However, it does not take into account the history of surge exposure of the varistor nor the lightning impulse current applied. Furthermore, the Arrhenius model requires physical measurements of the varistor's parameters such as temperature and applied voltage. Thus, it is evident that the existing models do not provide an indication on how the varistor, especially a MOV, degrade with respect to the applied single lightning impulse current. Therefore, a relationship between the lightning impulse current applied and the degradation of the MOV needs to be determined in order to accurately predict the life span of the MOV and to ensure that preventative maintenance is achieved whilst the MOV offers acceptable protection levels. The relationship should be defined with minimum varistor's measured parameters to ensure the versatility of the model without physical constraints of measurements required to minimise the dependency of the model on other parameters. Therefore, this research aims at determining the relationship between the lightning impulse current applied and the degree of degradation of the MOV. This relationship should be applicable for different magnitudes of lightning impulse currents.

The commonly used degradation diagnostic techniques and methods both in time and frequency domains were discussed in this chapter. Furthermore, this chapter discussed the existing varistor models and outlined the knowledge gap in the existing varistor models. The next chapter proposes a mathematical model that characterises the degradation of the MOV to answer the research question.

3. Proposed Degradation Model

This chapter presents the mathematical model proposed to describe a relationship between the lightning impulse current applied and the degree of degradation of the MOV. The model is primarily derived from the interpolation formula of the simplified varistor model and verified using the number of impulses given in the pulse rating curves.

3.1 Problem Analysis

Many investigations have been conducted in the past to determine the electrical degradation phenomena of a MOV after it has been exposed to various stresses. Different diagnostic and measuring techniques have been developed and implemented to provide a meaningful interpretation of the MOV's electrical degradation and ageing mechanism [1, 3, 48 - 51]. Studies on the microstructure of the MOV, especially those of grain size, grain boundary and crystalline bonding have been done extensively [52 – 54]. However, the relationship between the impulse currents injected and the degree of electrical degradation of the MOV is not clearly defined.

SPD monitors are employed to observe the operational status of SPDs, especially MOVs [55, 56]. The monitors constantly observe if the MOV's parameters, such as leakage current, reference voltage at 1 mA, internal temperature, etc. are above or below a certain threshold in order to deduce the operational status of the MOV. However, it is improbable and not always feasible to measure the parameters of every individual MOV. This is because of the limited space available and the complexity of the circuit the MOVs are connected in, especially in low voltage equipment. Furthermore, there are logistical cost related problems associated with measuring physical parameter of every individual MOVs, especially the MOVs installed on remote sites.

The life expectancy of a MOV, given on the pulse rating curves, is useful for estimating the life span of the MOV when subjected to surges of constant magnitudes. However, in reality, lightning and switching surges do not always have the same magnitudes and/or patterns as specified in the pulse rating curves. Hence, the pulse rating curves are not useful in estimating

the percentage of degradation of the MOV in order to determine whether or not the protection needs to be replaced (or reinforced) without measuring its parameters.

Therefore, it is imperative to determine the relationship between the lightning impulse current injected and the degree of degradation of the MOV in order to achieve preventative maintenance while ensuring that the lightning protection is in good state and offers acceptable protection level.

3.2 Defining a relationship between the 8/20 μs lightning impulse current and the electrical degradation of the MOV

The pulse rating curves of the varistor give an estimated life span of the varistor when it has been subjected to multiple surges of constant magnitudes. However, in reality, lightning and switching surges do not always follow the same pattern, nor yield sequential multiple impulses of same magnitudes. The lightning flash may consist multiple current surges (strokes) of different magnitudes, with the first stroke approximately three times larger than the subsequent strokes [57, 58]. Furthermore, the sequences of occurrence of surges are not always follow the same pattern. In the paper [59] submitted by the author to the IEEE International Conference on High Voltage Engineering and Application (see **Appendix A**), two sequences where considered: sequence 1 – a larger surge event, and then followed by a smaller surge event; and sequence 2 – a smaller surge event, followed by a larger surge event. It was concluded that the sequence of occurrence of surges and the surges of different magnitudes have significant effects on the degradation of the MOV. Therefore, defining a relationship between lightning impulse current injected and the degree of electrical degradation of the MOV will provide the level of degradation caused by the surges of different magnitudes and/or sequence of occurrence. This relationship can be used to give an accurate operational status of the MOV based on the level of exposure from surges of all magnitudes, including small magnitudes which are sometimes assumed to have no effects. Thus, the relationship will account for all lightning surges injected into the MOV irrespective of their magnitude, sequence of occurrence or frequency of occurrence.

The relationship is defined through proposing a mathematical model that outputs a percentage of degradation of the MOV caused by a particular lightning impulse current. The reason for proposing a mathematical model to characterise the relationship is due to versatility that comes with mathematical expressions – they can accurately model linear and non-linear relationships

if inputs and outputs are given. The expressions can then be adapted into getting a possible response out of unknown situation/behaviour. The next section proposes a mathematical model that describe the relationship between the lightning impulse current injected and the degree of electrical degradation of the MOV.

3.3 Determining the degradation characteristics of the MOV

The pulse rating curves of the MOV provides the estimated life span of the MOV through an estimate of the number of impulses the MOV can withstand when subjected to surge currents of same magnitudes and different shapes (i.e. impulse width). Figure 14 shows the pulse rating curves of the 14 mm size MOVs with the number of impulses the MOVs can withstand highlighted. Figure 14 is the manufacturer's specification of the 14 mm size MOVs; for every impulse width, starting from 20 μs, the relative impulse current value is provided with the number of impulses the MOV can withstand. Since the impulse width of a single 8/20 μs lightning impulse current is at least 20 μs, the corresponding number of impulses the MOV can withstand are only considered at 20 μs.

The model in this study is to be developed to characterise the degradation of the MOV when subjected to lightning impulse current with a current waveform rated at 8/20 μs as defined by the International standards (IEC 60-2, ANSI/IEEE Std 4-1978, and ANSI C62.1-1984) [60]. Therefore, from the pulse rating curves only the number of impulses of the surge currents at 20 μs is extracted to produce the estimated life span of the MOV when the MOV is subjected to 8/20 μs lightning impulse current. In order to match the estimated number of impulses, a ratio of the surge currents is computed instead of using the magnitude of the 8/20 μs lightning impulse current. The choice of using a computed ratio instead of the magnitude of lightning impulse is because the proposed model should be as generic as possible in order to be applicable on a variety of MOVs. Using the magnitude of the surge currents may limit the model to only work on few MOVs types of similar range of magnitudes of surge currents; however, the MOV have different ratings of surge current. Therefore, the surge current ratio is decided upon to normalise the model to accommodate a variety of MOVs of different surge current ratings. Equation 35 shows the expression used to compute the ratio for each lightning impulse current. The information about the number of impulses and the surge current ratio is then used to compute a degradation curve of a particular MOV. Figure 15 shows the plotted degradation curve of 14 mm size MOVs.

$$R_{imp} = \frac{I_{max}}{I_x} \tag{35}$$

Where:

R_{imp} = ratio of surge currents

I_{max} = maximum withstand surge current (8/20 µs) of respective MOV

I_x = surge current (8/20 µs) for which the degree of degradation is required

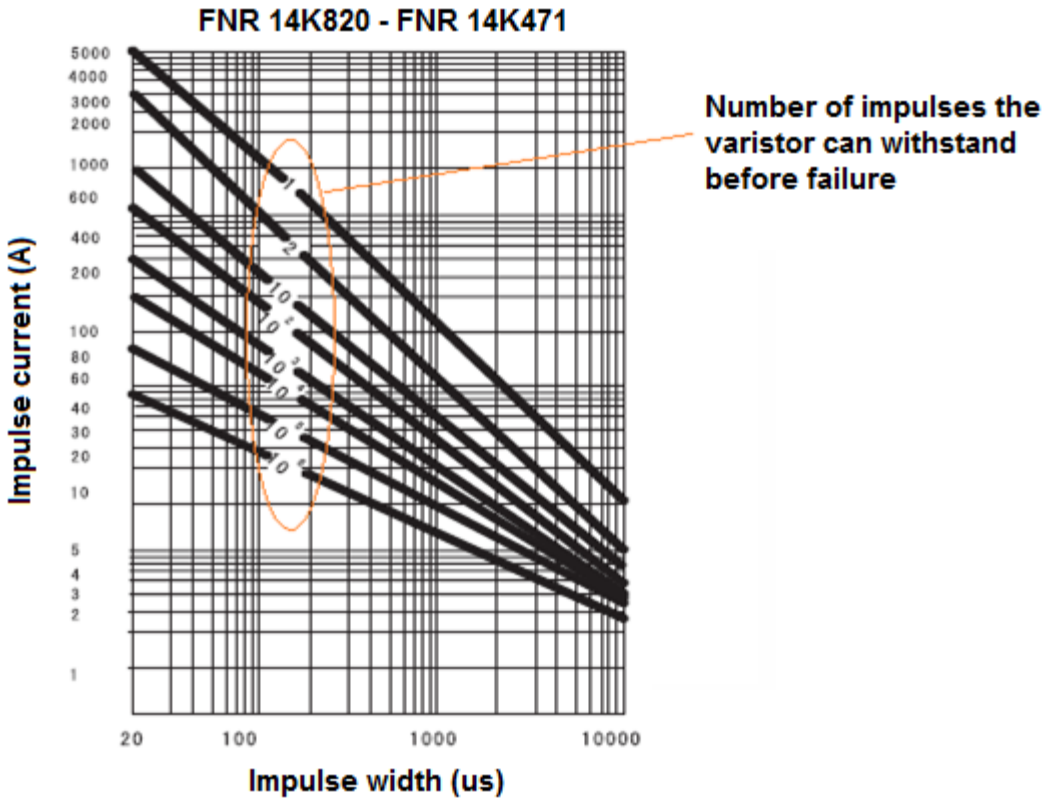

Figure 14: Pulse rating curves of 14 mm size MOVs [61].

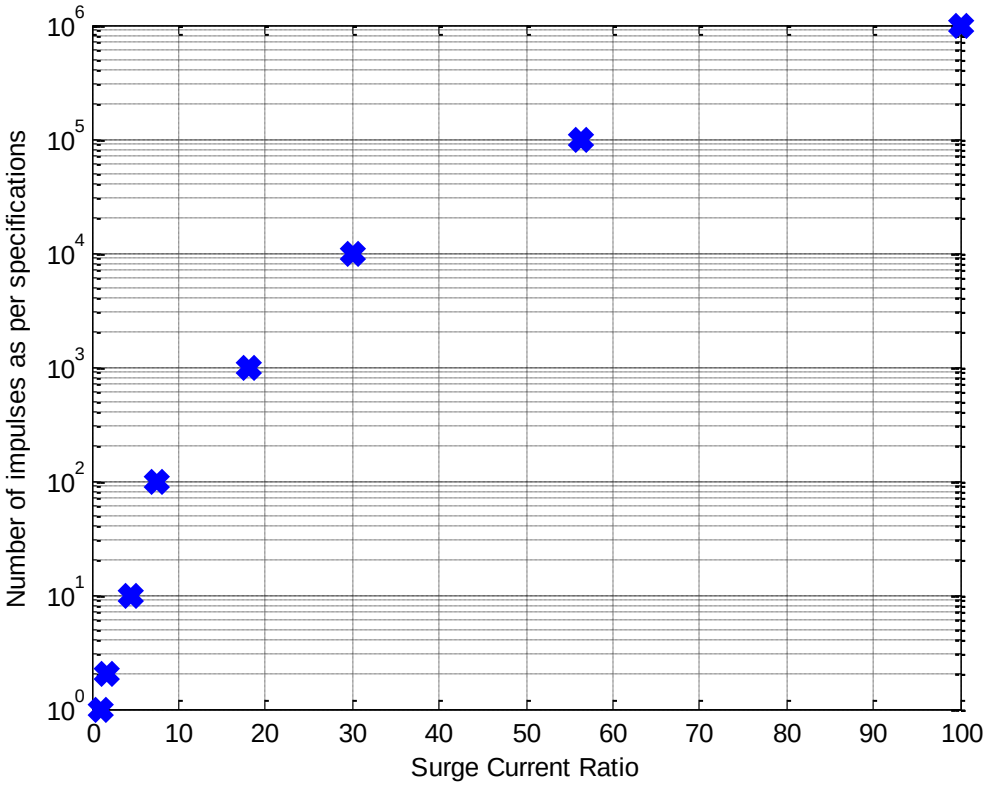

Figure 15: Degradation curve of 14 mm size MOVs.

Comparing the varistor degradation curve in Figure 15 and the varistor V-I curve shown in Figure 5, **Chapter 2** (by extracting the normal varistor operation region and the leakage region) it can be seen that both curves have similar shapes. The mathematical models of the varistor's V-I curve can therefore be used to describe the degradation curve of the MOV. The next section discusses the varistor model's interpolation formula that is suitable for the describing the degradation curve of the MOV in order to develop a degradation model.

3.4 Determining a suitable varistor model to describe the degradation characteristics of the MOV

There are several existing mathematical and electrical models, as described in **Chapter 2**, which characterise the behaviour of the MOV when subjected to lightning surges. These models mainly describe the V-I characteristics of the MOV, although the Arrhenius expression does describe the degradation of the MOV, but it does not consider the degradation caused by a single lightning impulse current and it is dependent on the measurement of the temperature of the MOV. Since one of the main objectives of this study is to minimise the dependency on

measuring physical parameters of the MOV before determining the operational status of the MOV, the Arrhenius expression is therefore not considered in developing the model.

The standard varistor model ($I = kV^{\alpha}$ as defined in equation 1) commonly used to describe the V-I characteristics of the MOV only describes the V-I relationship of the MOV at the 'normal varistor operation' (breakdown) region. The varistor exhibit an Ohmic behaviour at breakdown voltage and its V-I characteristics can be approximated using log-log scale with the expression shown in Equation 36 [62]. However, the varistor consists of three regions with the upturn region showing the response of the varistor when subjected to transients. Since the standard varistor model does not characterise the behaviour of the MOV after the breakdown region when it is subjected to transients (i.e. at the upturn region) it cannot be used to develop the degradation of the MOV when it is subjected to lightning impulse currents.

$$logI = logK + \alpha \cdot logV \tag{36}$$

The Durbak and simplified varistor models describe the V-I characteristics of a real varistor. The interpolation formula, in Equation 33, of the simplified varistor model describes the V-I characteristics of any varistor with its parameters given by the manufacturer, and the curve fitting formula, in Equation 34, of the Durbak model defines the V-I characteristics of only the two varistors given in the model as specified in the IEEE document [41]. The curve fitting formula of the Durbak model is limited to the two varistors' V-I curves given in [41] and the interpolation formula of the simplified varistor model is a generic formula of V-I characteristics of the varistor; therefore, the mathematical degradation model is to be based on the interpolation formula given in Equation 33 in ***Section 2.8.1***.

3.5 A proposed mathematical model to describe the degradation of the MOV

Since the interpolation of the simplified varistor model is found suitable to determine the degradation characteristics of the MOV, the proposed model is contextualised from the interpolation formula given in Equation 33. Comparing the V-I curve in Figure 5 and the degradation curve in Figure 15 it can be seen that the curves have similar shapes, with voltage and number of impulses being outputs and the currents and surge current ratio being inputs. Therefore, the initial degradation model is proposed by converting the interpolation in the manner that 'u' and 'i' in interpolation formula is replaced with N_{sw} and R_{imp} respectively, to get the proposed initial degradation mathematical model given in Equation 37.

$$\log(N_{sw}) = b_1 + b_2 \log\left(R_{imp}\right) + b_3 e^{-\log\left(R_{imp}\right)} + b_4 e^{\log\left(R_{imp}\right)} \quad (37)$$

Where:

N_{sw} = number of impulses

R_{imp} = ratio of surge currents

$b_1, b_2, b_3, \& \, b_4$ = parameters obtained by fitting the degradation curve

Since the number of impulses the MOV can withstand gives an indication about the degradation of the MOV caused by the applied impulse current, the N_{sw} from Equation 37 is then made a subject of the formula which results in Equation 38.

$$N_{sw} = 10^{\left(b_1 + b_2 \log\left(R_{imp}\right) + b_3 e^{-\log\left(R_{imp}\right)} + b_4 e^{\log\left(R_{imp}\right)}\right)} \quad (38)$$

Equation 38 provides an estimated number of impulses of particular magnitude of 8/20 µs current waveform the MOV can withstand. This information can be used to estimate the life span or degradation of the MOV when subjected to a single lightning impulse current.

The mathematical model is mainly proposed for MOVs with sizes ranging from 5 mm to 40 mm, which are commonly used in the low voltage equipment. These MOVs mostly encounter the challenges defined in the problem statement of this dissertation, in **Chapter 1**. Therefore, the proposed initial model, in Equation 38, was then tested on the 14 mm size MOVs as an initial point since this type of MOV is used frequently and its degradation curve is already computed as in Figure 15. The model is tested by inputting the different surge current ratios as per the pulse rating curves and then comparing the output (i.e. number of impulses N_{sw}) of the model with the number of impulses as per the pulse rating curves.

From the pulse rating curves, the number of impulses before failure ranges between 1 and 1000000 as highlighted in Figure 14. The proposed initial model was then found to accurately characterise four impulses, but not all impulses in relation to their number of impulses: it can accurately model the number of impulses either for 1 – 100 number of impulses or for 1000 – 1000000 number of impulses with maximum percentage error of below 1%. However, the proposed initial model cannot model the degradation of the MOV using number of impulses for the whole range (i.e. for 1 – 1000000 number of impulses). Table 2 shows the parameters

of the model for relevant number of impulses with maximum percentage error of below 1% relative to the pulse rating curves.

Table 2: Parameters for 14 mm size MOVs using initial degradation model defined by Equation 38.

Parameters	**For 1 – 100 number of impulses**	**For 1000 - 1000000 number for impulses**
b_1	-16.0921	-56.7103
b_2	3.5961	51.7103
b_3	10.5267	76.4057
b_4	5.5654	-6.9457

The model is intended to show the degradation of the MOV for whole range of number of impulses and lightning impulse current. Since the initial model only shows for either lower half (i.e. for 1 - 100 number of impulses) or upper half (i.e. for 1000 – 1000000 number of impulses) of the range of number of impulses it therefore requires modifications.

In order to accommodate all ranges of the number of impulses with the knowledge that the initial model can accurately model either halves of the range accurately; the initial model is extended by duplicating it for all ranges, which results in Equation 39 (modified initial degradation model). The first expression of the model in Equation 39 account for 1 - 100 number of impulses and the other expression of the model account for 1000-1000000.

$$N_{sw} = 10^{\left(b_1+b_2\log\left(R_{imp}\right)+b_3e^{-\log\left(R_{imp}\right)}+b_4e^{\log\left(R_{imp}\right)}\right)} + 10^{\left(b_5+b_6\log\left(R_{imp}\right)+b_7e^{-\log\left(R_{imp}\right)}+b_8e^{\log\left(R_{imp}\right)}\right)} \quad (39)$$

The modified initial model given by Equation 39 was tested on all MOVs (5K820 – 40K471) and it was found to accurately model most MOVs, but not all. On the other few MOVs, the model given by Equation 39 was found to accurately describe the degradation for 1 - 10000 number of impulses. However, the remaining 100000-1000000 number of impulses were modelled with a maximum error of 30% relative to the pulse rating curves. Therefore, additional parameters were added to improve the accuracy of the model and to ensure that it can model all MOVs accurately. The additional parameters were added based on the percentage error and degradation curve derived from the modified model. Furthermore, the addition of parameters was contextualised from the manner in which the standard V-I model in linear form, in Equation 36, was extended and converted into the interpolation formula of the simplified varistor model Equation 33.

During the addition of parameters into the model, it was clear that the more parameters are added the more accurate the model becomes. Therefore, the final proposed degradation model of the MOVs is given in Equation 40, and it was found to accurately model the number of impulses of all MOVs (with sizes ranging from 5 mm to 40 mm) with a maximum error of less than ±2% relative to the pulse rating curves. However, the parameters differ for each type of MOV. **Appendix B** shows the parameters of the model and the corresponding percentage error for each type of MOV. Table 3 shows the parameters of the proposed final degradation model for 14 mm size MOVs, and Table 4 shows the accuracy of the model for 14 mm size MOVs.

The parameters for all the MOVs are obtained using the **Fsolve** tool in Matlab (version 7.12.0 – R2011a) with the inputs defined as surge current ratios and outputs defined as respective specified number of impulses which were extracted from the pulse rating curves of the respective MOVs. **Appendix C** shows the Matlab code used to determine all the parameters of all the MOVs for the proposed model.

$$N_{sw} = 10^{\left(b_1+b_2\log(R_{imp})+b_3e^{-\log(R_{imp})}+b_4e^{\log(R_{imp})}+b_5e^{-2\log(R_{imp})}+b_6e^{2\log(R_{imp})}\right)} + 10^{\left(b_7+b_8\log(R_{imp})+b_9e^{-\log(R_{imp})}+b_{10}e^{\log(R_{imp})}+b_{11}e^{-2\log(R_{imp})}+b_{12}e^{2\log(R_{imp})}\right)} \quad (40)$$

Table 3: Parameters of the degradation model for 14 mm size MOVs as defined by Equation 40.

Parameters	**Values**
b_1	4.9785
b_2	31.3929
b_3	-17.0759
b_4	-12.2490
b_5	-15.5494
b_6	0.5740
b_7	-40.5783
b_8	-40.7520
b_9	21.7298
b_{10}	39.7058
b_{11}	-16.8345
b_{12}	-4.0222

Table 4: Accuracy of the proposed degradation model when compared to the degradation specified in pulse rating curves for 14 mm size MOVs.

Impulse (A)	Ratio	Number of impulses before failure as specified in pulse rating curves	Number of impulses before failure as per the proposed mathematical degradation model	Error (%)
4500	1	1	1.0014	-0.14
2500	1.8	2	1.9975	0.13
1000	4.5	10	10.0008	-0.01
600	7.5	100	100.0088	-0.01
250	18	1000	1000.3	-0.03
150	30	10000	9997	0.03
80	56.25	100000	99923	0.08
45	100	1000000	998440	0.16

Figure 16 shows the degradation curves of all the varistors simulated using the proposed final degradation model given by Equation 40 when compared to the specified reference curve (i.e. specified number of impulses as per the pulse rating curves). The x-axis of Figure 16, Term, is defined as a group of surge current ratios of different MOVs with the same number of impulses the MOVs can withstand before failure. For example, group 1 consists of different MOVs surge ratios with one number of impulses before failure; group 2 consists of different MOVs surge ratios with two number of impulses before failure; group 3 consists of different MOVs surge current ratios with ten number of impulses before failure; group 4 consists of different MOVs surge current ratios with 1000 number of impulses before failure; etc.

From Figure 16, it is apparent the model accurately matches the specified reference curve with a maximum error that is below ±2 % relative to the pulse rating curves. From these results it can be concluded that the proposed model best describes the degradation of the MOVs using the number of impulses specified in the pulse rating curves. Although, the number of impulses denote the degree of degradation the impulse causes on the MOV, the proposed final degradation model does not describe the actual percentage of degradation of the MOV caused by a particular impulse current. Therefore, the proposed final degradation model is to be modified and computed to estimate the percentage of degradation.

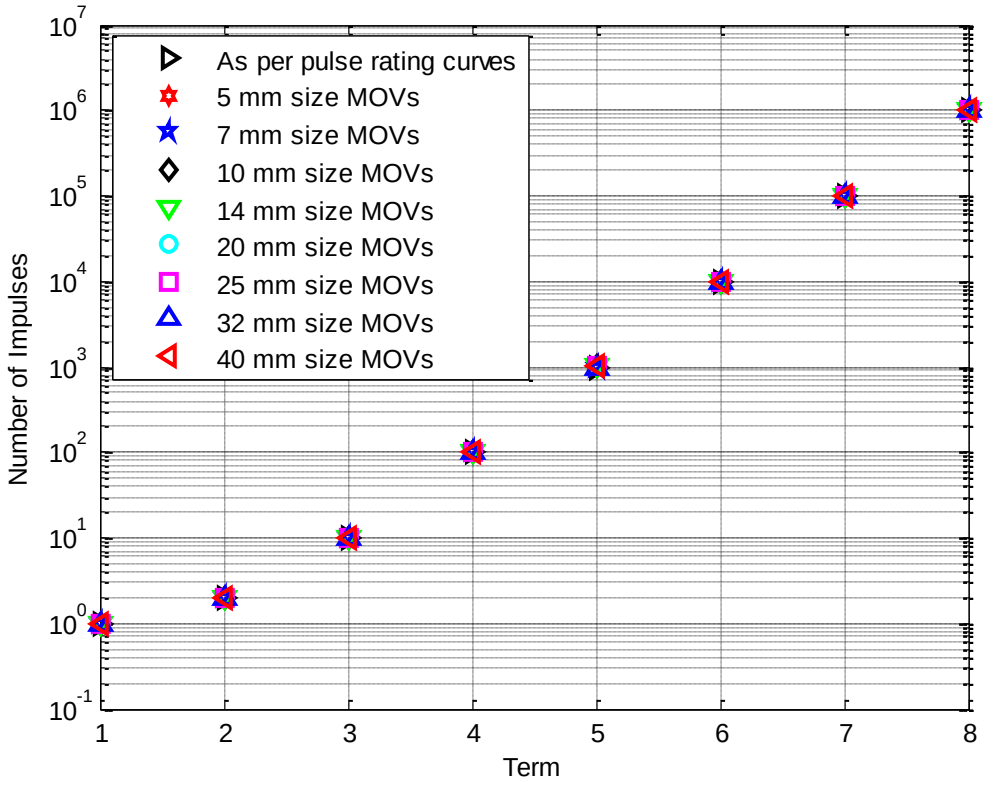

Figure 16: Degradation curves of all MOVs using proposed Model.

Computation: If the number of impulses is equal to one as per the pulse rating curve it implies that the particular surge will completely degrade the MOV (i.e. 100% degradation). Also, if the number of impulses is greater than one as per the pulse rating curve, it implies that the MOV is unlikely to fail immediately if subjected to the respective type of impulse; for example, if the number of impulses is equal to two, this implies that a strike/impulse of this type causes a 50% degradation. Since the model in Equation 40 outputs the number of impulses for a particular impulse current magnitude, the percentage of degradation of a MOV is given by a proposed degradation model described in Equation 41, where $N_{sw}$is as given in Equation 40. This degradation model has been proposed in the paper submitted by the author to South African Universities Power Engineering Conference (SAUPEC) 2017 and the paper has been accepted for oral presentation. **Appendix D** shows the paper the author submitted to SAUPEC 2017.

$$D_{imp} = \frac{1}{N_{sw}} \times 100\% \quad (41)$$

Where:

D_{imp} = percentage of degradation on the MOV caused by a particular 8/20 μs lightning impulse current

The accuracy of the proposed model is further required to be tested against experimental results to observe if it is able to provide the degradation rate of the MOV when it is subjected to surges of different magnitudes that are not specified in pulse rating curves; this will be discussed in the next Chapter.

4. Experimental Tests & Results, Model Evaluation and Discussion

This chapter discusses the test procedures and the test set ups used to conduct the experimental tests in order to validate the accuracy of the proposed degradation model. This chapter further discusses the results measured and computed during the experimental tests. The results computed using the proposed degradation model are also discussed. Thereafter, the results from both experimental tests and proposed model are compared and matched to evaluate the accuracy of the model for characterising the degree of degradation of the MOV in relation to the lightning impulse current applied.

4.1 Test set up

An impulse generator producing a lightning impulse current waveform of 8/20 μs, as defined by the international standards (IEC 62305, IEC 60-2, ANSI/IEEE Std 4-1978, and ANSI C62.1-1984), was used to inject a lightning impulse current into the MOV of type FNR 14K201. Figure 17 shows the 8/20 μs current waveform rated at approximately 5 kA which is generated by the impulse generator. The type FNR 14K201 MOV was used for testing mainly because of the availability and the frequency of it being used on the low voltage equipment/systems. Since the FNR 14K201 MOV have the same pulse rating curves as the 14 mm size MOVs, therefore, the test results of FNR 14K201 are regarded to be applicable to all 14 mm size MOVs.

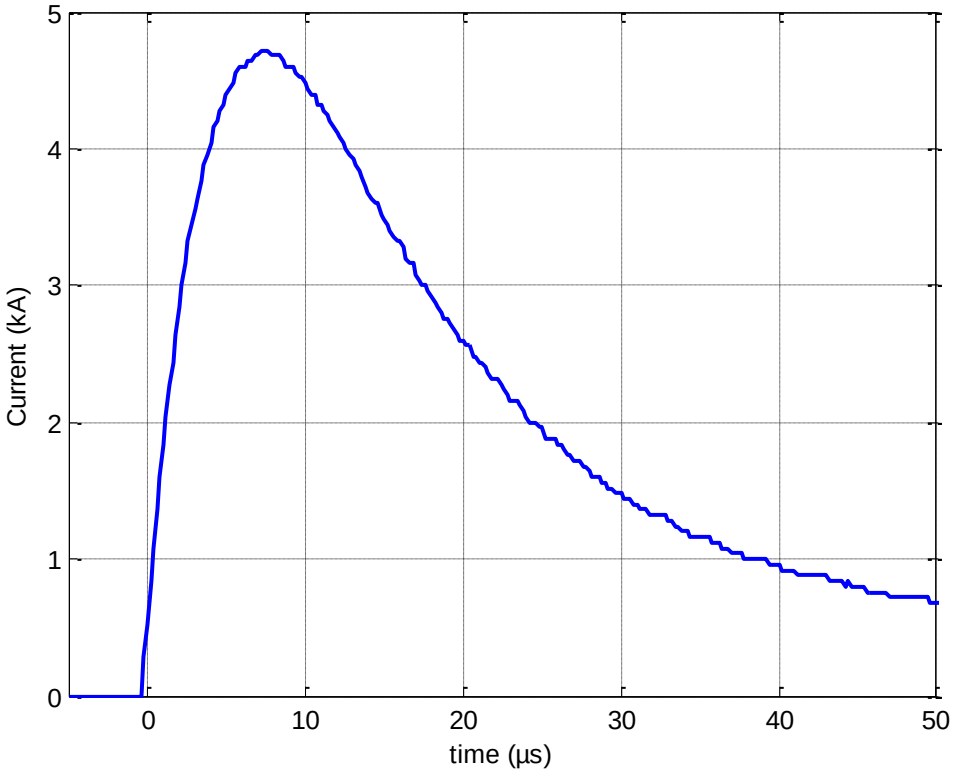

Figure 17: 8/20 µs Current waveform generated by the impulse generator.

Since the proposed degradation model is applicable to all types of MOVs with sizes ranging from 5 mm to 40 mm, it is therefore assumed that if the tests results of the 14 mm size MOVs validate the proposed model, then this would also be applicable to all the other MOVs types. This assumption is based on the versatility of the proposed model. Furthermore, it is based on the constraints of available resources to tests all the other MOVs types.

Figure 18 shows the circuit diagram of the test set up used to inject the MOV with the 8/20 μs lightning impulse current, whilst Figure 19 shows the circuit diagram of the test set ups used to excite the MOV with a DC voltage less than (or equal) the Maximum Continuous Operating Voltage (MCOV) and 1 mA d.c. in order to measure leakage current and reference voltage respectively. **Appendix E** provides a list of all components, equipment and tools used to conduct all the measurements for this study. The measured parameters were measured to gauge the degree of degradation of the MOV; the reference voltage was mainly measured to observe the pass/fail status of the MOV, and the leakage current is used to confirm the extent of degradation caused by a single lighting impulse current for matching with the proposed model. In this study the leakage current is chosen (over decay voltage, return voltage,

polarisation/depolarisation current, etc.) as a measured parameter to be used for matching/comparing the proposed model with the experimental test results since the leakage current can provide the degree of degradation of the MOV. From the literature review, where extensive tests were conducted to measure the failure of the MOV, the MOV was found to fail when the leakage current of the MOV had changed by at least 1000 %, which corresponds to 10 % change in reference voltage [4]. The other measured parameters such as decay voltage, return voltage, and polarisation current are often used as the parameters to measure the degradation of the MOV, however, the failing point somewhat differs for each varistor [3, 4].

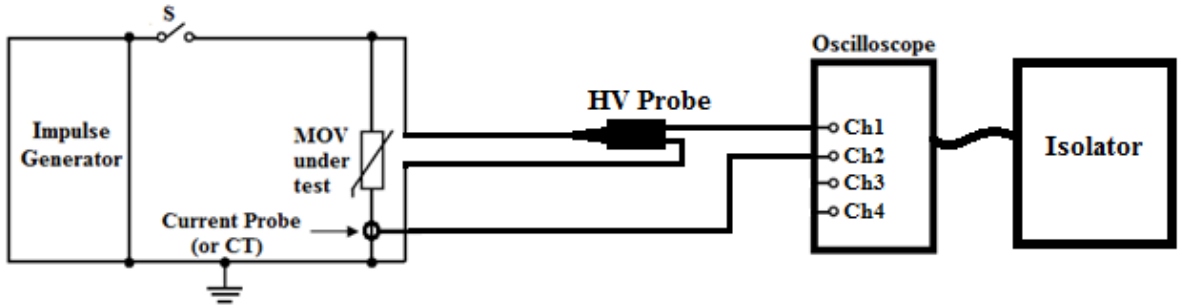

Figure 18: Lightning Impulse Current Test Circuit Diagram.

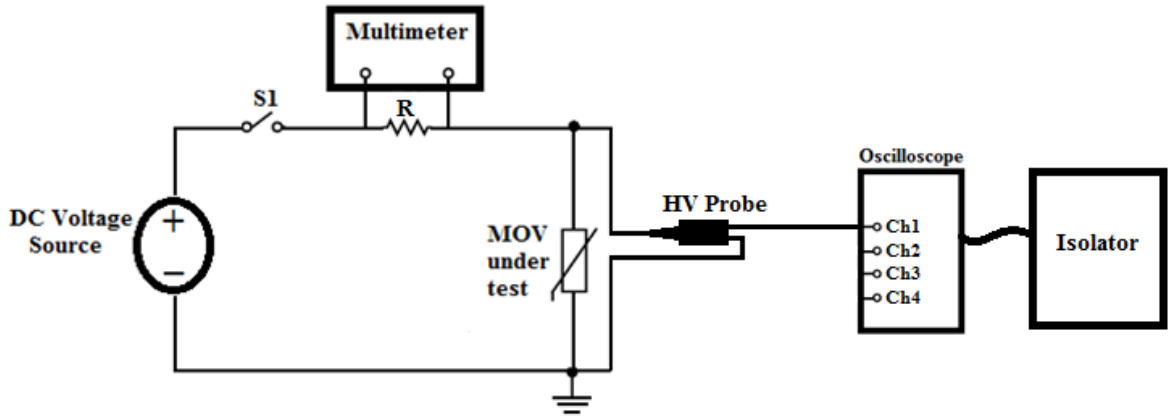

Figure 19: Leakage current and reference voltage measurements Test Circuit Diagram where R = 1 kΩ for leakage current tests and R = 1 Ω for reference voltage tests.

4.2 Test Procedure

The measurement were undertaken using 160 samples of MOV FNR 14K201 to compare the proposed degradation model against the experimental results. For each series of test, 16 samples were used. The 160 number of samples were chosen to ensure consistency between the results which subsequently ensures accuracy measurements.

In each test conducted when the MOV was subjected to single lightning impulse current, the leakage current and reference voltage was measured before and after the MOV was subjected to impulses in order to compute the percentage of change of the parameters which indicate the percentage of degradation. Figure 20 shows the flow diagram that summarises the test procedure used to conduct the tests for measurements of leakage current and reference voltage before and after the MOV was injected with impulse current.

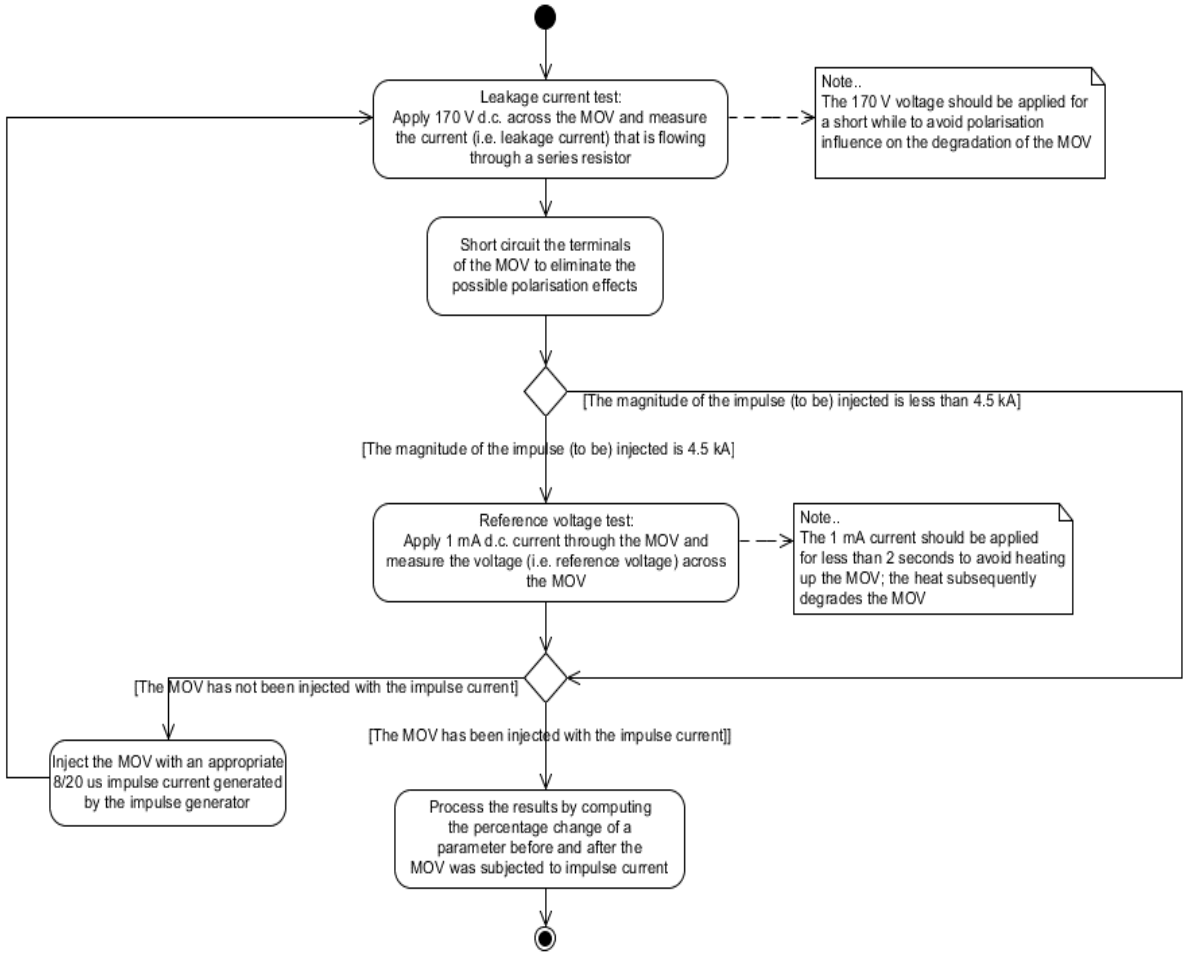

Figure 20: Test procedure flow diagram.

In order to observe the accuracy and consistency of the proposed model for all magnitudes of impulse current for a particular MOV, the MOV was injected with an 8/20 µs lightning impulse current with a magnitude ranging from 10 % of maximum withstand current (I_{max}) to 100% of I_{max}, where I_{max} = 4.5 kA. The impulse current was varied in steps of 10 % of I_{max} and for each magnitude of impulse current 16 samples were tested.

Since the reference voltage only indicates the pass/fail condition of the MOV and not the degree of degradation, the reference voltage was therefore measured only when the MOV was subjected to 4.5 kA lightning impulse current because it is a maximum withstand surge current of the MOV which has high chances of causing a failure. When the MOVs were subjected to impulse current less than 4.5 kA only the leakage current was measured.

4.3 Comparison between the operating duty test method and the test method used in this dissertation

In the test method discussed and used in this dissertation, the SPD, specifically the MOV, is subjected to a single lightning current impulse of positive polarity and thereafter, the leakage current and reference voltage of the MOV under test are measured in order to determine the extent of degradation of the MOV. Each time a single lightning current impulse with a peak value below or equal to the rated MOV I_{max} is applied, the degree of degradation corresponding to the applied impulse on the MOV is determined. Furthermore, with this test method, the MOV under test is not subjected to service conditions hence the follow current rating of the MOV is not considered in these tests.

On the other hand, the operating duty test method is based on subjecting the SPD to service conditions and to groups of current impulses. The tests in the method are performed to determine the capability of the SPD to withstand the specified discharge currents whilst it is subjected to service conditions. The follow current rating of the SPD is considered for configuring the power frequency voltage source. The pass criteria for SPDs under the operating duty test method includes: the thermal stability; absence of puncture or flashover; measured limit voltage is below or equal to U_P; absence of flashovers or puncture on the external and internal SPD disconnectors; acceptable leakage currents; maintaining the degree of protection (IP-code) of the SPD; etc.

Furthermore, in the operating duty test method, leakage current is measured by computing the resistive component of the current flowing through the SPD when it is connected to a power supply at reference test voltage U_{REF}. However, in the dissertation test method, the leakage current is measured as the current flowing through the SPD when it is connected to its rated d.c. maximum continuous operating voltage as stipulated by the manufacturer.

In conclusion, the operating duty test forms part of SPD type tests; which implies that it evaluates the conformity of the SPD to the manufacturer's specifications and specific requirements instead of the degree of degradation. However, the main purpose of this study is

to determine the degree of degradation of the SPD, specifically MOV, when it is subjected to a single lightning current impulse, hence the operating duty test method was not used.

The next section discusses the results measured and computed during the experimental tests. The results computed using the proposed degradation model are also discussed.

4.4 Experimental test results

As mentioned in previous section, the tests were done on 160 samples of MOV FNR 14K201 (rated at 4.5 kA) and for each test, the leakage current (and reference voltage – only when 4.5 kA was injected) was measured before and after the MOV was subjected to lightning impulse current. Table 5 and 6 respectively show the results of reference voltage and leakage current of the MOV for when it was subjected to 4.5 kA. The results of leakage currents for when all the MOVs were subjected to different magnitudes of impulse current are shown in **Appendix F**.

Table 5: MOV measured reference voltage when 4.5 kA is applied.

Sample number	**Before(V)**	**After(V)**	**%change**
1	215.8	188.1	12.84
2	197.1	160	18.82
3	205.1	170	17.11
4	205.3	182.3	11.20
5	204.9	176.5	13.86
6	208	195.5	6.01
7	198	171	13.64
8	200.3	180	10.14
9	199.3	169	15.20
10	204.1	178.9	12.35
11	197.1	177	10.20
12	205.1	187.7	8.48
13	195.6	160	18.20
14	199.8	180.3	9.76
15	202.7	179	11.69
16	201.7	169.8	15.82

Table 6: MOV measured leakage current when 4.5 kA is applied.

Sample number	Before(uA)	After(uA)	%change
1	5	70	-1300
2	1.6	75.5	-4618.75
3	4.1	48.5	-1082.93
4	3.3	71	-2051.52
5	3.8	42.6	-1021.05
6	8.8	56	-536.36
7	2.1	79.9	-3704.76
8	2.9	74.7	-2475.86
9	4.2	74	-1661.9
10	25	740	-2860
11	3.7	73.9	-1897.3
12	7.2	60	-733.33
13	11.5	742	-6352.17
14	2.5	26.7	-968
15	1.9	22.6	-1089.47
16	3.3	53.9	-1533.33

Comparing the results of the leakage current and reference voltage it can be seen that the MOV fails when the reference voltage changed by at least 10 %, which corresponds to at least 1000 % change in leakage current. This is also evident in the studies done by Bassi, 2016 [4].

4.5 Computed results of the proposed model

The percentage of degradation that can be caused by a particular magnitude of impulse current was computed using the proposed degradation model in Equation 41. The same magnitudes of lightning impulse currents used during experimental tests were also used in the model to compute the degree of degradation they each cause.

The percentage of degradation is used to determine the minimum expected percentage change of leakage current which indicate a degradation level that corresponds to the stipulated percentage degradation. Since 1000 % is the minimum percentage change of leakage current to indicate the MOV failure (which correspond to 10 % change in reference voltage), therefore, to determine the minimum expected leakage current for a respective magnitude of impulse, the 1000 % change is used as a reference value. The assumption made here is that all the MOVs respond the same to impulse current such that they fail at 1000. It is known that the MOV can fail at the percentage change of leakage current that is greater than 1000, however, for this study failure is regarded as 1000 to yield minimum possible degradation. Equation 42 shows

the expression used to compute the expected minimum percentage change of leakage current for a particular impulse current.

$$I_{lmin} = D_{imp} \times 1000 \quad (42)$$

Where:

I_{lmin} = expected minimum percentage change of the leakage current of the MOV

$D_{imp} = \frac{1}{N_{sw}} \times 100\%$ (As in Equation 41)

Table 7 shows the results for percentage of degradation and expected minimum percentage change of leakage current computed using the proposed model. The latter results will be compared to the minimum percentage changes of leakage current computed from the experimental results. The next section evaluates the accuracy of the proposed model.

Table 7: Percentages of degradation computed using proposed degradation model.

Impulse (kA)	**Ratio = $\frac{I_{max}}{I_x}$**	**Maximum number of impulses before failure as per the proposed degradation model**	**Percentage of degradation as per the proposed degradation model**	**Expected minimum percentage change of leakage current as per the proposed degradation model**
I_{max} = 4.5	1	1.0014	99.86	998.60
0.9I_{max} = 4.05	1.111111	1.2874	77.68	776.76
0.8I_{max} = 3.6	1.25	1.5513	64.46	644.62
0.7I_{max} = 3.15	1.428571	1.764	56.69	566.89
0.6I_{max} = 2.7	1.666667	1.9271	51.89	518.91
0.5I_{max} = 2.25	2	2.1079	47.44	474.41
0.4I_{max} = 1.8	2.5	2.528	39.56	395.57
03I_{max} = 1.35	3.333333	4.095	24.42	244.20
0.2I_{max} = 0.9	5	15.0413	6.65	66.48
0.1I_{max} = 0.45	10	395.1224	0.25	2.53

4.6 Evaluation of the model and discussion

The expected minimum percentage change of leakage currents computed using the proposed model is compared to the experimental results of the minimum percentage change of leakage currents. The comparison is done by matching the results to observe any correlations. Matching, in this dissertation, is defined as comparing the percentage change of leakage current from the experimental test results with the expected minimum percentage change of leakage

current (from Table 7), as per the proposed degradation model, at each impulse current level to determine whether the value of the percentage change of leakage current of each test sample is less, greater or equal to the value of the expected minimum percentage change of leakage current; if the measured value is greater or equal to the expected value, then that is regarded as matched, otherwise not matched.

Statistical analysis is conducted to observe the spread and consistence of the results. The experimental test results for all the MOV test samples are therefore computed at each impulse current level to determine the commonly used statistical parameters; mean, median and standard deviation of the percentage of change of leakage current after the MOV was subjected to single lightning current impulse. Table 8 shows the statistical spread of the results at each current level.

Table 8: Statistical spread of the experimental test results at each current level

Impulse (kA)	Mean	Median	Standard deviation
4.5	-2117.92	-1597.62	1585.863
4.05	-1302.5	-1082.86	1042.687
3.6	-932.192	-935.247	214.1495
3.15	-620.533	-630.189	229.3272
2.7	-636.904	-586.182	176.7325
2.25	-569.337	-552.68	175.5839
1.8	-528.605	-512.253	160.866
1.35	-385.244	-383.056	81.07989
0.9	-130.827	-130.278	43.66688
0.45	-36.1085	-39.3327	20.37889

From Table 8 it can be seen that the median values are not far apart from the mean values, except at higher impulse current levels. This is also evident on the standard deviation profile of the results, where the lower standard deviation values are found at the lower impulse current levels and the larger standard deviation values are found at the higher impulse current levels. Therefore, this can be interpreted as that the leakage current of the MOV is more sensitive at higher impulse current levels than at lower impulse current levels.

Therefore, the percentage of matching is computed using Equation 43. Table 9 shows the results of matching of the model.

$$M_{per} = \frac{N_{matched}}{N_{total}} \times 100 \tag{43}$$

Where:

M_{per} = percentage of matching of the proposed degradation model to experimental test results

$N_{matched}$ = number of samples matched per specific magnitude of impulse current

N_{total} = total number of samples tested per specific magnitude of impulse current

Table 9: Percentage of matching of the proposed degradation model to the experimental test results.

Impulse (kA)	Percentage of Matching to the proposed degradation model
I_{max} = 4.5	81.25
$0.9I_{max}$ = 4.05	75
$0.8I_{max}$ = 3.6	87.5
$0.7I_{max}$ = 3.15	75
$0.6I_{max}$ = 2.7	87.5
$0.5I_{max}$ = 2.25	81.25
$0.4I_{max}$ = 1.8	93.75
$03I_{max}$ = 1.35	87.5
$0.2I_{max}$ = 0.9	100
$0.1I_{max}$ = 0.45	93.75

From Table 9 it can be seen that the minimum percentage of accuracy of the model in relation to the experimental results is 75 %. Furthermore, it can be seen that the accuracy of the model is greater at lower impulse currents (i.e. from 0.45 kA to 1.8 kA) than at larger impulse currents (i.e. from 2.25 kA to 4.5 kA). This is a result of an assumption made that MOVs of the same type exhibit similar reaction when subjected to the same impulse current and as a result, an assumption that all MOVs fail when they are subjected to 4.5 kA impulse current was used during the matching process with a benchmark of 1000 % of change of leakage current to indicate a failure in the MOV. The 1000 % benchmark was used as reference in all the other magnitudes of impulse currents to get the expected minimum percentage of change of leakage current. An observation was made from the experimental test results that even though MOVs fail when the percentage change of leakage current is at least 1000, not all MOVs fail when subjected to 4.5 kA current impulse. This is due to the unique composition properties of each MOV which is a result of the manufacturing process, as a result, the MOV's varistor voltages are also not exactly the same regardless of the manufacture's specifications. Therefore, the proposed model gives an indication which ensures that the MOV is operated at safe margin; if the MOV is subjected to 4.5 kA, the model provides a percentage degradation which gives information about degradation status of the MOV - this allows the user to be cautious of the

condition of the MOV. This philosophy applies to the rest of the MOVs experimental results; the MOVs do not all react exactly the same to the same magnitude of impulse current, some tend to degrade more quicker than the others, however, the minimum possible degradation that may be caused should be noted to ensure that the MOV always offers acceptable protection level. Therefore, the model gives a minimum possible degradation that can be caused by a particular 8/20 µs lightning impulse current. The 75 % minimum accuracy matching serves as proof that the MOVs have distinct behaviour, however, most conform to manufacturer's specification. The proposed degradation model correctly describes the degradation of the MOVs which are more compliant to the manufacturer's specifications; for the MOVs that are less compliant to the specification, the proposed model provides an indication to the user to be aware of the condition of the respective MOV if it is operating within safety margin.

It is commonly known that human error in recording measurements have an influence in the results, however, these tests were conducted on multiple samples to observe the consistence and accuracy of the results. Furthermore, especially when the MOV was subjected to 4.5 kA, the leakage current and reference voltage results are aligned, i.e. when the percentage change of leakage current is at least 1000, the percentage change of reference voltage is at least 10. Therefore, the proposed model is deemed accurate with its intention of indicating possible minimum degradation caused by an impulse current. Furthermore, the indication given by the proposed degradation model can be used to compute the minimum protection level that can be offered by the MOV in order to note when the replacement or reinforcement of protection is required. However, further tests such as measuring reference voltage are still required to avoid replacing the MOV prematurely since it indicates a pass/fail status of the MOV.

One of the shortcomings of the proposed degradation model is its number of parameters. The model consist of 12 parameters of which are unique for every type of MOV. It was observed that the addition of parameters increase the accuracy of the model. However, the large number of parameters makes the model complex and be prone to errors when human insert the parameters for different types of MOVs. Therefore, the proposed degradation model is recommended to be further refined to constitute minimum parameters while maintaining (or improving) its accuracy.

5. Conclusion and Recommendations

This chapter provides the necessary conclusions drawn from the findings of this study when comparing the proposed degradation model with the experimental test results. Recommendations are given for further work to improve the proposed model and to ensure it caters for all conditions of lightning impulse currents.

5.1 Conclusion

Extensive work has been done in this study to determine the relationship between the lightning impulse current injected and the degree of degradation of the MOV. The relationship is described through a proposed degradation model which provides a percentage of degradation of the MOV caused by a respective 8/20 µs lightning impulse current. This model has been tested against experimental test results and it was found to match them by at least 75 %. The discrepancy in matching is due to the assumption used in the matching process that all the MOVs react the same when they are subjected to the same impulse current. Nonetheless, the proposed model provides a possible minimum degradation caused by a particular impulse current, and this information can be used to indicate the operational status of the MOV to ensure that the MOV operate in its safe margin and it always offers acceptable protection level. Therefore, the proposed model is deemed suitable to describe the relationship between the lightning impulse current injected and the degradation of the MOV.

5.2 Recommendations

The work conducted in this study provides a model that describes a relationship between an 8/20 µs lightning impulse current applied and the percentage of degradation of the MOV. However, further work is still recommended to be done to improve the model to cater for all possible conditions. Below are the recommendations for further work:

- Conduct experimental tests on all the other types of MOVs to verify if the accuracy of the model is consistent throughout, and also to observe if it does indeed cater for all the MOVs from different manufacturers it is developed for.

- The model is universal in a sense that it works for a range of MOVs with each MOV having unique model's parameters. It has been noted that MOVs with the same manufacturer's specification do not react the same under similar impulse conditions. Thus, further studies may be carried out to investigate the unique features of each MOV that can be included into the model to ensure that a respective MOV is modelled accurately, and whichever indication given by the model accurately describe the condition of the respective MOV.
- As it was proven in the work published by the author to the ICHVE 2016 that the sequence of occurrence of surges has an effect on the degradation of the MOV, the model should be refined to incorporate this development and should be tested on different types of MOVs.
- The proposed model is only based on an 8/20 μs lightning impulse current, however, in reality MOVs can also be subjected to switching surges and 10/350 μs lightning impulse current. Therefore, a study into how these aforementioned surges influence the degradation of the MOV may be carried out and the findings can be incorporated into the model to extend it in order to account for different shapes or types of impulse current that can possibly degrade the MOVs.
- The proposed model only provide information about the degradation caused by a particular lightning impulse current, but it does not consider the history of exposure before giving an overall status of the MOV. Therefore, the model may be extended to incorporate the history of exposure to output the actual status of the MOV.
- The proposed degradation model consist of a large number of parameters which make the model somewhat complex. It is therefore recommended for future work that the model be refined to reduce its number of parameters while maintaining its accuracy.
- A physical prototype, derived from the proposed degradation model, is recommended to be developed to monitor the status of the MOV. For every lightning current impulse the MOV is subjected to, the percentage of degradation can be computed using the proposed model. Therefore, the percentages of degradation may be summed up, and when the total percentage of degradation is at least 50 % an indication shall be conveyed to activate the maintenance personnel to perform physical tests on the MOV in the field, in order to verify the status of the MOV; this will subsequently achieve preventative maintenance.

- During the tests, the MOVs were not subjected to service conditions. Therefore, further tests are recommended to connect the MOV to a power supply in order to observe the effect of the power supply on the degradation of the MOV.

References

[1] K.P. Mardira, T.K. Saha, and R.A. Sutton, *The Effects of Electrical Degradation on the Microstructure of Metal Oxide Varistor*, IEEE 0-7803-7285-9/01, 2001.

[2] K.J. Brown, *Metal Oxide Varistor Degradation*, IAEI News: The Magazine, March/April 2004.

[3] K.P. Mardira and T.K. Saha, *Modern Electrical Diagnostics for Metal Oxide Surge Arresters*. IEEE transactions, 2001.

[4] W. Bassi and H. Tatizawa, *Early Prediction of Surge Arrester Failures by Dielectric Characterization*, IEEE Electrical Insulation Magazine, Vol. 32, No. 2, pp. 35-42, March/April 2016.

[5] IEC 61643-11, *Low-voltage surge protective devices – Part 11: Surge protective devices connected to low-voltage power systems – Requirements and test methods*, Edition 1.0, 2011.

[6] IEC 61643-12, *Low-voltage surge protective devices – Part 11: Surge protective devices connected to low-voltage power distribution systems – Selection and application principles*, Edition 2.0, 2008.

[7] M. Bazu and T. Bajenescu, *Failure Analysis: A Practical Guide for Manufacturers of Electronic Components and Systems*, Wiley, ISBN: 1119990009, 2011.

[8] Littlefuse, *Varistors - Basic Properties*, Terminology and Theory. Application Note AN9767.1, July 1999.

[9] Vishay BCComponents, *Varistors Introduction*, Technical note, document number 29079, http://www.vishay.com/docs/29079/varintro.pdf, last accessed: 03 February 2016.

[10] *Transient Surges and Surge Suppressor Technologies: Comparing Apples to Oranges – MOV versus SASD Design Discussion*, http://www.wago.us/surge.htm, last accessed: 03 February 2016.

[11] S. Han, H. Cho, Y. Lee, and H. Kang, *Modeling on the Failure for High-Voltage Arresters by Voronoi Network Simulation*, Proceedings of the 6th International Conference on Properties and Applications of Dielectric Materials, pp.676 – 680, June 2000.

[12] D. Birrell and R. B. Standler, *Failures of Surge Arrestors on Low-Voltage Mains*, IEEE Transactions on Power Delivery, Vol. 8, No. 1, 1993.

[13] W. Beech, *Comparing SPD Performance*, http://ecmweb.com/content/comparing-spd-performance, last accessed 30 March 2017.

[14] C. Stancu, P.V. Notigher, and L.V. Badicu, *Dielectric Response Function for Nonhomogeneous Insulations*, Conference on Electrical Insulation and Dielectric Phenomena (CEIDP), pp. 97 – 100, 2011.

[15] E. David and L. Lamarre, *Low-Frequency Dielectric Response of Epoxy-Mica Insulated Generator Bars during Multi-Stress Aging*, IEEE Transactions on Dielectrics and Electrical Insulation, Vol. 14, No. 1, pp. 212 – 226, February 2007.

[16] Littlefuse, *Varistor Testing*, Application Note AN9773, January 1998.

[17] V. Hinrichsen, *Monitoring of High Voltage Metal Oxide Surge Arresters*, VI Jornadas Internacionales de Aislamiento Electrico, pp. 1-15, October 1997.

[18] Maida Development Company, *Zinc-Oxide Varistors*, Catalog, pp. 5-7, 2001.

[19] M. Farahani, H. Borsi, and E. Gockenbach, *Calculation and Measurement of Dielectric Response Function in Insulation Systems of High Voltage Rotating Machines*, Proceeding of the 7th International Conference on Properties and Applications of Dielectric Materials, pp. 290 – 293, June 2003.

[20] A. Kozlovskis and J. Rozenkrons, *Temperature Dependence of Return Voltage Characteristics*, IEEE Transactions on Power Delivery, Vol. 14, No. 3, pp. 705 – 708, July 1999.

[21] A. Kozlovskis, *Dependence of Return Voltage Characteristics on Change of Insulation Conductivity and Polarization Resistance*, IEEE Transactions on Power Delivery, pp. 103 – 106, August 1999.

[22] A. Kozlovskis, *Diagnostic Measurements of Oil-Paper Insulation in Current Transformers*, Proc. of the 1996 NORD-IS, pp. 361-368, 1996.

[23] D. Allan, *Recent Advances in Automated Insulation Monitoring Systems, Diagnostic Techniques and Sensor Technology in Australia*, CIGRE Paper 15-101, 1998.

[24] E. Nemeth, *Some Newest Results of Diagnostic Testing of Impregnated Paper Insulated Cables*, Proc. of 10th ISH, Montreal Canada, 1997.

[25] T.K. Saha and T. Dinh, *Return Voltage Measurements on Metal Oxide Surge Arresters*, International Symposium on High Voltage Engineering, London, England, August 1999.

[26] K.P. Mardira, M. Darveniza, and T.K. Saha, *Search for New Diagnostics for Metal Oxide Surge Arrester,* International Conference on Properties and Applications of Dielectric Materials, pp. 947 – 950, June 2000.

[27] C. Heinrich and W. Kalkner, *Return Voltage Measurements on Metal Oxide Surge Arresters*, International Symposium on High Voltage Engineering, Vol. 5, pp. 137 – 140, 1997.

[28] A. Kozlovskis, *Recovery Voltage Method Application for Diagnostics of High Voltage Insulation*, Ph.D. Thesis, Riga Technical University, Riga Latvia, 1998.

[29] A. Bognar, *Comparing Various Methods for the Dielectric Diagnostics of Oil-Paper Insulation Systems in the Range of Low-Frequencies or Long Time-Constants*, Proc. of 8th ISH, Yokohama Japan, 1993.

[30] E. Nemeth, *Measuring Voltage Response: a non-destructive diagnostic test method of high voltage Insulation*, Science Measurement and Technology, Vol. 146, No.5, pp. 249 – 252, September 1999.

[31] E. Nemeth and T. Hrovath, *Fundamental of the Simulation of Dielectric Processes of Insulation*, International Symposium of High Voltage Engineering, pp. 177 - 180, 1993.

[32] E. Ildstad, U. Gafvert, and P. Tharning, *Relation Between Return Voltage and Other Methods for Measurements of Dielectric Response*, IEEE International Symposium on Electrical Insulation, pp. 25 – 28, June 1994.

[33] A.K. Jonscher, *Dielectric relaxation in solids*, Chelsea Dielectrics Press, London, 1983.

[34] R. Corn, *The Electric Susceptibility, Dielectric Constant, and Complex Index of Refraction*, Winter 2005, http://unicorn.ps.uci.edu/249/Handouts/EM2.pdf, Last accessed 21 March 2016.

[35] S. Ahmed, E. Ahmed, and M.D. Abd-Alla, *The Effect of Magnetic Field on the Electric Susceptibility*, Journal of Applied and Industrial Sciences, ISSN:2328-4609, pp. 16 – 19, October 2013.

[36] Y. Toyozawa, *Optical Processes in Solids – Chapter6: Electric Susceptibility and dielectric constant*, Cambridge University Press, ISBN: 9780511615085, pp. 89 – 106, December 2009.

[37] Agilent Technologies, *Basics of Measuring the Dielectric Properties of Materials*, pp. 4 – 6, June 2006.

[38] B. Zitnik, M. Babuder, M. Muhr, M. Zitnik, and R. Thottappillil, *Numerical Modelling of Metal Oxide Varistors*, Proceedings of the XIVth International Symposium on High Voltage Engineering, pp. 1-6, August 2005.

[39] R. Brocke, T. Goehlsch, and F. Noach, *Numerical Simulation of Low-Voltage Protective Devices*, International Zurich Symposium on EMC, 1993.

[40] I. Kim, T. Figunabashi, H. Sasaki, T. Hagiwara, and M. Kobayashi, *Study of ZnO Arrester model for Steep Front Wave*, IEEE Transactions on Power Delivery, Vol. 11, No. 2, pp. 834-841, April 1996.

[41] IEEE Working Group 3.4.11, *Modelling of Metal Oxide Surge Arresters*, IEEE Transactions on Power Delivery, Vol. 7, No. 1, January 1992.

[42] C. Chrysanthou and J. Boksiner, *Analysis of Coordination between Primary and Secondary Protectors*, IEEE Transactions on Power Delivery, Vol. 12, No. 4, pp. 1501 – 1507, October 1997.

[43] M. R. Meshkatoddini, *Metal Oxide ZnO-Based Varistor Ceramics*, Advances in Ceramics – Electric and Magnetic Ceramics, Bioceramics, Ceramics and Environment, Prof. Costas Sikalidis (Ed.), ISBN: 978-953-307-350-7, InTech, 2011.

[44] M. Edirisinghe, R. Montano, V. Cooray, and F. Roman, *Performance comparison of varistor models under high current derivative impulses*, International Letter of Chemistry, Physics and Astronomy, ISSN: 2299-3843, Vol. 11, pp. 40 – 53, September 2013.

[45] Siemens and Matshushita Componenta, *SIOV Metal Oxide Varistor*, Pspice model library, 1995.

[46] D. Durbak, *EMTP News Letter*, Vol. 5, No. 1, 1985.

[47] F. Fernandez and R. Diaz, *Metal-oxide surge arrester model for fast transient simulations*, Proceedings of the International Conference on Power Systems Transients, 2001.

[48] M. Darveniza, et al, *Laboratory Studies of the Effects of Multipulse Lightning Current on Metal Oxide Arresters*, IEEE Transaction on Power Delivery, Vol. 8, pp. 1035 – 1044, 1993.

[49] M. Darveniza, et.al, *Multiple Impulse Current Tests on a Zinc-Oxide Polymeric Distribution Surge Arrester*, International Power Engineering Conference, pp. 673 - 378, Singapore, March 1993.

[50] M. Darveniza, T.K. Saha, and S. Wright, *Comparison of in-service Laboratory Failure Modes of Metal Oxide Distribution Surge Arresters*, Proceedings of the IEEE Power Engineering Society Winter Meeting, Singapore, 2000.

[51] L.R. Tumma, M. Darveniza, and D.R. Mercer, *Stresses on Zinc Oxide Arrester Blocks Caused by Multiple Lightning Impulse Currents*, Inst. Eng. Aust., Electric Energy Conference (EECON 92), pp. 175 – 177, Brisbane, Oct. 1992.

[52] T.K. Gupta, *Influence of Microstructure and Chemistry on the Electrical Characteristic of ZnO Varistors*, Tailoring Multiphase and Composite Ceramics, pp. 493 – 5107, New York, 1986.

[53] L.M. Levinson and H.R. Phillip, *Zinc Oxide Varistors – A Review*, Ceram Bull., Vol. 65, No. 4, pp. 639 – 646, 1986.

[54] R.A. Sargent, G. Dunlop, and Darveniza, *Effects of Multiple Impulse Currents on the Microstructure and Electrical Properties of Metal-oxide Varistors*, IEEE Transactions on Electrical Insulation, Vol. 27, No. 33, pp. 586 – 592, 1992.

[55] H. Enomoto, Y. Takido, K. Yonezawa, Y. Takahashi, T. Idogawa, T. Hayashi, and Y. Niikura, *Development of Small-Sized Surge Monitoring Device for Measuring Invading Lightning Surge Currents*. 7th Asia-Pacific International Conference on Lightning, pp. 372 – 375, November 2011.

[56] J. Funke and F. Martzloff, *Monitoring of Surge-Protective Devices in Low-Voltage Power Distribution Systems*. Power Quality Exhibition and Conference, pp. 1 – 11, November 2004.

[57] IEC 62305-1, *Protection against lightning – Part 1: General Principles*, Edition 2.0, 2010.

[58] K.J. Nixon, J.M. Van Coller, and I.R. Jandrell, *Earthing and Lightning Protection, Revision 2.1*, School of Electrical and Information Engineering, University of the Witwatersrand, pp. 13-30, March 2010.

[59] M. Mashaba and K. Nixon, *Deducing Metal Oxide Varistor Life Span from Pulse Rating Curves for Surges of Different Magnitudes*, 2016 IEEE International Conference on High Voltage Engineering and Applications, September 2016.

[60] R.B. Standler, *Protection of Electronic Circuits from Overvoltages*, John Wiley & Sons, pp. 87, 1989.

[61] FENGHUA, *Zinc Oxide Varistor*, Manufacturer's Specification, Fenghua (HK) Electronics Ltd.

[62] EPCOS, *SIOV Metal Oxide Varistors – General technical information*, EPCOS AG 2011, pp. 1 – 21, April 2011.

Appendix A: Deducing the Metal Oxide Varistor Life Span from Pulse Rating Curves for Surges of Different Magnitudes – Presented at ICHVE 2016

This appendix presents a paper that was accepted and presented for publication by the 2016 IEEE International Conference on High Voltage Engineering and Applications (ICHVE), in Chengdu, China, 19th – 22nd September 2016. The paper is titled: ***Deducing the Metal Oxide Varistor Life Span from Pulse Rating Curves for Surges of Different Magnitudes***.

Deducing Metal Oxide Varistor Life Span from Pulse Rating Curves for Surges of Different Magnitudes

Mathews Mashaba
School of Electrical and Information Engineering
University of the Witwatersrand
Johannesburg, South Africa
Mathews.Mashaba@students.wits.ac.za

Ken Nixon
School of Electrical and Information Engineering
University of the Witwatersrand
Johannesburg, South Africa
Ken.Nixon@wits.ac.za

Abstract—**Metal Oxide Varistors (MOVs) are employed as surge protective devices due to their capability of dissipating reasonably large values of surges. The pulse (life span) rating curves of a MOV provide the estimated life span of the device when exposed to multiple surges of the same magnitude. However, in reality, a lightning event (flash) consists of multiple current surges (strokes), with the first stroke having a magnitude approximately three times that of the subsequent strokes. Furthermore, the sequence of occurrence of surge events (lightning and switching surges) is not always the same. In this paper two sequences are considered: sequence 1 – larger surge event, and then smaller; sequence 2 – smaller surge event, and then larger surge event. Several tests were conducted to deduce the life span of a MOV from pulse rating curves, and to determine the influence of sequence of occurrence of surges on the degradation of the MOV. A standard 20K201 MOV was tested under different levels of exposure of surges. The sequence of occurrence of surges was found to have a significant influence on the degradation of the MOV. The MOV showed a larger degree of degradation when it was first exposed to a surge of lower amplitude (2 kA) and then later to a surge of larger amplitude (4 kA), compared to when it was exposed to same surges but with opposite sequence. When the MOV was exposed to approximately 60% of rated surge current, it became more susceptible to surges and could easily fail when exposed to surges less than 32% of rated surge current.**

Keywords—degradation; life span; metal oxide varistor; sequence; surges

I. INTRODUCTION

Metal Oxide Varistors (MOVs) are commonly employed as surge protective devices for a range of systems from low voltage equipment to high voltage systems. MOVs can dissipate reasonably large values of surges, and they have a relatively long life span. The exposure of a MOV to surges higher than its rating, or exposure to multiple surges for a long period, results in failure in different forms, which include electrical puncture, thermal cracking, thermal runaway, etc. [1]. Depending on the level of surge exposure the MOV does not always show visual failure, which therefore makes visual inspection challenging and inaccurate. Therefore, to ensure that the MOV always offer acceptable protection, preventative maintenance mechanisms are sought.

The pulse (life span) rating curves of a MOV estimate its life span when it has been exposed multiple times to surges of the same magnitude. However, in reality, a lightning event (flash) consists of multiple current surges (strokes) of different magnitudes, with the first stroke approximately three times larger than the subsequent strokes [2, 3]. Furthermore, the sequence of occurrence of lightning events and switching surges does not always follow the same pattern. In this paper two sequences are considered: sequence 1 – a larger surge event, then a smaller surge event; and sequence 2 – a smaller surge event, then a larger surge event.

Therefore, this paper presents the findings of the research undertaken to deduce the life span of an MOV from the pulse rating curves if the MOV is exposed to surges of different amplitudes for the purpose of preventative maintenance. Furthermore, the sequence of occurrence of surges is investigated to examine its influences on degradation of the MOV.

The MOV under investigation is a standard 20K201 MOV; it has a varistor voltage rating of 200V, DC maximum continuous operating voltage (MCOV) rated at 170V, and a maximum withstand surge current (8/20 µs) rated at 6.5 kA [4].

II. DEGRADATION DIAGNOSTIC TECHNIQUES

Three MOV degradation evaluation and diagnostic techniques are considered, specifically Reference voltage, Leakage current and Decay voltage. The reference voltage is used to determine the pass/fail condition of the MOV, and the leakage current and decay voltage are used to determine the degree of degradation of the MOV.

A. Reference Voltage

Reference voltage is a measure of the varistor voltage of a MOV which influences the maximum operating voltage. It is the voltage across the MOV when a DC current of 1 mA is applied [5]. The Reference voltage test is done within few seconds to avoid heating up the MOV and subsequently degrading its performance; the reference voltage is determined to establish if the MOV is in a pass or fail condition. The pass or fail condition is determined through the percentage of deviation (tolerance) of the reference voltage before and after the MOV has been exposed to surges. It is a common practice to consider a MOV to be in a pass condition if the deviation ranges from ±5% to ±10% depending on the type of the MOV.

978-1-5090-0496-6/16/$31.00 ©2016 IEEE

For a 20K201 MOV the maximum allowable deviation is ±10%.

B. Leakage Current

Ideally when the MOV is in non-conductive state, i.e. at voltages less than the MCOV, no current is expected to flow. However, due to real elements composing the MOV, a small amount of current does flow during this non-conductive state, which is regarded as leakage current. Leakage current is measured to monitor the degradation of the MOV before and after it has been exposed to surges. Maximum leakage current is determined when MCOV is applied [5].

C. Decay Voltage Method

A MOV is considered to be an insulator when it is in a non conductive state, and the Decay voltage method is used determine the ohmic conductivity under this state. The ohmic conductivity is used to quantify the extent of degradation of the MOV as opposed to reference voltage, which only determines a pass or fail condition.

To determine the ohmic conductivity through Decay voltage method, the MOV is excited with a DC voltage less than the MCOV for shorter period, and thereafter the DC voltage supply is removed and the decay voltage is measured for longer period (approximately 5 times the charging period). When the voltage of a MOV decays, it discharges through the internal resistance of the MOV, hence the significance of determining the ohmic conductivity [6, 7]. Fig. 1 illustrates a typical decay voltage waveform of an insulator [7].

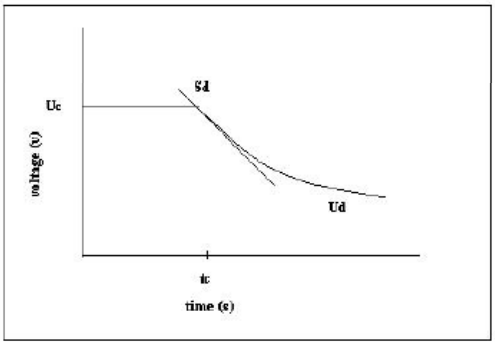

Fig. 1. Typical Decay voltage waveform [7]

Equation (1) is used to determine the ohmic conductivity of an insulator/MOV [7].

$$S_d \bullet d \bullet \varepsilon_o / U_c = \gamma \qquad (1)$$

Where d = length of the MOV

S_d = steepness of the initial tangent of decay voltage

U_C = DC voltage applied

γ = Ohmic Conductivity

ε_o = 8.854e-14 [A.s/V.cm]

III. TEST SET-UP

An 8/20 µs impulse current generator (IEC 62305) was used to inject surge impulses into type 20K201 MOVs. The degradation parameters of each MOV (i.e. reference voltage, leakage current and decay voltage) were measured before and after the MOV was injected with an impulse current in order to determine the percentage change in the aforementioned degradation parameters. The test procedure followed to conduct the tests is outlined in the following sections.

A. Tested MOV

A standard 20K201 MOV was tested to deduce its life span from the pulse rating curves, and also, to investigate the influence of the sequence of occurrence of surges. Fig. 2 illustrates the life span ratings of a 20K201 MOV [4].

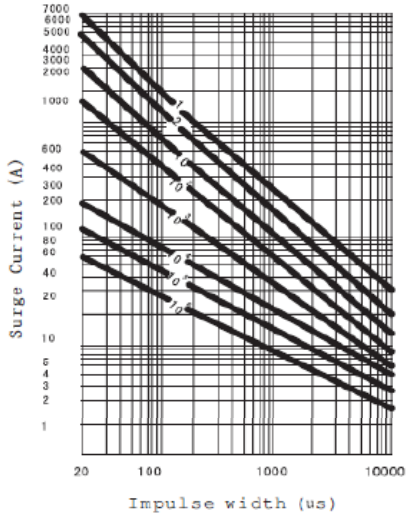

Fig. 2. MOV 20K201 Life span ratings [4]

The time intervals between impulses of the same magnitude as per Fig. 2 are as follows: up to 2 impulses is 5 minutes; up to 10 impulses is 2 minutes; and up to 10^6 impulses is 10 seconds.

B. Test Procedure

12 Samples of 20K201 MOVs were used for the tests. For every series of tests three samples of MOVs were used to ensure the accuracy of the results. The MOV was subjected to 8/20 µs impulses of different magnitudes, with 2 minutes intervals between impulses. The degradation parameters of the MOV (i.e. reference voltage, leakage current and ohmic conductivity) were measured before and after the MOV was exposed to surges to determine the degree of degradation. The test procedure is summarized as follows:

1. 1 mA DC current was applied and the voltage across the MOV was measured.
2. 170V (i.e. MCOV of a 20K201 MOV) was applied across the MOV and the current flowing (i.e. leakage current) was measured.
3. The MOV was excited with 82 V for 200s and then the supply was removed to measure the decay voltage for 1000s.
4. The terminals of the MOV were short circuited for 24 hours to eliminate polarization effects to ensure that the accuracy of the measurements is not affected.
5. The MOV was then subjected to 8/20 µs surges accordingly.
6. Tests 1-3 were then repeated to determine the degree of degradation of the MOV.

IV. TEST RESULTS

Table I, II and III present the measured reference voltage, leakage current, and ohmic conductivity of the MOV respectively. In the tables of results the sign '+' represent the time interval (which is 2 minutes) between impulses. The surges applied are rated at 8/20 µs with the magnitudes as shown in the tables of results.

TABLE I. Summary of MOV measured Reference Voltage

Level of Exposure (kA)	MOV Sample Number	Reference Voltage (V)		% Change
		Before	*After*	
2+4	S1	206.1	181.3	12.03
	S2	196.2	188.9	3.72
	S3	206.3	184.2	10.71
4+2	S4	216.2	210.3	2.73
	S5	220	212.5	3.41
	S6	201.7	176.9	12.30
4+2+2	S7	200.4	188.2	6.09
	S8	189.6	186.1	1.85
	S9	213.2	187.6	12.01
4+2+2+2	S10	210.6	182.3	13.45
	S11	193	180.1	6.68
	S12	209.1	184.5	11.77

TABLE II. Summary of MOV measured Leakage current

Level of Exposure (kA)	MOV Sample Number	Leakage current (µA)		% Change
		Before	*After*	
2+4	S1	174.5	558.4	-220.00
	S2	191.7	297.3	-55.09
	S3	174	479	-175.29
4+2	S4	172.2	193.7	-12.49
	S5	169.1	176.9	-4.61
	S6	178.5	744	-316.81
4+2+2	S7	186.5	314.5	-68.63
	S8	218.1	283.6	-30.03
	S9	172	407.9	-137.15
4+2+2+2	S10	173.6	519.8	-199.42
	S11	207	519.8	-151.11
	S12	173.4	519.9	-199.83

TABLE III. Summary of MOV measured Ohmic conductivity

Level of Exposure (kA)	MOV Sample Number	Ohmic Conductivity *e-15 (A/V.s)		% Change
		Before	*After*	
2+4	S1	2.148	2.153	-0.23277
	S2	2.147	2.138	0.41919
	S3	2.151	2.141	0.4649
4+2	S4	2.145	2.138	0.32634
	S5	2.145	2.163	-0.83916
	S6	2.150	2.166	-0.74419
4+2+2	S7	2.150	2.161	-0.51163
	S8	2.145	2.135	0.4662
	S9	2.157	2.167	-0.46361
4+2+2+2	S10	2.156	2.163	-0.32468
	S11	2.135	2.159	-1.12412
	S12	2.151	2.129	1.02278

V. DISCUSSION

Two key points, namely the sequence of occurrence of surges, and surges of different magnitudes, are considered for discussion. The first key point of discussion outlines the influence the sequence of occurrence of surge events has on the degradation of the MOV. The second key point discusses the effect of surges of different magnitudes on the degradation of the MOV.

A. Sequence of Occurrence of Surges

Referring to Table I between '2+4' and '4+2' results it is evident that the sequence of occurrence of the surges has an influence on the degradation of the MOV. Sequence '2+4' exhibits larger degradation which put the MOV in a fail state since the reference voltage change exceeds the maximum allowable tolerance of ±10%.

Table II shows that the degree of change of the leakage current on sequence '2+4' is very large when compared to the change of leakage current change of sequence '4+2'. This implies that when sequence '2+4' is injected into the MOV, the MOV experiences expedited degradation as compared to when sequence '4+2' is injected.

Table III shows that the internal resistance (through ohmic conductivity) of the MOV decreases when sequence '2+4' is injected which supports the increase of the leakage current compared to sequence '4+2'. The decrease of the ohmic conductivity implies that the MOV starts conducting at voltages lower than the rated MCOV, and this is evident from the decrease of reference voltage of the MOV from Table I and the increase in the leakage current of the MOV from Table II.

Therefore, the sequence of occurrence of surges has a significant influence on the degradation of a MOV. If an MOV is first exposed to a surge of larger amplitude and then later exposed to a surge of lower amplitude, it will yield lower degradation rate compared to when it is exposed to same surges but in an opposite sequence. This means that the sequence of occurrence of surges has to be considered when devising accurate mechanisms of achieving preventative maintenance on MOVs.

B. *Surges of Different Magnitudes*

According to the specification for the MOV it is expected to fail if it is exposed to 8/20 µs surges of 2 kA magnitude ten times, or of 4 kA magnitude two times.

Table I indicates that the MOV fails when it is exposed to one 4 kA impulse and three times 2 kA impulses with 2 minute intervals. This illustrates that the MOV does not have to be exposed to two times 4 kA impulses or 10 times 2 kA impulses, but the combination of 4 kA and 2 kA impulses causes the MOV to fail.

When the MOV is exposed to one 4 kA and two times 2 kA impulses it does not necessarily fail. However, it degrades by a larger amount, which makes it more susceptible to surges of any magnitudes.

From the tests conducted it is evident that after the MOV is exposed to a surge of approximately 60% of the rated surge current, it becomes more susceptible to surges, and it no longer exhibit the same behavior and performance as estimated by pulse rating curves.

Therefore, when monitoring the degradation of the MOV for preventative maintenance it is crucial to consider the combination of magnitudes of different surges in order to accurately deduce the life span of a MOV.

VI. CONCLUSION

The sequence of occurrence of surges has a significant influence on the degradation of the MOV. The MOV shows a larger level of degradation when it is first exposed to a surge of lower amplitude (2 kA) and then later to a surge of larger amplitude (4 kA), compared to when it is exposed to same surges but in an opposite sequence. Therefore, the sequence of occurrence of surges has to be taken into account when monitoring the degradation of a MOV for preventative maintenance.

When the MOV is exposed to approximately 60% of the rated surge current, it becomes more susceptible to surges and it can easily fail when exposed to surges less than 32% of the rated surge current. Therefore, the combination of magnitudes of different surges has to be considered in order to accurately infer the condition of a MOV.

REFERENCES

[1] K.J. Brown, "Metal Oxide Varistor Degradation," IAEI News: The Magazine, March/April 2004.

[2] IEC 62305-1 "Protection against lightning – Part 1: General Principles," Edition 2.0, 2010.

[3] K.J. Nixon, J.M. Van Coller, and I.R. Jandrell, "Earthing and Lightning Protection, Revision 2.1," School of Electrical and Information Engineering, University of the Witwatersrand, pp. 13-30, March 2010.

[4] FENGHUA "Zinc Oxide Varistor: FNR-20K201," Fenghua (HK) Electronics Ltd.

[5] W. Bassi and H. Tatizawa, "Early Prediction of Surge Arrester Failures by Dielectric Characterization," IEEE Electrical Insulation Magazine, Vol. 32, No. 2, pp. 35-42, March/April 2016.

[6] E. Nemeth, "Measuring Voltage Response: a non-destrictive diagnostic test method of high voltage insulation," Science Measurement and Technology, Vol. 146, No. 5, pp. 249-252, September 1999.

[7] K.P. Mardira and T.K. Saha, "Modern Electrical Diagnostics for Metal Oxide Surge Arresters," IEEE transactions, pp. 672-676, 2002.

APPENDIX B: Proposed Model's Simulation Results

This Appendix presents the pulse rating curves and the proposed model's simulation results, with parameters, of all the MOVs with sizes ranging from 5 mm to 40 mm. The model's simulation results are compared to the number of impulses given in the pulse rating curves to outline the percentage of error.

B1: FNR 5K820 to FNR 5K561

The FNR 5K820 – FNR 5K561 MOVs have a diameter of 5 mm. These MOVs have a one-time maximum withstand surge current (8/20 µs) of 400 A and the rated power of 0.1 W. The maximum energy (2 ms) of these MOVs ranges from 1.8 J to 14 J with a maximum operating DC voltage ranging from 65 V to 460 V depending on the type of MOV.

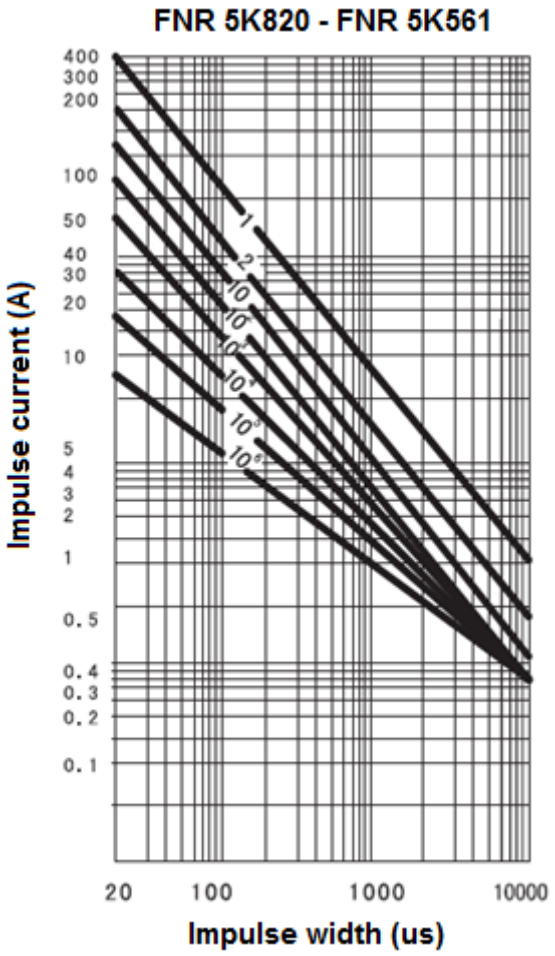

Figure B1: Pulse rating curves of MOVs FNR 5K820 – FNR 5K561 [58].

Table B1: Parameters of the proposed degradation model for MOVs FNR 5K820 – FNR 5K561.

Parameters	Values
b_1	0.6702
b_2	10.2826
b_3	-6.0490
b_4	-2.5423
b_5	7.8326
b_6	0.0872
b_7	12.4734
b_8	6.0918
b_9	-3.5501
b_{10}	-2.9439
b_{11}	-20.6478
b_{12}	-0.2448

Table B2: Accuracy of the proposed degradation model for MOVs FNR 5K820 – FNR 5K561.

Impulse (A)	Ratio (R_{imp}) = 400/I	Number of impulses before failure as specified in pulse rating curves	Number of impulses before failure as per the proposed mathematical degradation model	Error (%)
400	1	1	0.997	0.3
200	2	2	2.0077	-0.39
133	3.007519	10	10.0013	-0.01
100	4	100	100.0317	-0.03
80	5	1000	1000.4	-0.04
60	6.666667	10000	9976.4	0.24
18	22.22222	100000	100140	-0.14
8	50	1000000	1002700	-0.27

B2: FNR 7K820 to FNR 7K681

The FNR 7K820 – FNR 7K681 MOVs have a diameter of 7 mm. These MOVs have a one-time maximum withstand surge current (8/20 µs) of 1.2 kA and the rated power of 0.25 W. The maximum energy (2 ms) of these MOVs ranges from 4.2 J to 26 J with a maximum operating DC voltage ranging from 65 V to 561 V depending on the type of MOV.

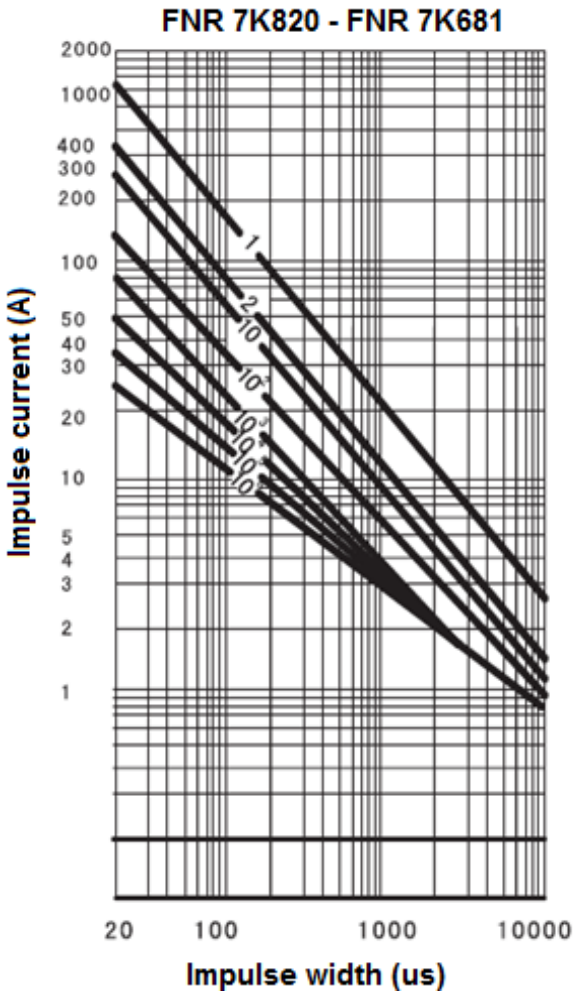

Figure B2: Pulse rating curves of MOVs FNR 7K820 – FNR 7K681 [58].

Table B3: Parameters of the proposed degradation model for MOVs FNR 7K820 – FNR 7K681.

Parameters	Values
b_1	-32.1205
b_2	4.4482
b_3	-22.3621
b_4	14.2903
b_5	-9.7428
b_6	-1.4471
b_7	31.8516
b_8	-42.5623
b_9	-61.1654
b_{10}	14.1462
b_{11}	15.8575
b_{12}	-0.6940

Table B4: Accuracy of the proposed degradation model for MOVs FNR 7K820 – FNR 7K681.

Impulse (A)	Ratio	Number of impulses before failure as specified in pulse rating curves	Number of impulses before failure as per the proposed mathematical degradation model	Error (%)
1200	1	1	0.9906	0.94
600	2	2	2.0232	-1.16
300	4	10	9.9868	0.13
141	8.510638	100	99.9391	0.06
80	15	1000	999.0416	0.10
50	24	10000	9986.2	0.14
35	34.28571	100000	99818	0.18
25	48	1000000	997540	0.25

B3: FNR 10K820 to FNR 10K471

The FNR 10K820 – FNR 10K471 MOVs have a diameter of 10 mm. These MOVs have a one-time maximum withstand surge current (8/20 µs) of 2.5 kA and the rated power of 0.4 W. The maximum energy (2 ms) of these MOVs ranges from 8.4 J to 58 J with a maximum operating DC voltage ranging from 65 V to 385 V depending on the type of MOV.

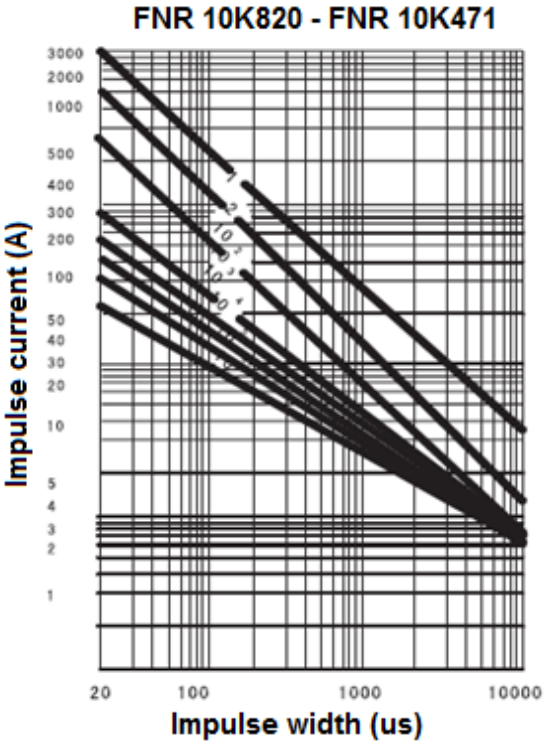

Figure B3: Pulse rating curves of MOVs FNR 10K820 – FNR 10K471 [58].

Table B5: Parameters of the proposed degradation model for MOVs FNR 10K820 – FNR 10K471.

Parameters	Values
b_1	18.9053
b_2	31.4606
b_3	-16.1990
b_4	-17.3930
b_5	-26.6517
b_6	1.1071
b_7	-4.0016
b_8	0.6972
b_9	-1.0806
b_{10}	3.4135
b_{11}	2.1683
b_{12}	-0.4979

Table B6: Accuracy of the proposed degradation model for MOVs FNR 10K820 – FNR 10K471.

Impulse (A)	Ratio	Number of impulses before failure as specified in pulse rating curves	Number of impulses before failure as per the proposed mathematical degradation model	Error (%)
2500	1	1	1.0039	-0.39
1250	2	2	1.993	0.35
650	3.846154	10	10.0051	-0.05
300	8.333333	100	100.0308	-0.03
200	12.5	1000	1000.6	-0.06
150	16.66667	10000	10008	-0.08
100	25	100000	100120	-0.12
60	41.66667	1000000	1001900	-0.19

B4: FNR 14K820 to FNR 14K471

The FNR 14K820 – FNR 14K471 MOVs have a diameter of 14 mm. These MOVs have a one-time maximum withstand surge current (8/20 µs) of 4.5 kA and the rated power of 0.6 W. The maximum energy (2 ms) of these MOVs ranges from 15 J to 104 J with a maximum operating DC voltage ranging from 65 V to 385 V depending on the type of MOV.

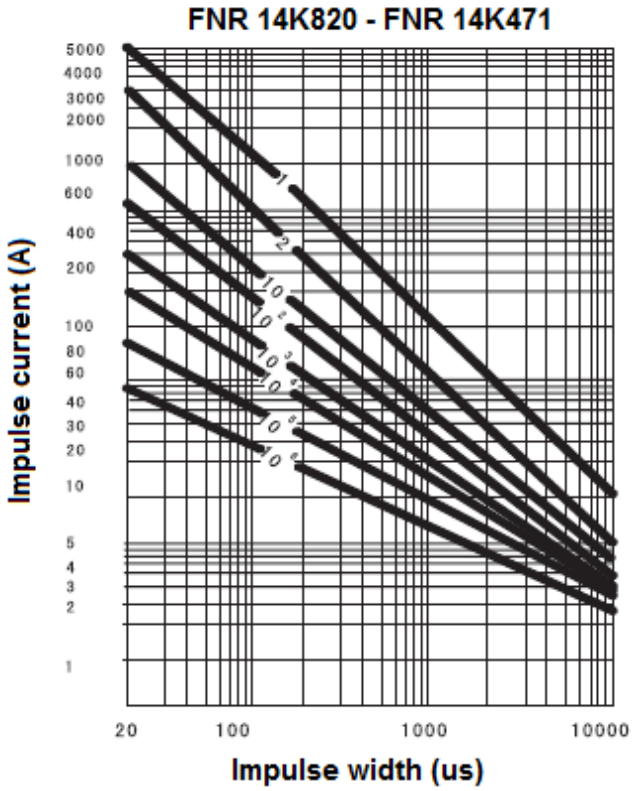

Figure B4: Pulse rating curves of MOVs FNR 14K820 – FNR 14K471 [58].

Table B7: Parameters of the proposed degradation model for MOVs FNR 14K820 – FNR 14K471.

Parameters	Values
b_1	4.9785
b_2	31.3929
b_3	-17.0759
b_4	-12.2490
b_5	-15.5494
b_6	0.5740
b_7	-40.5783
b_8	-40.7520
b_9	21.7298
b_{10}	39.7058
b_{11}	-16.8345
b_{12}	-4.0222

Table B8: Accuracy of the proposed degradation model for MOVs FNR 14K820 – FNR 14K471.

Impulse (A)	Ratio	Number of impulses before failure as specified in pulse rating curves	Number of impulses before failure as per the proposed mathematical degradation model	Error (%)
4500	1	1	1.0014	-0.14
2500	1.8	2	1.9975	0.13
1000	4.5	10	10.0008	-0.01
600	7.5	100	100.0088	-0.01
250	18	1000	1000.3	-0.03
150	30	10000	9997	0.03
80	56.25	100000	99923	0.08
45	100	1000000	998440	0.16

B5: FNR 20K820 to FNR 20K471

The FNR 20K820 – FNR 20K471 MOVs have a diameter of 20 mm. These MOVs have a one-time maximum withstand surge current (8/20 µs) of 6.5 kA and the rated power of 1 W. The maximum energy (2 ms) of these MOVs ranges from 27 J to 195 J with a maximum operating DC voltage ranging from 65 V to 385 V depending on the type of MOV.

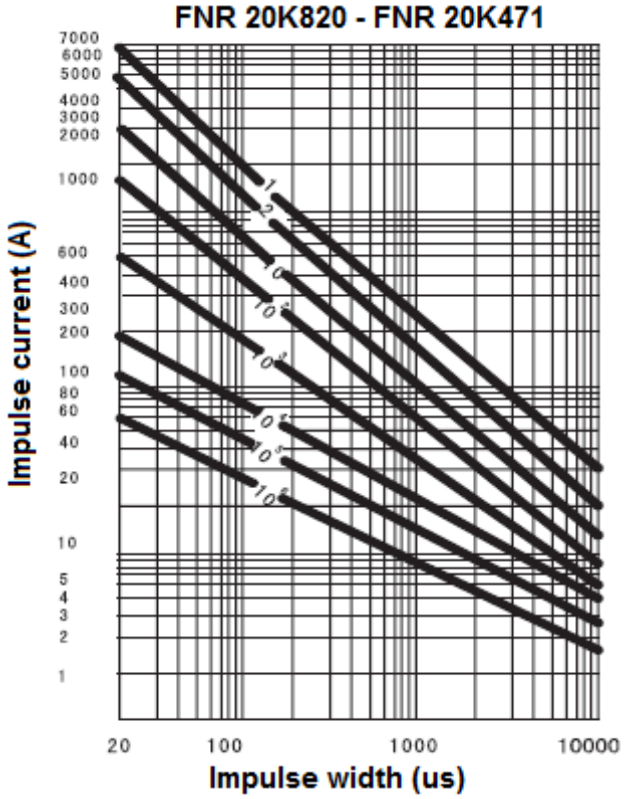

Figure B5: Pulse rating curves of MOVs FNR 20K820 – FNR 20K471 [58].

Table B9: Parameters of the proposed degradation model for MOVs FNR 20K820 – FNR 20K471.

Parameters	Values
b_1	-2.9570
b_2	3.0633
b_3	-3.8004
b_4	3.1558
b_5	-2.6373
b_6	-0.5763
b_7	0.3937
b_8	3.7227
b_9	-1.9763
b_{10}	-0.6204
b_{11}	2.1514
b_{12}	0.0513

Table B10: Accuracy of the proposed degradation model for MOVs FNR 20K820 – FNR 20K471.

Impulse (A)	Ratio	Number of impulses before failure as specified in pulse rating curves	Number of impulses before failure as per the proposed mathematical degradation model	Error (%)
6500	1	1	0.9993	0.07
4000	1.625	2	2.0018	-0.09
2000	3.25	10	10.0046	-0.05
1000	6.5	100	100.0696	-0.07
600	10.83333	1000	1000.9	-0.09
200	32.5	10000	10025	-0.25
100	65	100000	100480	-0.48
60	108.3333	1000000	1007300	-0.73

B6: FNR 25K820 to FNR 25K471

The FNR 25K820 – FNR 25K471 MOVs have a diameter of 25 mm. These MOVs have a one-time maximum withstand surge current (8/20 µs) of 10 kA and the rated power of 1 W. The maximum energy (2 ms) of these MOVs ranges from 35 J to 286 J with a maximum operating DC voltage ranging from 65 V to 385 V depending on the type of MOV.

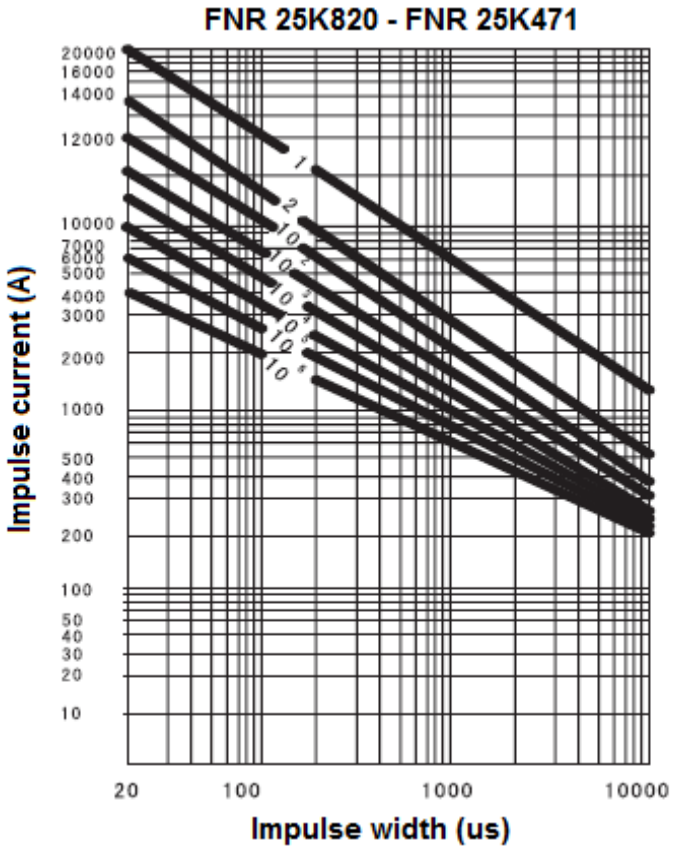

Figure B6: Pulse rating curves of MOVs FNR 25K820 – FNR 25K471 [58].

Table B11: Parameters of the proposed degradation model for MOVs FNR 25K820 – FNR 25K471.

Parameters	Values
b_1	-8.6075
b_2	-4.0805
b_3	0.6999
b_4	7.6255
b_5	0.9412
b_6	-0.6581
b_7	-1.2413
b_8	7.1062
b_9	-6.8441
b_{10}	4.7442
b_{11}	-8.5724
b_{12}	-1.5266

Table B12: Accuracy of the proposed degradation model for MOVs FNR 25K820 – FNR 25K471.

Impulse (A)	Ratio	Number of impulses before failure as specified in pulse rating curves	Number of impulses before failure as per the proposed mathematical degradation model	Error (%)
10000	1	1	1.0023	-0.23
5000	2	2	1.995	0.25
3000	3.333333	10	10.0013	-0.01
2000	5	100	100.0094	-0.01
1500	6.666667	1000	1000.2	-0.02
1000	10	10000	10002	-0.02
600	16.66667	100000	100030	-0.03
400	25	1000000	1000400	-0.04

B7: FNR 32K820 to FNR 32K471

The FNR 32K820 – FNR 32K471 MOVs have a diameter of 32 mm. These MOVs have a one-time maximum withstand surge current (8/20 µs) of 20 kA and the rated power of 1.2 W. The maximum energy (2 ms) of these MOVs ranges from 35 J to 390 J with a maximum operating DC voltage ranging from 65 V to 385 V depending on the type of MOV.

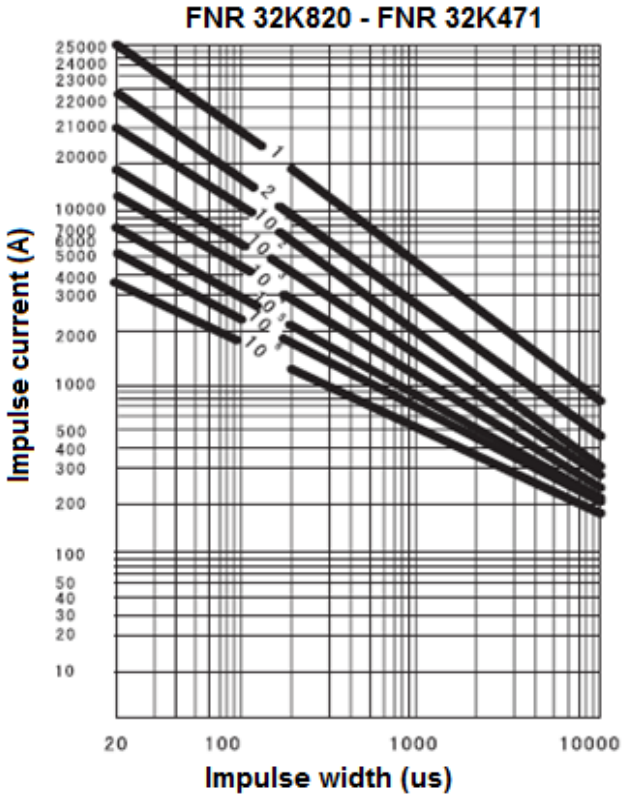

Figure B7: Pulse rating curves of MOVs FNR 32K820 – FNR 32K471 [58].

Table B13: Parameters of the proposed degradation model for MOVs FNR 32K820 – FNR 32K471.

Parameters	Values
b_1	-2.9733
b_2	1.8822
b_3	-1.9283
b_4	1.9726
b_5	3.0346
b_6	-0.1056
b_7	-1.7368
b_8	4.8267
b_9	-4.6983
b_{10}	3.9540
b_{11}	-4.7667
b_{12}	-1.0763

Table B14: Accuracy of the proposed degradation model for MOVs FNR 32K820 – FNR 32K471.

Impulse (A)	Ratio	Number of impulses before failure as specified in pulse rating curves	Number of impulses before failure as per the proposed mathematical degradation model	Error (%)
20000	1	1	1	0
10000	2	2	2.0005	-0.03
6000	3.333333	10	10.0003	-0.003
4000	5	100	99.9942	0.01
2800	7.142857	1000	999.8329	0.02
1600	12.5	10000	9996.9	0.03
1000	20	100000	99960	0.04
700	28.57143	1000000	999390	0.06

B8: FNR 40K820 to FNR 40K471

The FNR 40K820 – FNR 40K471 MOVs have a diameter of 40 mm. These MOVs have a one-time maximum withstand surge current (8/20 µs) of 40 kA and the rated power of 1.4 W. The maximum energy (2 ms) of these MOVs ranges from 80 J to 546 J with a maximum operating DC voltage ranging from 65 V to 385 V depending on the type of MOV.

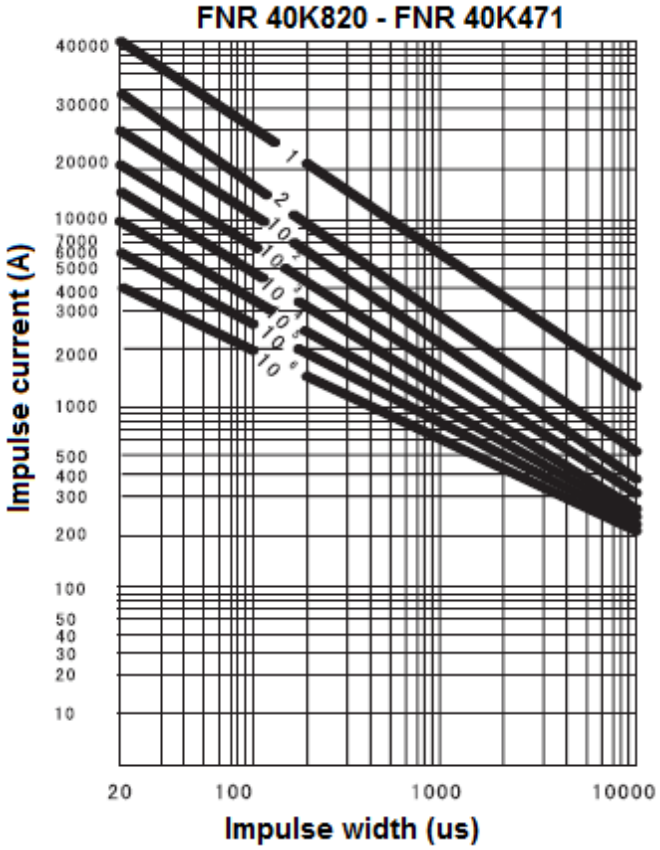

Figure B8: Pulse rating curves of MOVs FNR 40K820 – FNR 40K471 [58].

Table B15: Parameters of the proposed degradation model for MOVs FNR 40K820 – FNR 40K471.

Parameters	Values
b_1	-8.6075
b_2	-4.0805
b_3	0.6999
b_4	7.6255
b_5	0.9412
b_6	-0.6581
b_7	-1.2413
b_8	7.1062
b_9	-6.8441
b_{10}	4.7442
b_{11}	-8.5724
b_{12}	-1.5266

Table B16: Accuracy of the proposed degradation model for MOVs FNR 40K820 – FNR 40K471.

Impulse (A)	Ratio	Number of impulses before failure as specified in pulse rating curves	Number of impulses before failure as per the proposed mathematical degradation model	Error (%)
40000	1	1	1.0014	-0.14
20000	2	2	1.9975	0.13
12000	3.333333	10	10.0008	-0.01
8000	5	100	100.0088	-0.01
6000	6.666667	1000	1000.3	-0.03
4000	10	10000	9997	0.03
2400	16.66667	100000	99923	0.08
1600	25	1000000	998440	0.16

Appendix C: Matlab code for determining the proposed model's parameters

This appendix shows the Matlab code used to determine the parameters of the proposed model in order to characterise the degradation of the MOVs with sizes ranging from 5 mm to 40 mm.

```
% Name: Mathews Mashaba
% Student number: 361994
% Date: June 2016
% matlab version 7.12.0 - R2011a

% This code is for determining the parameters of the proposed degradation model for
% all the MOVs in order to determine the relationship between the lightning impulse
% current injected and the degree of degradation of the MOV



%xdata -> is the surge current ratio of respective MOVs
%ydata -> is the specified number of strikes extracted from the pulse rating curves

%FNR 05K820-05K561
%xdata = [1 2 3 4 5 6.67 22.22 50];
%FNR 07k820-07K681
%xdata = [1 2 4 8.571 15 24 34.286 48];
%FNR 10k820-10K471
%xdata = [1 2 3.846 8.333 12.5 16.667 25 41.667];
%FNR 14k820-14K471
%xdata = [1 1.8 4.5 7.5 18 30 56.25 100];
%FNR 20k820-20K471
%xdata = [1 1.625 3.25 6.5 10.833 32.5 65 108.333];
%FNR 25k820-25K471
%xdata = [1 2 3.333 5 6.667 10 16.667 25];
%FNR 32k820-32K471
%xdata = [1 2 3.333 5 7.143 12.5 20 28.571];
%FNR 40k820-40K471
xdata = [1 2 3.333 5 6.667 10 16.667 25];
ydata = [1 2 10 100 1000 10000 100000 1000000];

% NB: All the ratios (xdata) and specified number of strikes (ydata)for respective MOVs
% are given above. In order to determine the proposed model's parameters for a specific
% MOV, the rest of the ratios of other MOVs have to be commented out.


fun = @(x,xdata) 10.^(x(1)+((x(2))*log10(xdata))+((x(3))*exp(-log10(xdata)))+((x(4))↙
*exp(log10(xdata)))+((x(5))*exp(-2*log10(xdata)))+((x(6))*exp(2*log10(xdata))))+ 10.^(x↙
(7)+((x(8))*log10(xdata))+((x(9))*exp(-log10(xdata)))+((x(10))*exp(log10(xdata)))+((x↙
(11))*exp(-2*log10(xdata)))+((x(12))*exp(2*log10(xdata))));

x0 = [0,0,0,0,0,0,0,0,0,0,0,0];
options = optimset('lsqcurvefit');
options.MaxFunEvals = 100000000;
options.MaxIter = 100000000;
lb = [ ];
ub = [ ];
[x,resnorm,~,exitflag,output] = lsqcurvefit(fun,x0,xdata,ydata,lb,ub,options)

% End of code
```

Appendix D: A Proposed Mathematical Model of Metal Oxide Varistor Degradation – paper submitted to SAUPEC 2017

This appendix presents a paper the author submitted to South African Universities Power Engineering Conference (SAUPEC) 2017 which will be held in Stellenbosch University, on 30th January – 1st February 2017. The paper has been accepted for oral presentation. The paper is titled: ***A Proposed Mathematical Model of Metal Oxide Varistor Degradation***.

A PROPOSED MATHEMATICAL MODEL OF METAL OXIDE VARISTOR DEGRADATION.

M.M. Mashaba* and K.J. Nixon**

School of Electrical and Information Engineering, University of the Witwatersrand, Johannesburg, South Africa
** Mathews.Mashaba@students.wits.ac.za*
*** Ken.Nixon@wits.ac.za*

Abstract: Lightning and switching surges propagate through incoming and outgoing (power and signal) cables to reach electrical and electronic equipment, and subsequently may cause catastrophic damage and operational malfunction. Surge Protective Devices composed of Metal Oxide Varistors are commonly used to protect the equipment against surges, however, over time the MOVs degrade depending on the severity and frequency of surges. Measuring the physical parameters of the MOV to deduce its condition is not always practical, and thus preventative maintenance mechanisms are sought. The purpose of this paper is to propose a mathematical model that characterises the degradation of a MOV 14K201 with respect to an 8/20 µs lightning impulse current injected. The proposed model can accurately predict the degradation with a maximum error that is below ±0.2% relative to the pulse rating curves. Further work is recommended in order to refine and improve the model.

Key words: Degradation, lightning surges, metal oxide varistor, proposed mathematical degradation model.

1. INTRODUCTION

Lightning and switching surges propagate through incoming and outgoing power and signal cables to reach electrical and electronic equipment, and subsequently may cause damage and operational malfunction. Surge Protective Devices (SPDs) are employed to protect the electrical and electronic equipment against the catastrophic and harmful effects of surges. Most SPDs, especially the ones used in low-voltages, are commonly composed of Metal Oxide Varistors (MOVs) [1-3]. MOVs are bipolar ceramic semiconductor devices with a non-linear voltage-current characteristics; their resistance decreases with an increase in voltage magnitude [1, 2]. A MOV acts as an open circuit during normal operating voltage and conducts current during voltage transients or when voltage is elevated above the rated Maximum Continuous Operating Voltage (MCOV).

Depending on the level of surge exposure the MOV does not always show visual failure which therefore makes visual inspection challenging and inaccurate. Therefore, to ensure that the MOV always offers acceptable protection, preventative maintenance mechanisms are sought.

Numerous studies have been undertaken to determine the degradation of a MOV. Most of these studies utilise methods and diagnostic techniques which focus on observing the degradation of the MOV's microstructure and how the change in microstructure actually affects the electrical performance of the MOV with respect to its specification [1, 3]. However, not much attention has been focused on quantifying the electrical degradation of the MOV relative to lightning impulses.

The pulse (life span) rating curves of a MOV estimate its life span when it has been exposed multiple times to surges of the same magnitude. However, in reality, a lightning event (flash) consists of multiple current surges (strokes) of different magnitudes, with the first stroke approximately three times larger than the subsequent strokes [4, 5]. Furthermore, the sequence of occurrence of lightning events and switching surges does not always follow the same pattern.

This paper proposes a mathematical model that defines the relationship between the 8/20 µs lightning impulse current injected and the degree of degradation of the MOV 14K201. The type 14K201 MOV is chosen mainly because of the availability and the frequency of it being used on the low voltage equipment/systems.

2. MOV DEGRADATION AND FAILURE

This section discusses the factors that contribute to the degradation of a MOV, and the mechanisms by which a MOV frequently fails. Furthermore, the methods that are commonly used to determine the degradation/failure of the MOV are discussed.

2.1 MOV Failure

MOVs are subjected to different types of failure which include long-term degradation, electrical puncture, thermal cracking, thermal runaway, etc. mainly caused by the limited capacity of the MOV to absorb energy. A surge in excess of the rated surge current or voltage may cause short circuits which can lead to a rupture with expulsion of

the material. The significant failure mechanisms of a MOV are briefly described below [4, 6-7]:

- **Puncture** – occurs in the centre of varistor which results from non-uniform distribution of heat and current density that is caused by the higher temperature and larger current grown alternately at the centre. This phenomenon may be caused by long-duration over-voltages.
- **Cracking** – occurs due to higher thermal tensile stresses on the varistor which are caused by very large impulse currents during lightning surges.
- **Thermal runaway** – occurs due to continuous operating voltage following lightning surge current, because of the inability of the varistor to sufficiently cool temperature down, and consequently the temperature of the varistor is increased by leakage current caused by degradation of the varistor. As a result, this causes a notable disorder on the microstructure of the varistor.
- **Repeated conduction of currents** – are associated with momentary system over-voltages (swells), which lead to an increase in leakage current. The conduction is limited to a highly thermally activated low current region where the performance of the varistor is determined by the parameters of the potential barriers. This results in the movement of ions and the deformation of potential barriers.
- **Mechanical degradation** – leads to the corresponding increase in the forward voltage drop which results in electrical degradation. This degradation leads to local thermal runaway and total failure.
- **Misalignment** – results in a very small insulation path, where moisture or ion concentration may lead to high leakage. Large and unstable leakage currents may occur as a result of the oxide passivation being bridged by effects such as purple plague.

2.2 MOV Degradation

It is known that MOVs experience degradation due to single and multiple current impulses. The MOVs degrade when they are exposed to a few large surges, or many smaller surges [2]. However, many MOVs show no signs of degradation when they are operated below rated voltage. Hence, the degradation of MOVs is dependent on their composition and fabrication. Furthermore, the degradation depends on their application or use.

From the degradation tests conducted in [1] it was found that a MOV starts to degrade at 8/20 µs surge current that is 1.5 times the rated MOV surge current. Degraded MOVs were found to have smaller grain size and changed diffraction peak position compared to new samples.

In high current conditions, especially above the rated surge current of a MOV, the zinc oxide junctions begin to degrade, and as a result it lowers the MCOV of the MOV. As the degradation continues, the MCOV is lowered to a level that the MOV conducts continuously, shorting or fragmenting within several seconds [2].

The life span of a MOV is generally determined by the magnitude of the internal current and its increase in temperature and voltage with time. The end of life is generally reached when measured nominal voltage of the varistor (V_n) has changed by more than ±10%. Arrhenius expression defines the failure of the varistor (or life span) as the time to reach thermal runaway [2]. Equation 1 shows the Arrhenius rate expression which is used to describe the degradation of the MOV to reach thermal runaway [2]. However, the Arrhenius expression does not consider the energy of the surge applied nor the history of surge exposure of the MOV. The environment (such as lightning surges, switching transients, temporary overvoltages, etc.) in which the MOV is exposed to is the primary factor that contribute to the degradation of a MOV. Thermal runaway is primarily caused by large surge currents and/or long duration voltages which change the physical and/or chemical properties of the MOV. As a result, the leakage current and temperature of the MOV increase and cause the MOV to reach thermal runaway.

$$t = t_0 e^{\frac{(E_a - f(V))}{RT}} \quad (1)$$

Where:

t = time to thermal runaway [s]
t_0 = constant time [s]
E_a = activation energy [J]
$f(V)$ = applied energy [J]
R = material constant [J/K]
T = temperature in Kelvin [K]

Since the MOV does not conduct at normal operating voltages (i.e. voltages below MCOV), it is then regarded as an insulator. Most diagnostic techniques refer to the MOV as an insulating material when assessing its degree of degradation. There are several recommended methods for diagnosing and monitoring electrical equipment insulation systems (such as rotating machines, power transformers, cables, MOV, etc.) and the common and widely used methods are the Time Domain Spectroscopy (TDS) method and Frequency Domain Spectroscopy (FDS) method [8].

Time Domain Spectroscopy (TDS): TDS is based on the measurements of polarisation (also referred to as absorption) and depolarisation (also referred to as resorption) currents. These currents are used to determine the dielectric response function (which describes the behaviour) and the DC conductivity of the insulation.

Frequency Domain Spectroscopy (FDS): FDS is based on the measurements of complex permittivity components of the insulation. These components such as capacitance of

insulation at different frequencies are used to determine the loss factor as the insulation degrades.

The aging of MOV involves changes in the physical and/or chemical structure of the insulation material, which subsequently change the dielectric response [9]. The degree of aging of the MOV depends on the nature of MOV, and the nature and duration of the stresses applied. There are various types of stresses which cause aging or degradation in the MOV such as electrical, mechanical, thermal, or environmental.

The quantification of electrical degradation of the MOV aims to allow reasonable estimates of service life expectancy of the MOV and to assess its reliability in operating conditions after being subjected to stresses. The commonly used non-destructive electrical degradation diagnostic parameters and techniques of a MOV include reference voltage; leakage current; return voltage characteristics; decay voltage measurement; and Polarisation/Depolarisation current measurement.

3. CHARACTERISING THE DEGRADATION OF THE MOV

The pulse rating curves of the MOV provides the estimated life span of the MOV through an estimate of the number of strikes the MOV can withstand when subjected to surge currents of same magnitudes and different shapes (i.e. impulse width). Figure 1 shows the pulse rating curves of the MOVs 14K820 – 14K471 with the number of strikes the MOVs can withstand highlighted. The model in this study is to be developed to characterise the degradation of the MOV when subjected to lightning impulse current with a current waveform rated at 8/20 µs as defined by the International standards (IEC 60-2, ANSI/IEEE Std 4-1978, and ANSI C62.1-1984) [10]. Therefore, from the pulse rating curves only the number of strikes of the surge currents at 20 µs is extracted to produce the estimated life span of the MOV when the MOV is subjected to 8/20 µs lightning impulse current. In order to match the estimated number of strikes, a ratio of the surge currents is computed instead of using the magnitude of the 8/20 µs lightning impulse current. The choice of using a computed ratio instead of the magnitude of lightning impulse is because the proposed model should be as generic as possible in order to be applicable on a variety of MOVs. Using the magnitude of the surge currents may limit the model to only work on few MOVs types of similar range of magnitudes of surge currents; however, the MOV have different ratings of surge current. Therefore, the surge current ratio is decided upon to normalise the model to accommodate a variety of MOVs of different surge current ratings. Equation 2 shows the expression used to compute the ratio for each lightning impulse current. The information about the number of strikes and the surge current ratio is then used to compute a degradation curve of a particular MOV. Figure 2 shows the plotted degradation curve of MOVs 14K820 – 14K471.

$$R_{imp} = \frac{I_{max}}{I_n} \quad (2)$$

Where:

R_{imp} = ratio of surge currents

I_{max} = is the maximum withstand surge current (8/20 µs) of respective MOV

I_n = is the surge current (8/20 µs) for which the degree of degradation is required

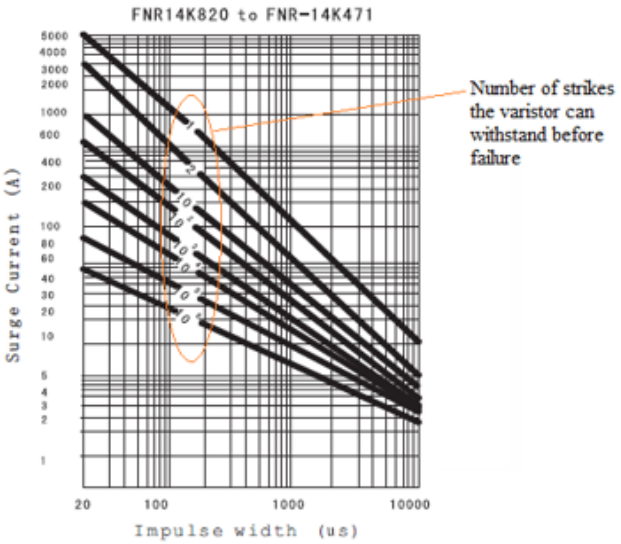

Figure 1: Pulse rating curves of MOVs FNR 14K820 – FNR 14K471 [11]

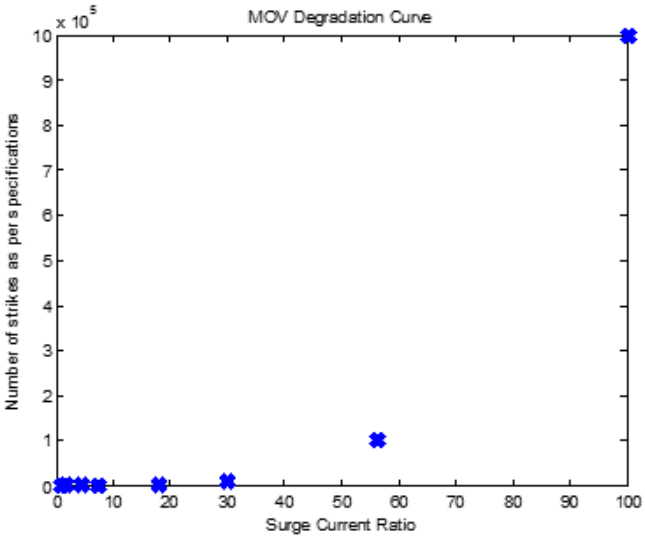

Figure 2: Degradation curve of MOVs FNR 14K820 – FNR 14K471

Comparing the varistor degradation curve in Figure 2 and the generic varistor VI curve [2] (by extracting the normal

varistor operation region and the upturn region) it can be seen that both curves have similar exponential shapes. This implies that the mathematical models of the varistor's VI curve can be used to describe the degradation curve of the MOV. The next section discusses the varistor model's interpolation formula that is suitable for the describing the degradation curve of the MOV in order to develop a degradation model.

3.1 Determining a suitable varistor model to describe the degradation characteristics of the MOV

There are several existing mathematical and electrical models [12-13] which characterise the behaviour of the MOV when subjected to lightning surges. These models mainly describe the V-I characteristics of the MOV, although the Arrhenius expression does describe the degradation of the MOV, it does not consider the lightning impulse current and it is dependent on the measurement of the temperature of the MOV. Since one of the main objectives this study aims to achieve is to minimise the dependency on measuring physical parameters of the MOV before determining the operation status of the MOV the Arrhenius expression is therefore excluded from being contextualised in developing the model.

The Durbak and simplified varistor models [12-13] describe the VI characteristics of a real varistor. The interpolation formula (33) of the simplified varistor model describes the VI characteristics of any varistor with its parameters given by the manufacturer, and the curve fitting formula (34) of the Durbak model defines the VI characteristics of only the two varistors given in the model as specified in the IEEE document [12]. The curve fitting formula of the Durbak model is limited to the two varistors' VI curves given in [12] and the interpolation formula of the simplified varistor model is a generic formula of VI characteristics of the varistor; therefore, the mathematical degradation model to be proposed is based on the interpolation formula given in [13].

4. A PROPOSED MATHEMATICAL MODEL FOR THE DEGRADATION OF THE MOV

Since the interpolation of the simplified varistor model is found suitable to describe the degradation characteristics of the MOV, the proposed model is contextualised from the interpolation formula given in [13]. Comparing the generic MOV VI curve in [2] and the degradation curve in Figure 2 it can be seen that the curves have similar shapes, with voltage and number of strikes being outputs and the currents and surge current ratio being inputs. Therefore, the initial degradation model is proposed by converting the interpolation in the manner that 'u' and 'i' in interpolation formula is replaced with N_{sw} and R_{imp} respectively, to get the proposed initial degradation mathematical model given in equation 3.

$$\log(N_{sw}) = b_1 + b_2 \log(R_{imp}) + b_3 e^{-\log(R_{imp})} + b_4 e^{\log(R_{imp})} \quad (3)$$

Where:

N_{sw} = number of strikes

R_{imp} = ratio of surge currents

$b_1, b_2, b_3, \& b_4$ = parameters obtained by fitting the degradation curve

Since the number of strikes the MOV can withstand gives an indication about the actual degradation of the MOV caused by the applied impulse current, the N_{sw} from equation 3 is then made a subject of the formula which results in equation 4.

$$N_{sw} = 10^{\left(b_1 + b_2 \log(R_{imp}) + b_3 e^{-\log(R_{imp})} + b_4 e^{\log(R_{imp})}\right)} \quad (4)$$

Equation 4 provides an estimated number of strikes of particular magnitude of 8/20 µs current waveform the MOV can withstand. This information can be used to estimate the life span or degradation of the MOV when subjected to a particular lightning impulse current.

The mathematical model is mainly proposed for MOVs 5K820 – 40K471, however, the emphasis is on MOV 14K201 because it is frequently used in the low voltage equipment. The model is tested by inputting the different surge current ratios as per the pulse rating curves and then comparing the output (i.e. number of strikes N_{sw}) of the model with the number of strikes as per the pulse rating curves.

From the pulse rating curves, the number of strikes before failure ranges between 1 and 1000000 as highlighted in Figure 1. The proposed initial model was then found to accurately characterise 4 impulses, but not all impulses in relation to their number of strikes: it can accurately model the number of strikes either for 1 – 100 strikes or for 1000 – 1000000 strikes with maximum percentage error of below 1% relative to the pulse rating curves. However, the proposed initial model cannot model the degradation of the MOV using number of strikes for the whole range (i.e. for 1 – 1000000 number of strikes). Table 1 shows the parameters of the model for relevant number of strikes with maximum percentage error of below 1%.

Table 1: Parameters for MOVs FNR 14K820-14K471 using initial degradation model defined by eq. 4

Parameters	**For 1 – 100 number of strikes**	**For 1000 - 1000000 number for strikes**
b_1	-16.0921	-56.7103
b_2	3.5961	51.7103
b_3	10.5267	76.4057
b_4	5.5654	-6.9457

The model is intended to show the degradation of the MOV for whole range of number of strikes and lightning impulse current. Since the initial model only shows for either lower half (i.e. for 1 - 100 number of strikes) or upper half (i.e. for 1000 – 1000000 number of strikes) of the range of number of strikes it therefore requires modifications.

In order to accommodate all ranges of the number of strikes with the knowledge that the initial model can accurately model either halves of the range accurately; the initial model is extended by duplicating it for all ranges, which results in equation 5 (modified initial degradation model). The first expression of the model in equation 5 account for 1-100 number of strikes and the other expression of the model account for 1000-1000000.

$$N_{sw} = 10^{\left(b_1+b_2\log(R_{imp})+b_3e^{-\log(R_{imp})}+b_4e^{\log(R_{imp})}\right)} + 10^{\left(b_5+b_6\log(R_{imp})+b_7e^{-\log(R_{imp})}+b_8e^{\log(R_{imp})}\right)} \quad (5)$$

The modified initial model given by equation 5 was tested on all MOVs (5K820 – 40K471) and it was found to accurately model most MOVs, but not all. On the other few MOVs, the model given by equation 5 was found to accurately describe the degradation for 1- 10000 number of strikes. However, the remaining 100000-1000000 number of strikes were modelled with a maximum error of 30%. Therefore, additional parameters were added to improve the accuracy of the model and to ensure that it can model all MOVs accurately. The additional parameters were added based on the percentage error and degradation curve derived from the modified model. Furthermore, the addition of parameters was contextualised from the manner in which the standard VI model in linear form [2] was extended and converted into the interpolation formula of the simplified varistor model.

During the addition of parameters into the model, it was clear that the more parameters are added the more accurate the model becomes. Therefore, the final proposed degradation model of the MOVs is given in equation 6. Table 2 shows the parameters of the proposed final degradation model for MOVs 14K820 – 14K471, and Table 3 shows the accuracy of the model for MOVs 14K820 – 14K471 with maximum error of less than ±0.2% relative to the pulse rating curves.

$$N_{sw} = 10^{\left(\begin{matrix} b_1+b_2\log(R_{imp})+b_3e^{-\log(R_{imp})}+b_4e^{\log(R_{imp})} \\ +b_5e^{-2\log(R_{imp})}+b_6e^{2\log(R_{imp})} \end{matrix}\right)} + 10^{\left(\begin{matrix} b_7+b_8\log(R_{imp})+b_9e^{-\log(R_{imp})}+b_{10}e^{\log(R_{imp})} \\ +b_{11}e^{-2\log(R_{imp})}+b_{12}e^{2\log(R_{imp})} \end{matrix}\right)} \quad (6)$$

Table 2: Parameters of the proposed degradation model for MOVs FNR 14K820 – FNR 14K471

Parameters	Values
b_1	4.9785
b_2	31.3929
b_3	-17.0759
b_4	-12.2490
b_5	-15.5494
b_6	0.5740
b_7	-40.5783
b_8	-40.7520
b_9	21.7298
b_{10}	39.7058
b_{11}	-16.8345
b_{12}	-4.0222

Table 3: Accuracy of the proposed model when compared to specified degradation model for MOVs FNR 14K820 – FNR 14K471

Impulse (A)	Ratio	Number of strikes before failure as per pulse rating curves	Number of strikes before failure as per the proposed model	Error (%)
4500	1	1	1.0014	-0.14
2500	1.8	2	1.9975	0.13
1000	4.5	10	10.0008	-0.01
600	7.5	100	100.0088	-0.01
250	18	1000	1000.3	-0.03
150	30	10000	9997	0.03
80	56.25	100000	99923	0.08
45	100	1000000	998440	0.16

From these results it can be concluded that the proposed model best describes the degradation of the MOVs using the number of strikes specified in the pulse rating curves. Although, the number of strikes denote the degree of degradation the impulse causes on the MOV, the proposed final degradation model does not describe the actual percentage of degradation of the MOV caused by a particular impulse current. Therefore, the proposed final degradation model is to be modified and computed to estimate the percentage of degradation.

Computation: If the number of strikes is equal to one as per the pulse rating curve it implies that the particular surge will completely degrade the MOV (i.e. 100% degradation). Also, if the number of strikes is greater than one as per the pulse rating curve, it implies that the MOV is unlikely to fail immediately if subjected to the respective type of impulse; for example, if the number of strikes is equal to two, this implies that a strike/impulse of this type causes a 50% degradation. Since the model in equation 6 outputs the number of strikes for a particular impulse current magnitude, the percentage of degradation of a MOV is

given by a proposed degradation model described in equation 7, where N_{sw} is as given in equation 6.

$$D_{imp} = \frac{1}{N_{sw}} \times 100\% \quad (7)$$

Where:

D_{imp} = percentage degradation caused by a lightning impulse current

5. FUTURE RECOMMENDATIONS

The proposed mathematical model accurately describe the percentage of degradation of the MOV FNR 14K820-14K471 (14K201is included). However, the model has many parameters which make the model somewhat complicated. Therefore, for future work it is recommended to possibly refine the model to consist of less parameters while remain accurate.

The mathematical model was computed based on the pulse rating curves. It is therefore recommended to test the proposed model against the experimental test results of the MOV to observe the discrepancy and thus, to include a correction factor.

6. CONCLUSION

A mathematical model has been proposed to model the degradation of the MOV 14K201 with respect to the 8/20 µs lightning impulse current injected. The proposed model can accurately model the degradation with a maximum error that is below ±0.2% relative to the pulse rating curves. Further work is recommended to refine the proposed model to reduce the number of parameters, and to test the proposed model against experimental test results.

REFERENCES

[1] K.P. Mardira, T.K. Saha, and R.A. Sutton, "The Effects of Electrical Degradation on the Microstructure of Metal Oxide Varistor", *IEEE 0-7803-7285-9/01*, 2001.

[2] K.J. Brown, "Metal Oxide Varistor Degradation", *IAEI News: The Magazine*, March/April 2004.

[3] K.P. Mardira and T.K. Saha, "Modern Electrical Diagnostics for Metal Oxide Surge Arresters", *IEEE transactions*, 2001.

[4] IEC 62305-1 "Protection against lightning – Part 1: General Principles," Edition 2.0, 2010.

[5] K.J. Nixon, J.M. Van Coller, and I.R. Jandrell, "Earthing and Lightning Protection, Revision 2.1," *School of Electrical and Information Engineering, University of the Witwatersrand*, pp. 13-30, March 2010.

[6] Transient Surges and Surge Suppressor Technologies: "Comparing Apples to Oranges – MOV versus SASD Design Discussion", http://www.wago.us/surge.htm, last accessed: 03 November 2016.

[7] S. Han, H. Cho, Y. Lee, and H. Kang, "Modeling on the Failure for High-Voltage Arresters by Voronoi Network Simulation", *Proceedings of the 6th International Conference on Properties and Applications of Dielectric Materials*, pp.676 – 680, June 2000.

[8] C. Stancu, P.V. Notigher, and L.V. Badicu, "Dielectric Response Function for Nonhomogeneous Insulations", *Conference on Electrical Insulation and Dielectric Phenomena (CEIDP)*, pp. 97 – 100, 2011.

[9] E. David and L. Lamarre, "Low-Frequency Dielectric Response of Epoxy-Mica Insulated Generator Bars during Multi-Stress Aging", *IEEE Transactions on Dielectrics and Electrical Insulation*, Vol. 14, No. 1, pp. 212 – 226, February 2007.

[10] R.B. Standler, "Protection of Electronic Circuits from Overvoltages", John Wiley & Sons, pp. 87, 1989.

[11] FENGHUA, "Zinc Oxide Varistor", Fenghua (HK) Electronics Ltd.

[12] IEEE Working Group 3.4.11, "Modelling of Metal Oxide Surge Arresters", *IEEE Transactions on Power Delivery*, Vol. 7, No. 1, January 1992.

[13] Siemens and Matshushita Componenta, "SIOV Metal Oxide Varistor", Pspice model library, 1995.

Appendix E: Tools, Equipment and Components used

This appendix provides the list of components, equipment and tools used to conduct the experimental tests for this study. A brief description on-, and the purpose of-, each tool/equipment/component is given.

Table D1: Tools, Equipment and Components used to conduct experimental tests.

Tool/Equipment/Component	**Description**
FNR 14K201	A metal oxide varistor tested to compare the proposed model results with the experimental test results. It is rated at 4.5 kA (8/20 µs) and 170 V_{DC} (Maximum Continuous Operating Voltage)
1 kΩ and 1 Ω carbon film resistors	Are shunt resistors (with ±5% tolerance) used to measure the leakage current and reference voltage of the MOV respectively
Fluke 15B+ Digital multimeter	A multimeter used measure the voltage across the shunt resistor and the MOV
Fluke 177 and Fluke 336	Multimeters used to verify the readings obtained by Fluke 15B+
Pearson Current Monitor Model 301X	Current meter used to measure the lightning impulse current from the impulse generator
SPELLMAN SA4 High Voltage power supply	DC Power supply used to excite the MOV for leakage current and reference voltage tests.
RIGOL DS1064B Digital Oscilloscope	Oscilloscope used to display measurements
Harper Transformer rated at 220V, 1 kVA {manufactured by Harper Electrical Industries (PTY.) LTD}	Isolator used to protect the Oscilloscope against surge currents and overvoltages.
Fluke 80K-40 HV Probe with a ratio of 1000:1	High Voltage probe used in connection with oscilloscope and mutlimeters to safely measure high voltages

APPENDIX F: Experimental Test Results

This appendix provides the results of all the experimental tests conducted on type FNR 14K201 MOV. In total, 160 samples of the MOVs were tested, and 16 samples were used per particular magnitude of 8/20 µs lightning impulse current.

F1: Reference voltage and leakage current results for MOV FNR 14K201

The MOVs were subjected to 8/20 µs lightning impulse current and the parameters were measured before and after it was subjected to the impulse current.

I_{rs} = Rated surge current (i.e. Maximum current 8/20 µs the MOV can withstand only for 1 time)

Table F1: Reference voltage results at I_{rs} = 4.5 kA.

Sample number	Before(V)	After(V)	%change
1	215.8	188.1	12.84
2	197.1	160	18.82
3	205.1	170	17.11
4	205.3	182.3	11.20
5	204.9	176.5	13.86
6	208	195.5	6.01
7	198	171	13.64
8	200.3	180	10.14
9	199.3	169	15.20
10	204.1	178.9	12.35
11	197.1	177	10.20
12	205.1	187.7	8.48
13	195.6	160	18.20
14	199.8	180.3	9.76
15	202.7	179	11.70
16	201.7	169.8	15.82

Table F2: Leakage current results at I_{rs} = 4.5 kA.

Sample number	Before(uA)	After(uA)	%change
1	5	70	-1300
2	1.6	75.5	-4618.75
3	4.1	48.5	-1082.93
4	3.3	71	-2051.52
5	3.8	42.6	-1021.05
6	8.8	56	-536.364
7	2.1	79.9	-3704.76
8	2.9	74.7	-2475.86
9	4.2	74	-1661.9
10	25	740	-2860
11	3.7	73.9	-1897.3
12	7.2	60	-733.33
13	11.5	742	-6352.17
14	2.5	26.7	-968
15	1.9	22.6	-1089.47
16	3.3	53.9	-1533.33

Table F3: Leakage current results at $0.9I_{rs}$ = 4.05 kA.

Sample number	Before(uA)	After(uA)	%change
17	5	25.4	-408
18	3.5	73.8	-2008.57
19	1.6	16	-900
20	3.6	39	-983.33
21	4.2	13.9	-230.95
22	9	131	-1355.56
23	8	97.6	-1120
24	2.1	30.4	-1347.62
25	9.5	449	-4626.32
26	2.5	12.6	-404
27	9.2	100	-986.96
28	3.5	23.2	-562.86
29	70	802	-1045.71
30	5.7	80	-1303.51
31	14.6	350	-2297.26
32	3.2	43.5	-1259.38

Table F4: Leakage current results at $0.8I_{rs}$ = 3.6 kA.

Sample number	Before(uA)	After(uA)	%change
33	2.1	28.7	-1266.67
34	3.2	35	-993.75
35	4.1	38.6	-841.46
36	2.7	25.1	-829.63
37	5.2	36	-592.31
38	3.8	41.4	-989.47
39	5.3	76.8	-1349.06
40	5.8	59.9	-932.76
41	19.7	180.3	-815.23
42	4	43.2	-980
43	5.3	55	-937.74
44	4.5	43	-855.56
45	5.9	61.6	-944.09
46	4.2	54.9	-1207.14
47	9.3	87.6	-841.94
48	4.7	30	-538.30

Table F5: Leakage current results at $0.7I_{rs}$ = 3.15 kA.

Sample number	Before(uA)	After(uA)	%change
49	7.6	16	-110.53
50	9.6	67	-597.92
51	1.5	11.6	-673.33
52	2.9	24.4	-741.38
53	14.1	98.7	-600
54	6.9	55	-697.10
55	4.9	43.6	-789.80
56	3.4	23.4	-588.24
57	1.5	16.8	-1020
58	5.3	40.3	-660.38
59	4.1	33	-704.88
60	8.1	88	-986.42
61	9.3	48	-416.13
62	5.2	20.4	-292.31
63	19.3	111	-475.13
64	6	40.5	-575

Table F6: Leakage current results at $0.6I_{rs}$ = 2.7 kA.

Sample number	Before(uA)	After(uA)	%change
65	9.6	61.3	-538.54
66	6.9	44.4	-543.48
67	1.4	7.4	-428.57
68	2.2	15.7	-613.64
69	5.1	55	-978.43
70	3.7	32	-764.87
71	2.2	15.1	-586.36
72	4	38	-850
73	4	41.9	-947.5
74	4.4	17.9	-306.82
75	9.5	71.5	-652.63
76	8.1	55.5	-585.19
77	5	34.3	-586
78	3.3	21.6	-554.55
79	4.7	37	-687.23
80	2.4	16	-566.67

Table F7: Leakage current results at $0.5I_{rs}$ = 2.25 kA.

Sample number	Before(uA)	After(uA)	%change
81	1.8	10.1	-461.11
82	2.9	23.5	-710.35
83	8.6	57.6	-569.77
84	7.4	46.2	-524.32
85	5.2	30.8	-492.31
86	4	23.9	-497.5
87	4.4	29	-559.09
88	1.6	15.1	-843.75
89	2.5	13.3	-432
90	7.5	44	-486.67
91	7	57	-714.29
92	6.7	43.3	-546.27
93	6.2	50	-706.45
94	1.6	13.9	-768.75
95	6.2	49.4	-696.77
96	2.5	5	-100

Table F8: Leakage current results at $0.4I_{rs}$ = 1.8 kA.

Sample number	Before(uA)	After(uA)	%change
97	3.3	19.4	-487.88
98	2.2	15.3	-595.45
99	4	20	-400
100	4.5	27.2	-504.44
101	1.8	11.6	-544.44
102	5.1	13.5	-164.71
103	9.9	51	-415.15
104	2.3	19	-726.09
105	1.7	10.9	-541.18
106	5.9	31.7	-437.289
107	4.4	22.8	-418.18
108	4.4	27	-513.64
109	2.3	18	-682.61
110	18.1	133	-634.81
111	2.1	20.6	-880.95
112	9.2	56.2	-510.87

Table F9: Leakage current results at $0.3I_{rs}$ = 1.35 kA.

Sample number	Before(uA)	After(uA)	%change
113	4.1	17.2	-319.51
114	3.7	23	-521.62
115	2.3	9.8	-326.09
116	1.4	7	-400
117	4.5	22.1	-391.11
118	3	12.1	-303.33
119	11.4	49.9	-337.72
120	4.4	25	-468.18
121	18.5	99	-435.14
122	2	6.7	-235
123	8.2	46	-460.98
124	18.2	110.4	-506.59
125	3.2	15.2	-375
126	3.2	17	-431.25
127	4.2	19	-352.38
128	1.4	5.6	-300

Table F10: Leakage current results at $0.2I_{rs}$ = 0.9 kA.

Sample number	Before(uA)	After(uA)	%change
129	3.7	9.9	-167.57
130	9.4	23.2	-146.81
131	2	3.4	-70
132	0.4	0.9	-125
133	11.9	22.2	-86.56
134	4.5	10.6	-135.56
135	5.4	11.3	-109.26
136	2.7	7	-159.26
137	4	11.9	-197.5
138	3.8	8.2	-115.79
139	4.1	12	-192.68
140	3.5	6.1	-74.29
141	2	3.4	-70
142	6.1	18	-195.08
143	19	45.2	-137.90
144	2	4.2	-110

Table F11: Leakage current results at $0.1I_{rs}$ = 0.45 kA.

Sample number	Before(uA)	After(uA)	%change
145	4.2	5	-19.05
146	7	11.1	-58.57
147	1.3	2	-53.85
148	3.2	4	-25
149	5.4	9.6	-77.78
150	2.3	3.2	-39.13
151	3.4	5.2	-52.94
152	6.6	8	-21.21
153	6.3	8.5	-34.92
154	6.6	6.7	-1.52
155	5.8	8.6	-48.28
156	4.3	6	-39.54
157	7.7	10.9	-41.56
158	3.1	3.4	-9.68
159	10.4	14.9	-43.27
160	9.6	10.7	-11.46